THE DESIGN AND IMPLEMENTATION OF A VERSATILE MICROPROCESSOR-BASED DIRECTIONAL OVERCURRENT RELAY

A Thesis

Submitted to the College of Graduate Studies and Research

in Partial Fulfilment of the Requirements

for the Degree of

Master of Science

in the

Department of Electrical Engineering

University of Saskatchewan

by

Wayne Allan Guttormson

Saskatoon, Saskatchewan

June 1993

COPYRIGHT

Dedicated to my beloved parents,
Neil and Alice.

ACKNOWLEDGEMENTS

The author would like to express his deep appreciation and gratitude to Dr. M.S. Sachdev for his thoughtful guidance and assistance in the supervision and preparation of this thesis.

The author also acknowledges the helpful advice received from Dr. T.S. Sidhu and Ph.D. students Bijoy Chattopadhyay and Thompson Adu.

The author also takes this opportunity to acknowledge his parents and friends for their moral support and patience throughout the course of this work.

Financial assistance provided by the Saskatchewan Power Corporation in the form of a scholarship is also gratefully acknowledged.

UNIVERSITY OF SASKATCHEWAN

Electrical Engineering Abstract 93A378

THE DESIGN AND IMPLEMENTATION OF A VERSATILE MICROPROCESSOR-BASED DIRECTIONAL OVERCURRENT RELAY

Student: Wayne A. Guttormson Supervisor: Dr. M.S. Sachdev

M.Sc. Thesis Submitted to the
College of Graduate Studies and Research

June 1993

ABSTRACT

Due to advancements in the field of electronics, relay designers are able to implement practical microprocessor-based relay designs which are being used more and more by utilities. With the increasing number of digital overcurrent relays being developed for use in electrical power systems need has arisen for the development of directional relays. In many situations, the magnitudes of fault currents do not provide enough information for correctly discriminating faults in a power system where the lines form loops, rings or grids. As power systems have become increasingly complex and interconnected, this scenario occurs more often. Directional relays can sense the direction of power flow and often act as sensors and logical switches for activating other types of relays. An example of this type of monitoring is the directional overcurrent relay.

This thesis is concerned with the design and implementation of a versatile microprocessor-based directional overcurrent relay for phase and ground fault detection. The user is able to specify various design parameters at the time of commissioning the relay so that it may be used in distribution networks, transmission networks or other power flow applications. Some of these parameters are the maximum torque angles, torque offsets, directional sensing voltage-current pairs, pickup settings, time multiplier settings, current-time characteristics and configuration of the relay. The relay design is implemented on an Ariel Corporation's PC-C25 DSP Coprocessor Board which contains a Texas Instruments TMS320C25 digital signal processor.

The relay's software structure is divided into a main program and numerous support functions. The main program and several functions are written in TMS320C25 C to take advantage of the flexibility of the C programming language. The C code is cross-compiled into TMS320C25 assembly language and linked with other developed assembly language support functions. The majority of time critical code is directly implemented in assembly language and some code employs floating point arithmetic instead of fixed point.

The capabilities of the designed relay are demonstrated by including cases of transmission line shunt faults. These tests were performed off line using (*i*) data generated by the Electro-Magnetic Transients Program using a six-bus model of the Saskatchewan Power Corporation's (SPC) transmission network and (*ii*) fault data recorded by SPC.

Table of Contents

List of Figures

List of Tables

1. INTRODUCTION

1.1. Power System Protection

The primary function of a power system is to generate, transmit, and distribute electrical energy with a high degree of continuity. However, faults and other abnormal conditions can occur in a power system which disrupt this function. This poses a serious problem to utilities and consumers of electricity because faults can cause expensive damage to equipment, injuries to personnel, severe drops in system voltage, loss of synchronism and losses in revenues. Protective relays try to reduce or eliminate these effects by activating/tripping circuit breakers to isolate faults from the rest of the system. The two main types of faults experienced by power systems are shunt faults and open circuit faults.

The present philosophy in power system protection is to divide the system into zones and then protect each zone by a set of relays and circuit breakers [1, 2, 3]. A protective zone normally consists of one major electrical component and its protective equipment. An example of a power system and its relay protection zones is shown in Figure 1.1. If a fault occurs in a zone, relays will activate the appropriate circuit breakers to isolate the fault; thus limiting damage to the system.

1.2. Microprocessor-Based Relays

Protective relays can be grouped into three general classifications, electro-mechanical, solid state and digital. Because of rapid advancements in integrated circuit technology and its related computer technologies, recent developments in relay designs have been in the area of microprocessor-based relays.

G.D. Rockefeller proposed the use of a single computer for protecting all the major

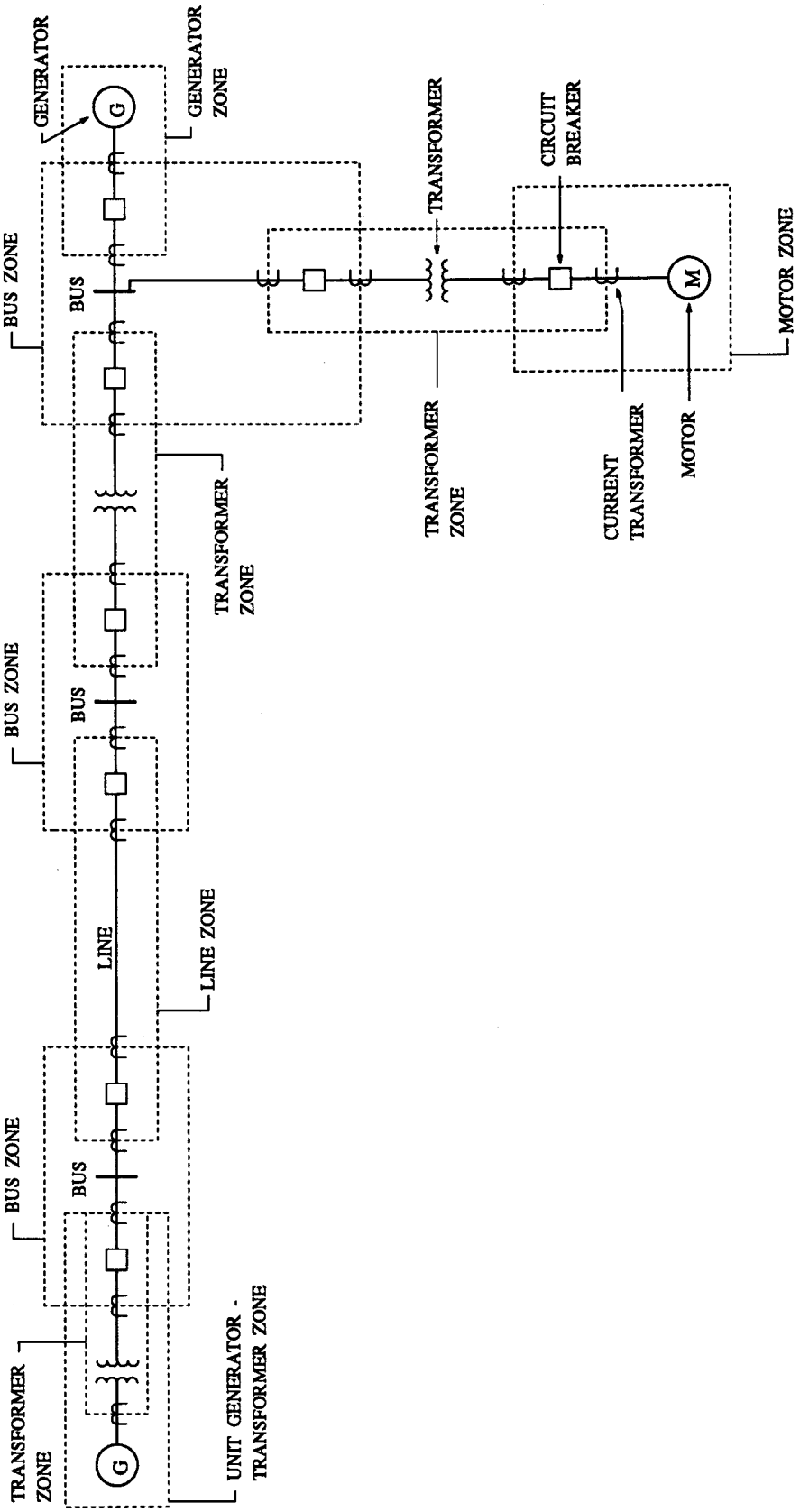

Figure 1.1: Typical relay protection zones in a power system.

components of a substation [4] in 1969. Several years later the first digital relay was installed at the Tesla substation of the Pacific Gas and Electric Company (PG&E) as a joint venture between the Westinghouse Electric Corporation and PG&E [5]. Since these efforts, great strides have been made in the design and application of microprocessor-based relays [6, 7, 8] to power system protection. There are many reasons why the interest in this area of research is so great; some of these are:

1. Economic: The prices of electro-mechanical and solid state relays have been increasing steadily, whereas the cost of digital relays have been decreasing, making them an appealing alternative for use in protective schemes.
2. Performance: Properly designed digital relays perform at least as well as, if not better than, presently available electro-mechanical and solid state relays. With the rapid improvements in microcomputer technology, the performance of digital relays can only get better.
3. Reliability: The self-diagnostic capabilities of digital relays allow them to monitor the state of their components for failures and either switch to backups and/or alert operators if a problem is encountered.
4. Flexibility: Digital relays can have multiple characteristics which can be modified by altering the relay's software; therefore digital relays can be made more flexible without a substantial increase in cost.
5. Background Tasks: Digital relays can perform background tasks such as storage and analysis of fault data, transmitting data to control centers and monitoring maintenance and supervisory alarms.
6. By Products: Digital relays present less burden to voltage and current transducers. They can also accept data over fiber optic cables; thus reducing the cost of providing cables in a station.

The functional block diagram of a stand-alone microprocessor-based relay is shown in Figure 1.2. The relay consists of analog and digital input subsystems, a digital output subsystem, a microprocessor platform (i.e., a microcomputer) and a power supply [9]. The analog input subsystem acquires low level signals proportional to power system voltages and currents via voltage and current transformers. These signals are pre-processed by auxiliary transformers, surge suppression circuits and low-pass filters. The auxiliary transformers reduce the levels of the signals to avoid saturation of the analog to digital (A/D) converters and provide electrical isolation. The surge suppression circuits limit the levels of the signals to protect the relay's electronic components against transients. Low-pass filters are used to band limit the signals to avoid aliasing. The cut

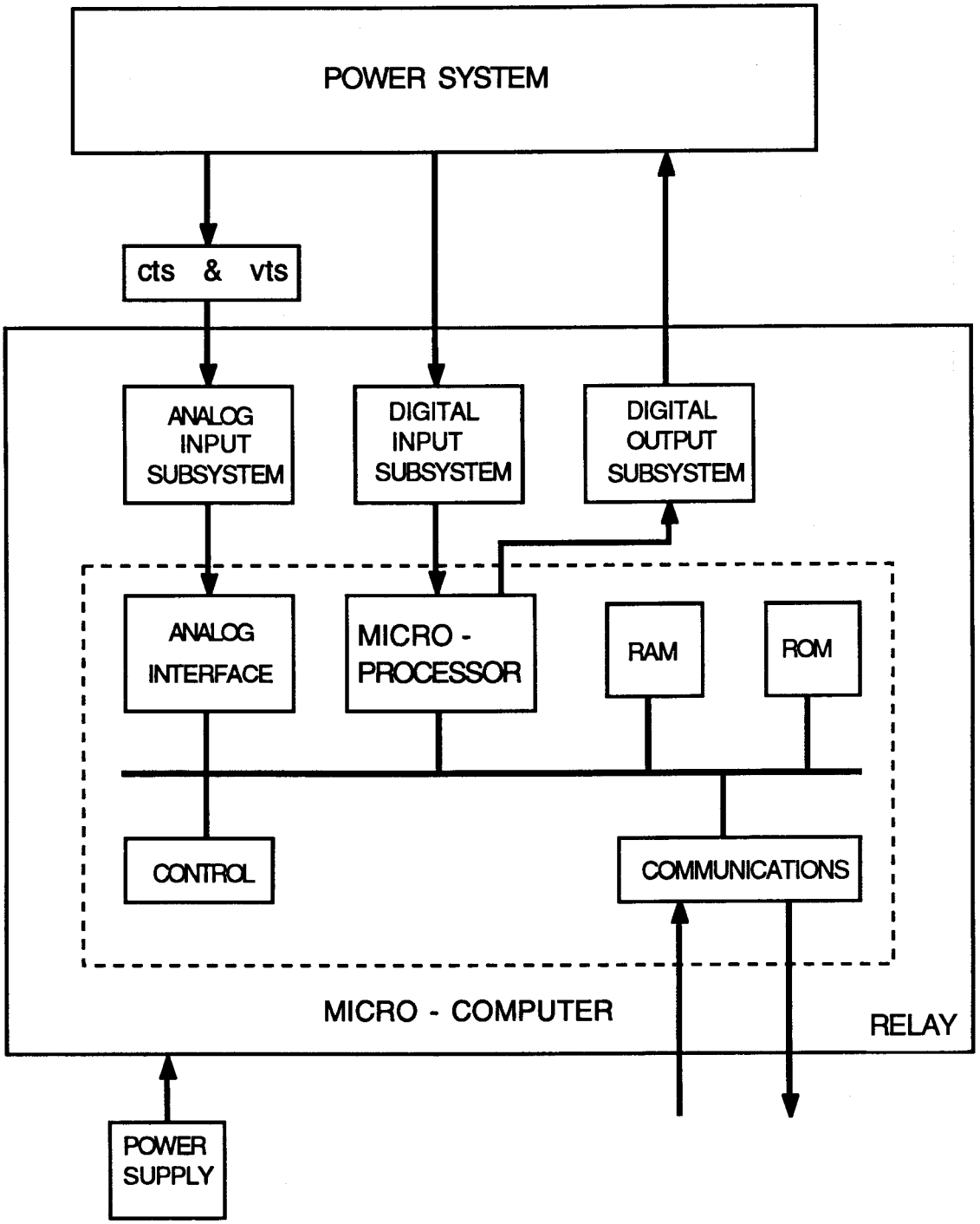

Figure 1.2: A functional block diagram of a stand-alone microprocessor-based relay.

off frequency of the filters is chosen considering the sampling frequency used to acquire the inputs. The processed time-continuous signals are then converted to time-discrete signals using sample and hold amplifiers. A multiplexer then applies each signal to an A/D converter that digitizes the time-discrete signal. The status of the circuit breakers and switches are transmitted to the relay by the digital input subsystem. Using digital relay algorithms, the microprocessor estimates the parameters of interest from the digitized signals and then decides if there is a fault in the zone of protection or not. Finally, the decision of the relay is conveyed to the power system through the digital output subsystem. A record of important events is stored in random access memory (RAM) for retrieval at a later time for permanent storage. To ensure that the relay operates properly under all conditions its power supply should be independent of the station ac supply. Usually, a dc-dc converter is used to provide energy to the relay from a substation battery.

The research, design and economics of microprocessor-based relays reached a level where commercial production began several years ago. One class of commonly produced digital relays are overcurrent relays. These are used in a variety of situations, such as distribution and sub-transmission networks. However, with the increasing complexity and greater interconnections between power systems, the direction of power flow as well as the magnitude of the fault current becomes important. The direction of power flow must be established when power lines form loops because in these situations overcurrent relays cannot provide adequate protection.

Singh, Sachdev, Fleming and Krause [10] designed and implemented an inverse definite minimum time (IDMT) directional overcurrent relay on a PDP-11 computer. They used hyperbolic equations to model IDMT current-time characteristics and the Fourier approach to estimate the rms values of the fundamental frequency components of the voltages and currents. Their directional algorithm was based on the torque equation for an electro-mechanical directional relay.

Later Murty and Smolinski [11] used a weighted least squares derived polynomial of exponential International Electrotechnical Commission (IEC) current-time

characteristics, implemented them in an overcurrent relay and determined the directionality by calculating the real power flow in the line. They used a recursive discrete Fourier transform algorithm to estimate the rms values of the fundamental frequency components of the voltages and currents and implemented their design on a TMS32010 microprocessor.

1.3. Objectives of the Thesis

The main objective of this thesis is to design and develop a versatile microprocessor-based directional overcurrent relay that can be applied in distribution networks, transmission networks or other power flow applications. To accomplish this task the relay should provide:

- phase and ground fault directional monitoring,
- single phase or polyphase configuration of the directional phase units,
- zero or negative sequence polarization of the ground unit,
- the commonly used directional-sensing connections for phase faults,
- standard current-time characteristics for use with the overcurrent element, and
- user selectable maximum torque angles, torque offsets, relay constants, pickup settings and time multiplier settings.

1.4. Outline of the Thesis

The thesis is organized in six chapters and six appendices. The first chapter introduces the subject of the thesis, outlines its organization and provides a brief overview of power system protection. Chapter 2 describes some of the applications and theory of directional relaying for power system protection. Chapter 3 provides some background information on digital relaying algorithms considered for estimating the parameters of voltages and currents. Chapter 4 describes the modelling and implementation of the directional overcurrent relay. Chapter 5 describes the tests performed and system studies done to verify the performance of the relay. A brief conclusion and summary of the thesis are given in Chapter 6.

Appendix A describes the design of the anti-aliasing filter used in off-line testing. Appendix B presents a technique that estimates the rms value of the fundamental frequency component of a current. The model of the analog to digital converter used in off-line testing is presented in Appendix C. Appendix D lists the electrical parameters of the six-bus model of the transmission system of the Saskatchewan Power Corporation (SPC) used in system studies. Appendix E describes the use of the Electro-Magnetic Transients Program (EMTP) to simulate faults on the six-bus model. Further results are given in Appendix F.

2. APPLICATIONS OF DIRECTIONAL RELAYING IN POWER SYSTEM PROTECTION

Chapter two presents some applications of directional relaying to power system protection. In particular, it provides background information and theory on how directional relays determine the direction of power flow for phase and ground faults. The direction of flow is established by monitoring the electrical torque generated by pre-specified combinations of system voltages and currents. Also discussed is directional overcurrent relaying for line protection and other power flow applications, such as generator and transformer protection.

2.1. Directional Relays

Directional relays discriminate between power flowing in one direction or the other by recognizing differences in the phase angle between two actuating quantities, usually a voltage and a current. Figure 2.1 shows a schematic diagram of a directional relay. These relays are basically power measuring devices in which a system voltage is used as a polarizing quantity for establishing the relative direction of power flow. However, they generally do not respond to the actual power flow in the system because [12]:

1. The power system is mainly reactive and, therefore, the power factor during a fault is usually quite low. A relay responding to the real power flow would not develop sufficient torque for the relay to operate without excessive delay.
2. The system voltage collapses at the short circuit and, therefore, voltage signals received by the relay are unbalanced. The developed torque by the phase units of the relay would vary widely in magnitude and in sign. By polarizing the relay with a voltage, that will not be reduced significantly under most fault conditions, a satisfactory reference is maintained for directional discrimination.

Generally, directional relays are not applied alone but are used in combination with other relays to provide outputs to control the system.

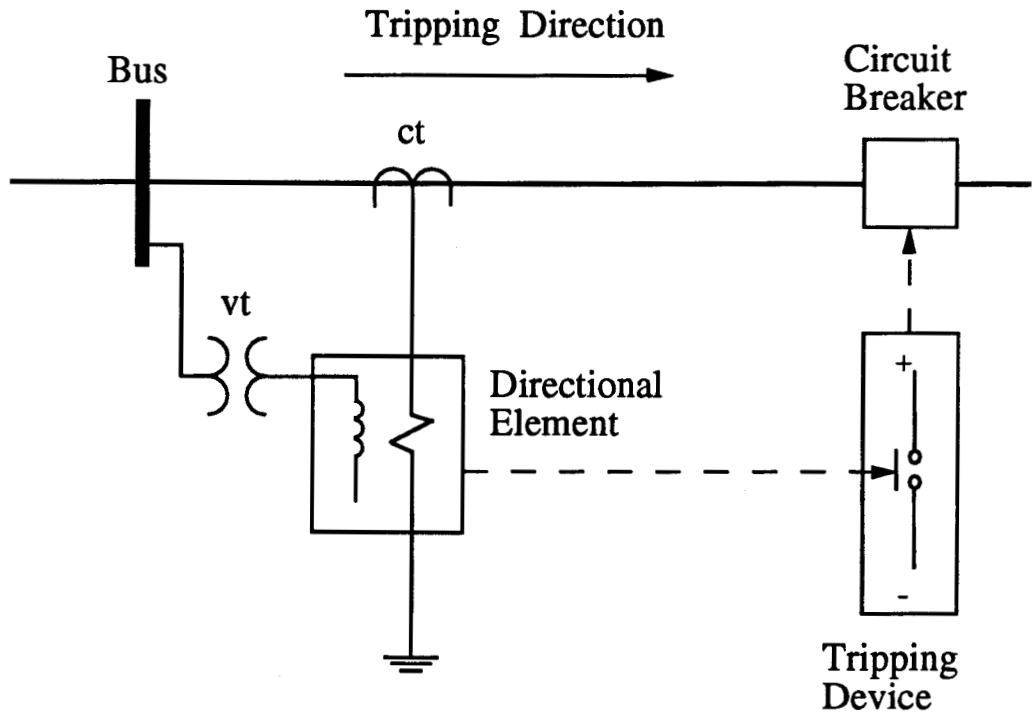

Figure 2.1: The schematic diagram of a directional relay.

The electrical torque produced by an electro-mechanical single's phase directional relay is given in Equation 2.1 [1].

$$T = K_1 |V_{pol}||I| \cos(\theta - \tau) - K_2, \tag{2.1}$$

$$\theta = \theta_I - \theta_V, \tag{2.2}$$

where:

V_{pol}	is the rms phasor representing the polarizing voltage applied to the relay,
I	is the rms phasor representing the current applied to the relay,
θ	is the phase angle between V and I phasors,
θ_I	is the phase angle of the current phasor,
θ_V	is the phase angle of the voltage phasor,

τ is the maximum torque angle (MTA),

K_1 is a relay constant and

K_2 is the torque offset, i.e., the restraining torque.

A polarizing quantity is an input that has a reasonably stable phase angle under fault conditions. It is used as a reference for other quantities whose phase angle will vary considerably due to a fault. In Equation 2.1 voltage is the polarizing quantity and the directional relay is concerned with the phase angle of the current with respect to that of the voltage. If the generated torque is greater than the torque offset, $|V_{pol}||I|\cos(\theta-\tau) > K_2$, the power flow is assumed to be in the forward direction and the fault on the line side of the relay. The ability of the directional relay to distinguish between power flow in one direction or the other depends on the polarizing quantity and the maximum torque angle used.

2.1.1. The Operating Characteristic of a Directional Relay

The operating characteristic or zero torque line of a directional relay is the dividing line between the development of positive and negative torque by the relay. When the relay is on the verge of operating, the net torque is zero and Equation 2.1 can be expressed as:

$$|V_{pol}||I|\cos(\theta-\tau) = \frac{K_2}{K_1} = Constant. \tag{2.3}$$

Figure 2.2 shows the operating characteristic in polar-coordinates with the polarizing voltage as reference. When the voltage magnitude is held constant, Equation 2.3 generates an operating characteristic that is a straight line offset from the origin and perpendicular to the maximum torque line. Pickup of the relay occurs if the tip of a current vector lies in the positive torque region. If the tip lies in the negative torque region the directional relay will either reset or not pickup. The relay generates maximum torque if the current vector lies along the maximum torque line. As the phase angle of the current approaches 90° from the maximum torque line the pickup current will become very large.

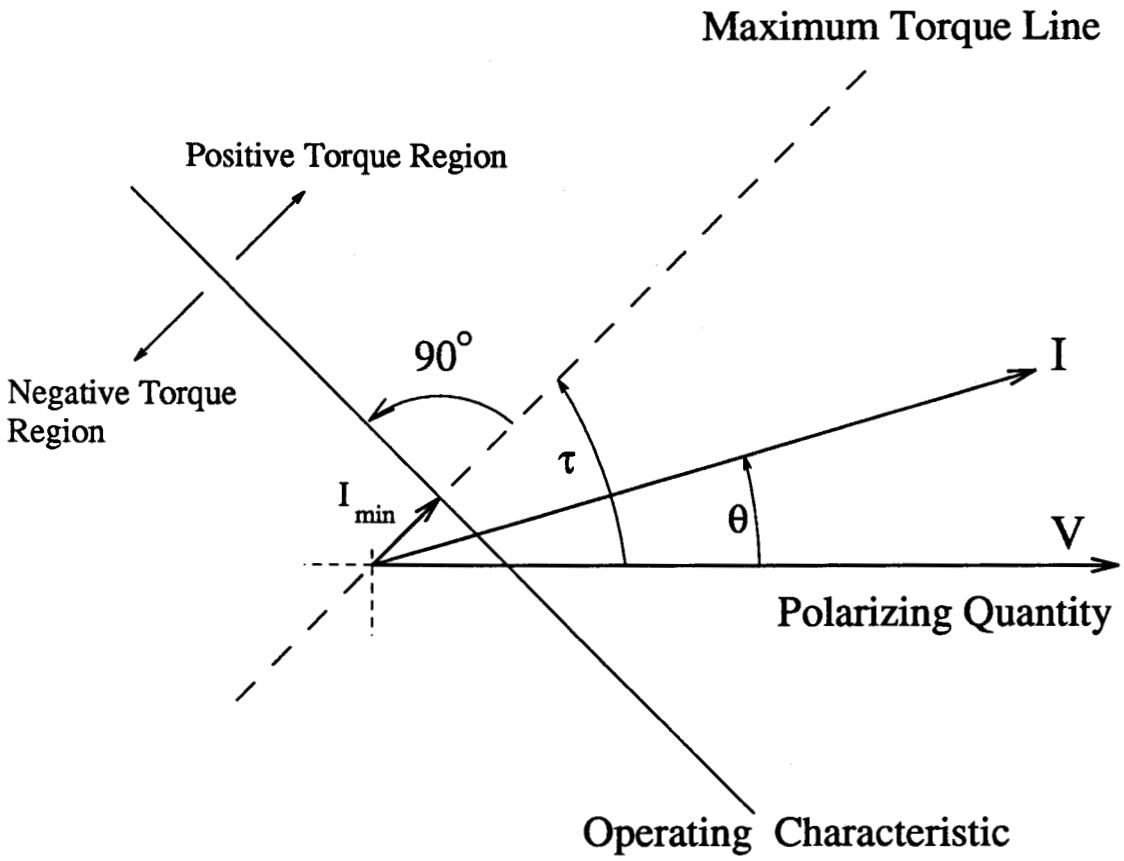

Figure 2.2: The general operating characteristic of a single's phase directional relay [1].

Different magnitudes of input voltage will generate different operating characteristics parallel to the one shown in Figure 2.2. Therefore, an infinite number of characteristics are possible, all related by:

$$|V_{pol}||I_{min}| = Constant,$$

where:

$|I_{min}|$ is the smallest magnitude of the pickup current that will cause the relay to operate.

2.1.2. Directional Sensing for Interphase Faults

For interphase faults directional relays can be configured in one of two ways, polyphase or single's phase. In a single's phase arrangement there are three single's phase directional relays or units, each one monitoring a separate phase. A polyphase directional relay operates on the net torque from all three directional phase units; thus monitoring all three phases as a whole. The voltage and current inputs for both types of configurations are determined by the directional-sensing connection used.

The commonly used connections that are used for interphase faults are the 90°, 30°, 60° delta/#1 and the 60° wye/#2 [3]. Table 2.1 describes these connections in greater detail. The suitability of each connection for a particular application involves determining the limiting conditions of the voltage and current applied to each phase unit of the relay for all fault conditions and taking into account the possible range of source and line impedances. The most versatile connection is the 90° connection the others are more application specific [12, 13, 14, 15].

Table 2.1: The directional-sensing connections for phase fault monitoring.

Connection	Phase A Unit		Phase B Unit		Phase C Unit	
	I	V_{pol}	I	V_{pol}	I	V_{pol}
90°	I_a	V_{bc}	I_b	V_{ca}	I_c	V_{ab}
30°	I_a	V_{ac}	I_b	V_{ba}	I_c	V_{cb}
60° Delta/#1	I_{ab}	V_{ac}	I_{bc}	V_{ba}	I_{ca}	V_{cb}
60° Wye/#2	I_a	$-V_{cn}$	I_b	$-V_{an}$	I_c	$-V_{bn}$

The 90 Degree Connection

Because most faults involve currents that lag their unity power factor positions by large angles it is desirable that the directional relay develop maximum torque under such

conditions. One of the most commonly used connections to accomplish this is the 90° connection with a maximum torque angle of 30° or 45°. The 90° connection applies a system voltage that lags the system unity power factor (UPF) current by 90°. Generally, the fault currents lag their unity power factor position by approximately 60°; therefore a maximum torque angle of 30° should produce maximum torque.

Figure 2.3 shows a typical three-line connection diagram for phase fault directional sensing with the directional units using a connection of 90°. From Table 2.1 the inputs to the unit monitoring phase *A*, with a MTA of 30°, are I_a and V_{bc}, with V_{bc} as the polarizing quantity. Substituting these inputs into Equation 2.1 the torque produced by the unit is:

$$T = K_1|V_{bc}||I_a|\cos(\theta_a - 30°) - K_2, \tag{2.4}$$

where:

θ_a is the phase angle between the voltage and current inputs for the directional unit monitoring phase *A* and

K_2 is the torque offset for the phase A unit.

Figure 2.4 shows the operating characteristic of the directional unit and from this figure it is evident that whenever the input current lags its unity power factor position by 60° the unit will generate the maximum amount of torque possible. If this torque is greater than K_2 the power flow is to the line side of the relay. For a large fault current with a relatively small torque offset the range of possible operation is from almost 30° leading to 150° lagging the unity power factor position. The two remaining directional units for phases *B* and *C* would have similar operating characteristics. If a MTA of 45° is used the units would have an operating range of approximately 45° leading to 135° lagging the UPF.

A polyphase configured directional relay operates on the net torque of all three phase units. With a connection of 90° and a MTA of 30° the torque would be determined as follows:

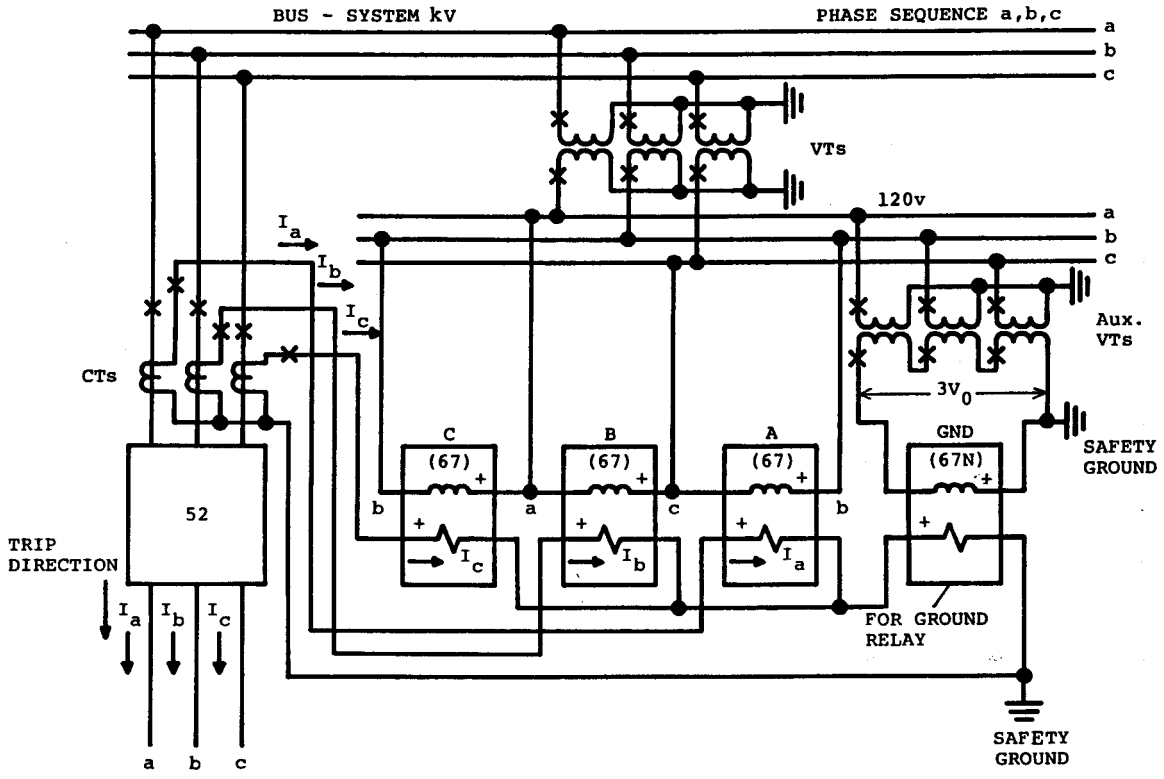

Figure 2.3: Typical three line connection for phase fault directional sensing [3].

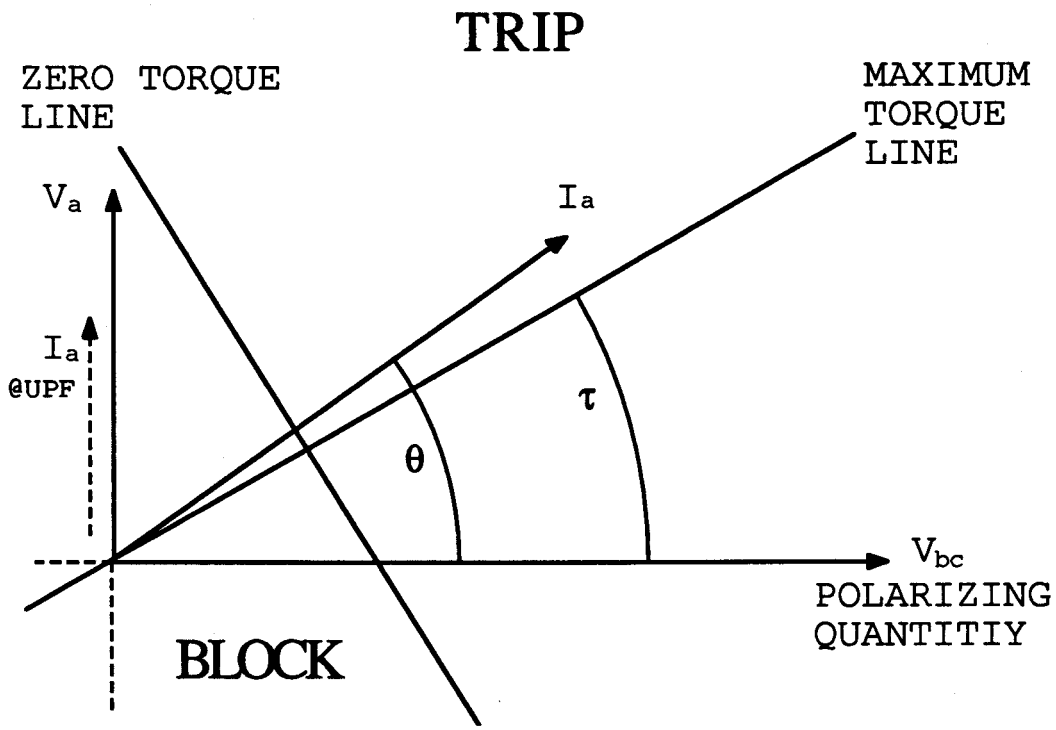

Figure 2.4: The operating characteristic of a directional unit for a three phase system using the 90° connection and a MTA of 30°.

$$T = T_a + T_b + T_c - K_2, \tag{2.5}$$

$$T_a = K_1 |V_{bc}||I_a| \cos(\theta_a - \tau), \tag{2.6}$$

$$T_b = K_1 |V_{ca}||I_b| \cos(\theta_b - \tau) \text{ and} \tag{2.7}$$

$$T_c = K_1 |V_{ab}||I_c| \cos(\theta_c - \tau), \tag{2.8}$$

where:

K_2 is the torque offset for all three phase units.

If the summation of the torques generated by the phase units minus the torque offset is positive, $\Sigma T_{a,b,c} > K_2$, the power flow is to the line side or in the tripping direction of the relay.

The 30 Degree Connection

The phase *A* unit is supplied with the current I_a and the system voltage V_{ac}. The most suitable MTA for this connection is 0°. Therefore maximum torque will occur when the current lags the unity power factor position by 30°. This results in a zone of operation for currents from 60° leading to 120° lagging the UPF.

The 60 Degree Delta/No. 1 Connection

The phase *A* unit is supplied with the current I_{ab} and the system voltage V_{ac}. The most suitable MTA for this connection is 0°. Therefore maximum torque will occur when the current lags the unity power factor position by 60°. This results in a zone of operation for currents from 30° leading to 150° lagging the UPF.

The 60 Degree Wye/No. 2 Connection

The phase *A* unit is supplied with the current I_a and the system voltage $-V_c$. The most suitable MTA for this connection is 0°. Therefore maximum torque will occur when the current lags the unity power factor position by 60°. This results in a zone of operation for currents from 30° leading to 150° lagging the UPF.

2.1.3. Directional Sensing for Ground Faults

A single-phase-to-ground fault on any phase will produce the same magnitude of zero sequence current and voltage, I_0 and V_0, and in the same phase relation. Therefore, only one single phase directional relay is required, and it is energized from the residual circuit, $I_{res}=3I_0$ and $V_{res}=3V_0$, with the negative of the residual voltage, $-3V_0$, used as the polarizing quantity. Using symmetrical components the relay inputs can be expanded into:

$$3I_0 = I_a+I_b+I_c, \tag{2.9}$$

$$-3V_0 = -(V_a+V_b+V_c). \tag{2.10}$$

To illustrate how a directional ground relay operates, consider a phase-*A*-to-ground fault in the tripping direction for the simple system shown in Figure 2.5(a). For this type of fault the following assumptions can be made, referring to Figure 2.5(b):

1. V_{ag} collapses and I_a proceeds to a lagging position.
2. $I_b=I_c=0$ and therefore $I_a=3I_0$.
3. V_b and V_c remain uncollapsed.

To ensure proper operation of the relay it becomes necessary to use $-3V_0$ as the polarizing voltage instead of $3V_0$ because the sum of the phase voltages results in $3V_0$ at –90°, as shown in Figure 2.5(c). It is more desirable to have the reference voltage at +90° due to the position of the fault current, as shown in Figure 2.5(d). If a MTA of –60° is used the relay will then operate for currents from nearly 30° leading to 150° lagging the polarizing voltage.

Figure 2.3 also shows the three-line connection diagram of a directional ground unit. The polarizing voltage is acquired from a broken delta transformer connection and a MTA of -60° is used to produce maximum torque. If the generated ground torque is greater than its torque offset, the power flow is assumed to be in the tripping direction of the relay.

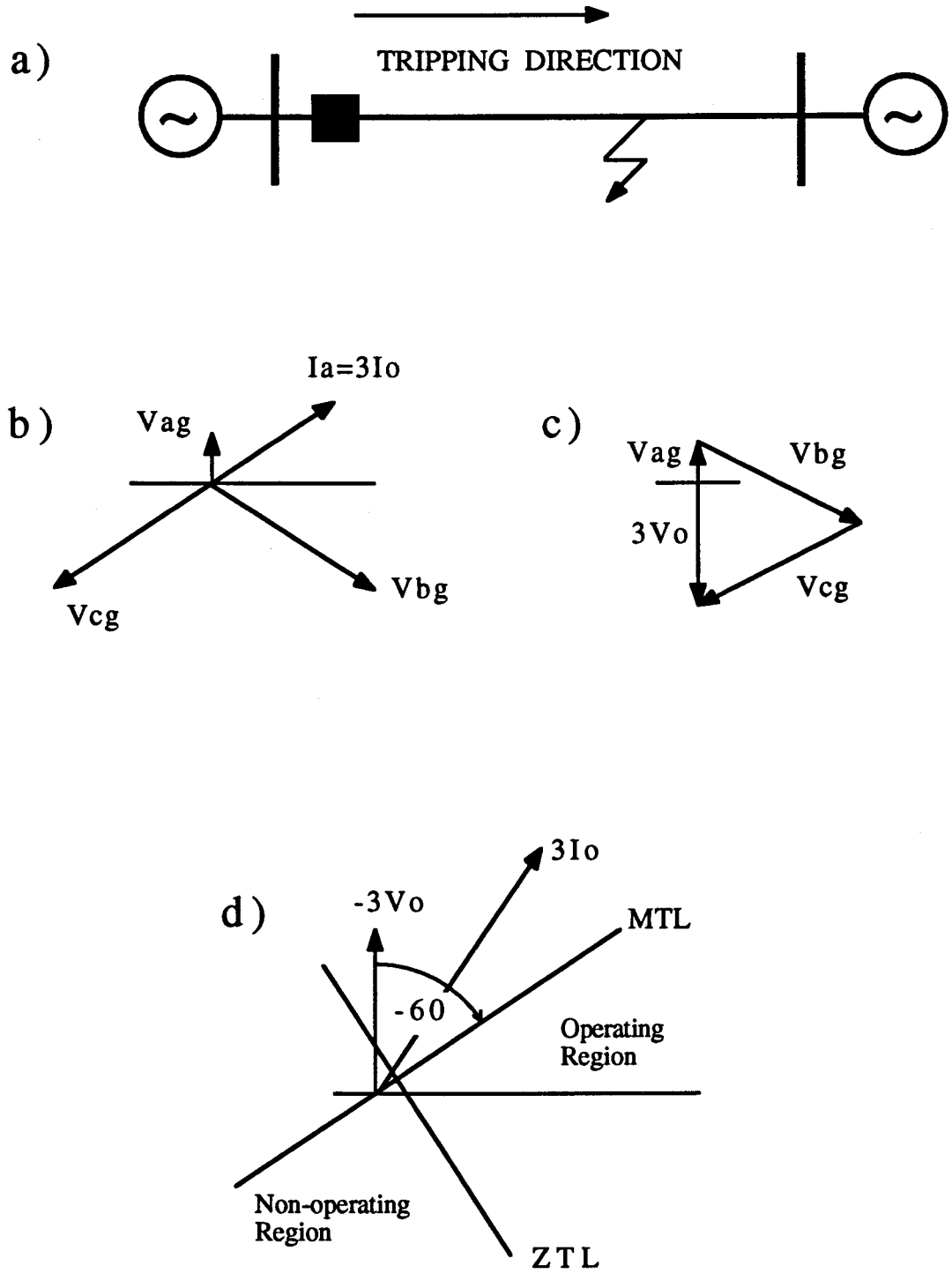

Figure 2.5: Diagrams illustrating ground fault directional sensing [3].

2.1.3.1. Current Polarization

If the residual voltage in the system is insufficient for polarization, current polarization of the relay can be used for ground fault detection. The current that flows in the grounded neutral of a wye-delta power or distribution transformer bank can be used to provide an effective reference for a directional ground relay. Figure 2.6 shows the three-line connection diagram of a current polarized ground unit. As long as the power system is balanced no current can flow to the ground relay either from the fault or the transformer bank neutral. For a fault in the tripping direction the current flowing into the fault will essentially be in phase with the current flowing up the transformer bank neutral; a MTA of 0° will produce maximum torque for this situation. The relay currents will be approximately 180° out of phase for a fault in the non-tripping direction and as a result produce negative torque.

2.1.4. Directional Power and Var Relays

Other directional-sensing connections can also be derived for directional relays to measure the different power factor areas. Directional power relays are used to protect prime movers on induction and synchronous generators from being motored by the generator due to a loss of mechanical power. Power relay connections and MTA's are designed to produce maximum torque when unity power factor load is carried by the protected circuit. For example, the following wye/delta currents and corresponding polarizing voltages I_a and V_{an} or I_{ab} and V_{ab} could be used for watt measurement with a MTA of 0°. The 30° connection can also be used with a MTA of 30° to perform this function. Both arrangements align the maximum torque line with the input current's unity power factor position.

Directional var relays are used to to protect synchronous motors and generators from receiving vars from the external power system due to loss of field excitation. Using I_a and V_{bc} as the polarizing voltage, with a MTA of 0°, the relay would produce maximum torque when I_a lags by 90° and zero torque when I_a is at UPF and flowing in either direction. Another alternative is to use I_a and V_{bn} with a MTA of 30° to generate maximum torque when I_a lags its unity power factor position by 90°.

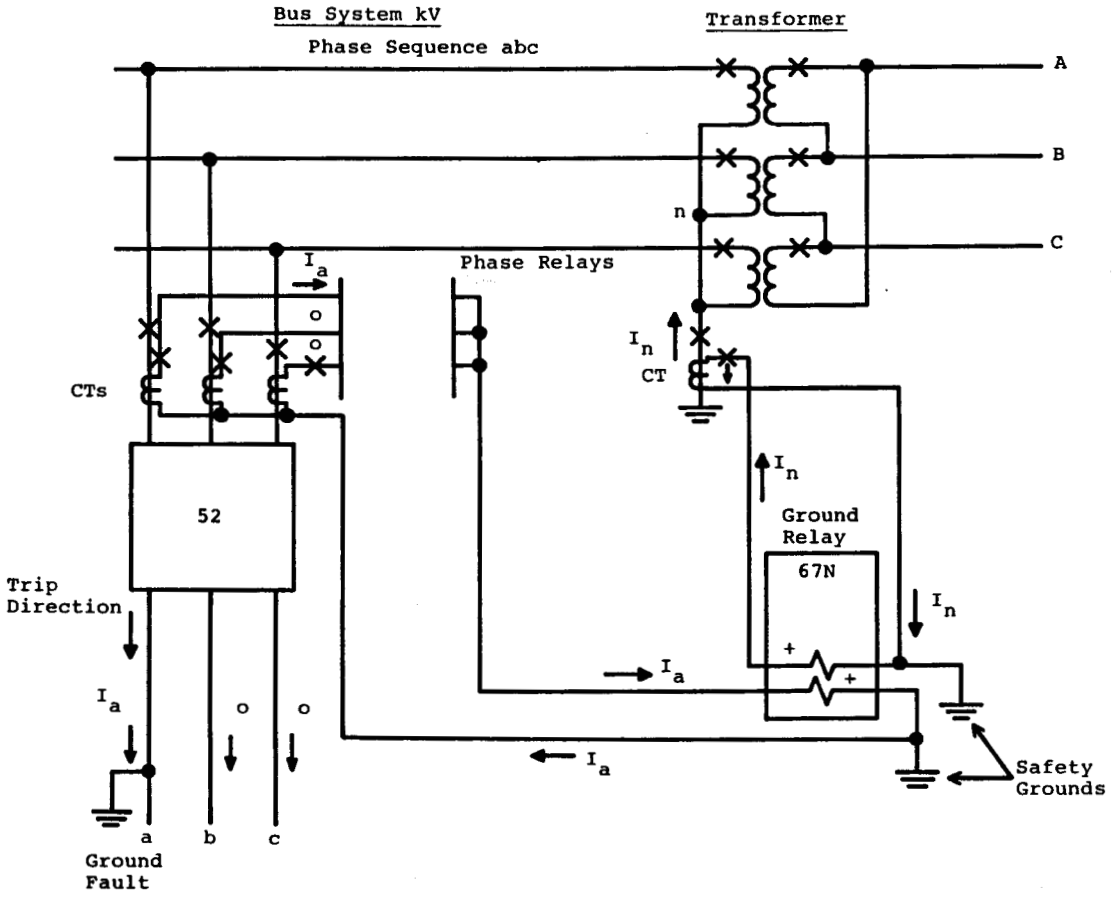

Figure 2.6: Three-line connection diagram for ground-fault directional sensing with current polarization [3].

2.2. Line Protection Using Directional Overcurrent Relays

Electrical power lines form the links that interconnect the various parts of a power system. Power generated at low voltage is stepped up and transmitted to distribution points for consumers to use. These interconnections often form loops, rings or grids which can create difficult protection problems. In these situations protective relays must be directional to provide adequate and effective protection to the system. A common practice is to use the output of directional relays to control the operation of overcurrent relays, which are often instantaneous or inverse-time units.

Overcurrent relays on single radial lines do not have to be directional because the direction of the fault current is obvious. But, with parallel lines or lines that form loops the magnitude of the fault currents may be the same in two lines except for their relative direction and that may change with the location of the fault. Figure 2.7 illustrates this point with a simple loop network.

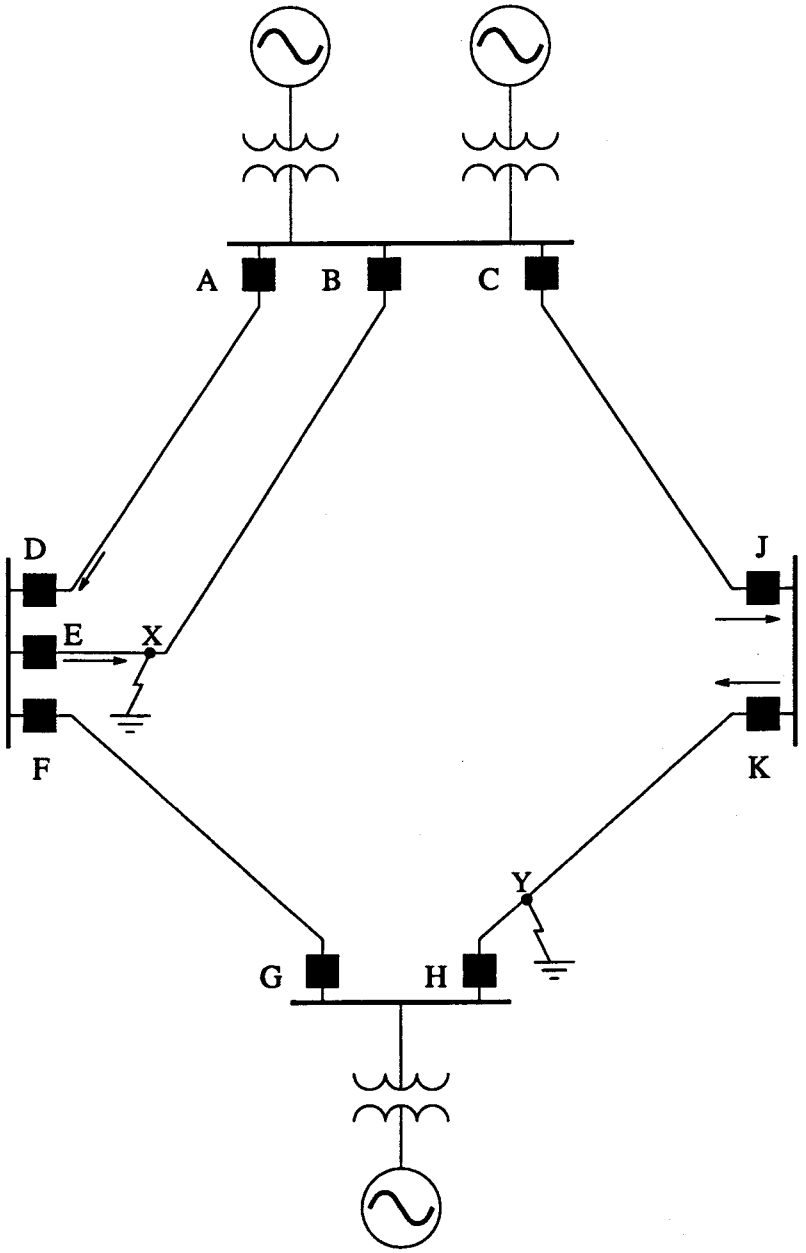

Figure 2.7: A simple loop network [2].

Consider a fault at point X which produces comparable levels of fault current in overcurrent relays D and E except that their directions are different, one is towards the bus and the other is away from the bus. If relays D and E are not directional D would remove its unfaulted line from service when this is neither necessary or desirable. Similarly, a fault at point Y could produce the same situation for relays G and H. Directional control of these relays prevent D and G from disconnecting their sound lines from the power system.

A schematic diagram of a directional overcurrent relay is shown Figure 2.8. It is composed of two main elements an overcurrent element/relay and a directional element/relay. The only operating criterion for the directional unit is the direction of the

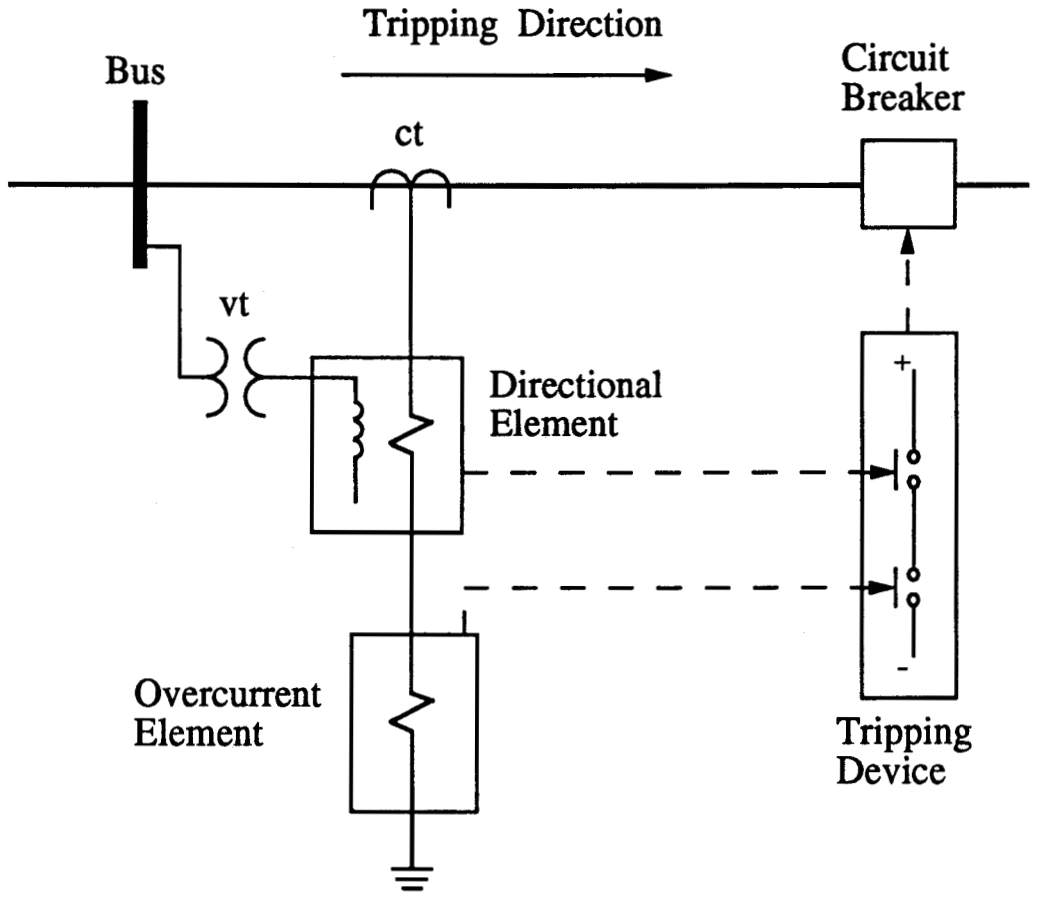

Figure 2.8: A schematic diagram of a directional overcurrent relay.

fault current. Both current and voltage signals are required to determine the direction of power flow because it is a function of the phase angle between the two input signals. The overcurrent element is sensitive only to current and usually operates as an inverse time unit. If a fault occurs in the protected zone the directional element closes its contacts and allows the overcurrent element to trip the circuit breakers if the current is above the pickup setting.

2.2.1. Current-Time Characteristics

The current-time characteristics of inverse-time overcurrent relays are represented by families of curves relating the contact closing time of the relay to the observed current. Figure 2.9 shows a typical current-time characteristic for an electro-mechanical overcurrent relay [16]. The characteristics are plotted on a linear versus log scale with the relay current in multiples of pickup or tap current as the abscissa and the ordinate is the contact closing time in seconds. From this figure it is evident that as the multiples of pickup current increase the relay operating time decreases. The operating times for current multiples of less than 1.5 are not shown as relay operation is inconsistent in this region. To achieve a desired contact closing time for a specified current the time dial (TDS) or time multiplier (TMS) setting is changed. The TDS/TMS is continuous which results in an infinite number of operating curves, usually only 10 to 12 curves are published.

2.2.2. Instantaneous Overcurrent Relays

Where a reasonable difference in fault current exists between close-in and far-bus faults, instantaneous units can be utilized to provide fast protection for faults out on the line. The greater the difference between the two fault currents the more of the line that is protected. At minimum they provide fast operation for close-in faults that generate large currents; but care must be taken so that they do not overreach any other protective device. Instantaneous overcurrent units operate with no intentional time delay and usually the operating time is approximately 0.015 to 0.05 s. The guidelines for setting instantaneous units and whether they need to be directional are:

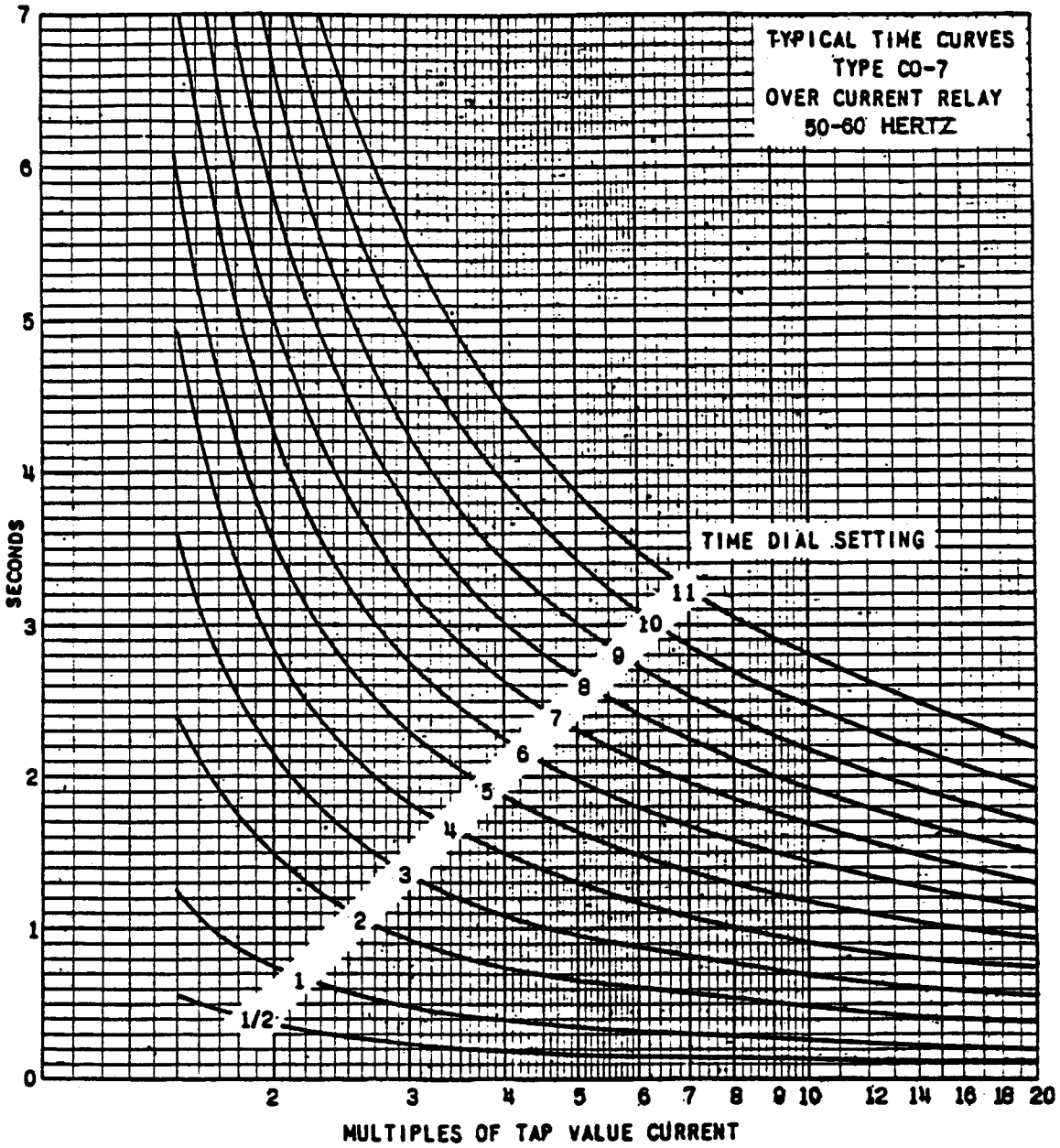

Figure 2.9: Typical current-time characteristics of an overcurrent relay [16].

1. The pickup is set at $kI_{Far\ Bus\ Max}$, k is typically 1.1 to 1.33 depending on the response of the unit to a fully offset current and the conservatism of the protection engineer. k is a constant representing a combined asymmetry factor and safety margin.
2. If this setting is greater than the maximum near-bus fault current a nondirectional instantaneous unit may be used.
3. If this is not the case a directional instantaneous unit must be used.

The reach of an instantaneous unit on a radial line can be determined from Equation 2.11 [3]. The percent coverage on a loop system is not linear as on a radial system and is therefore less than what would be calculated using Equation 2.11.

$$\%\,Instantaneous\ \ Coverage\ =\ 100\,\frac{I_{CI}-I_{IT}}{I_{CI}-I_{FB}}, \tag{2.11}$$

where:

I_{CI} is the close-in fault current,
I_{FB} is the far-bus fault current and
I_{IT} is the instantaneous unit current setting.

2.2.3. Polyphase Versus Single Phase Directional Monitoring of Overcurrent Relays

There are advantages and disadvantages to both polyphase and single phase directional monitoring of overcurrent relays [1]. Using single phase directional units not only provides protection against interphase faults but phase-to-ground faults as well; with polyphase relays this is not possible unless the minimum ground fault current is greater than three times the maximum load current. The main advantage of polyphase relays is that they are less likely to misoperate than their single phase counterparts. Under certain conditions a single phase configuration can cause unwanted tripping for ground faults in the non-tripping direction. One of the single phase relays may develop enough torque to turn on its overcurrent unit, and if the current is large enough issue a trip signal when this is undesirable. Since a polyphase directional relay operates on the sum of the torques from its directional units the other two will counteract this tendency and produce a proper indication of power flow.

2.2.4. Directional Sensing for Ground Overcurrent Relaying

Since most line faults (approximately 80 - 90%) involve ground, directional overcurrent relays can provide effective protection in most cases. For multigrounded loop systems overcurrent units need to be directional. Instantaneous units may or may not need to be directional depending on the relative magnitude of the maximum near-bus and maximum far-bus fault currents. Pickup settings for overcurrent ground units can be set at a more sensitive level than phase relays because the residual components are normally zero except for situations involving unbalanced phases.

2.2.4.1. Ground Directional Sensing With Negative Sequence Quantities

Directional ground relays commonly use zero sequence quantities for directional discrimination. A useful alternative is the use of negative sequence voltage and current, V_2 and I_2, with a MTA of approximately 100° to operate the directional unit [17]. Residual current, $3I_0$, is still used for the fault-detecting overcurrent element. The use of negative sequence quantities can alleviate some of the application problems associated with autotransformer stations, mutual induction on parallel lines and with some of the limitations of zero sequence voltage polarization. Negative sequence components for ground faults are generally smaller than their zero sequence counterparts but usually have sufficient magnitude to function as the voltage-current pair of a directional unit. Figure 2.10 shows a typical voltage profile of V_2 and $3V_0$ for a ground fault.

At stations with large, solidly grounded transformer banks, the residual voltage levels, $3V_0$, should be checked to ensure sufficient amounts are generated by remote ground faults. While the residual voltage is maximum at the fault location the value at the grounding bank may be quite small, this is shown in Figure 2.10. In the diagram the impedance of the transformer is small because of the large bank and the zero sequence impedance of the lines is large because of the distance and the $3Z_1$ factor.

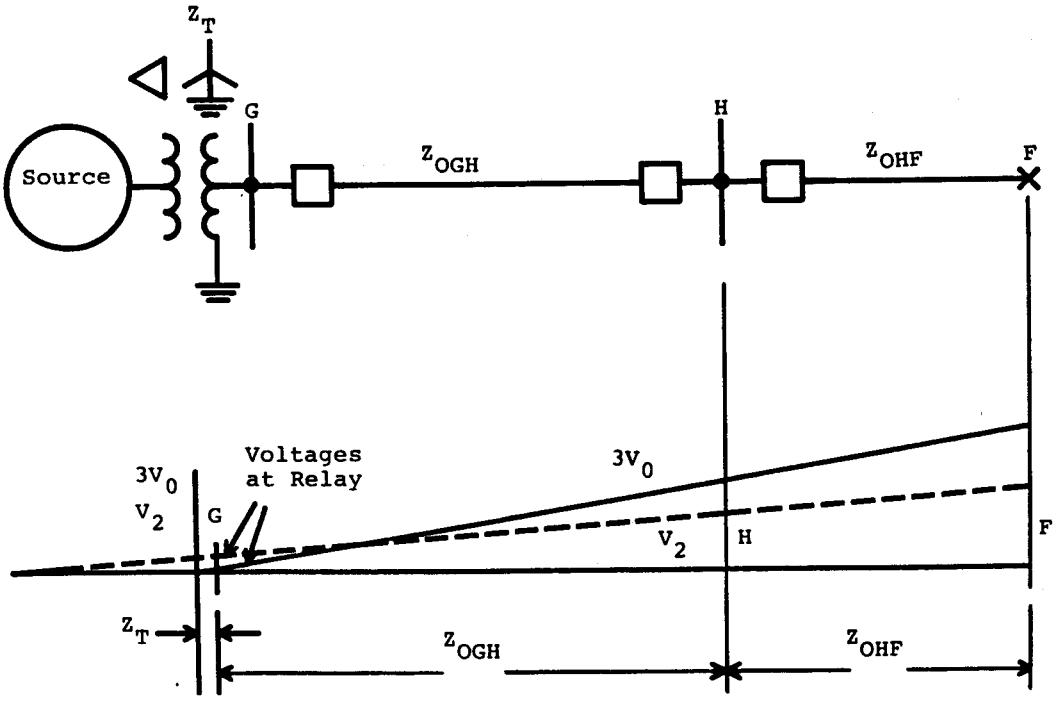

Figure 2.10: Typical voltage profiles of V_2 and $3V_0$ for ground faults [3].

2.2.4.2. Mutual Coupling and Directional Ground Relaying

Employing negative sequence quantities for directional ground relaying can also provide effective directional discrimination where mutual induction is involved between parallel transmission lines. Zero sequence coupling between lines that are parallel for part or all of their length can induce false information in the unfaulted circuit and cause protection problems in both when standard residual voltage and current polarization schemes are used. When a ground fault occurs on one of the parallel lines a zero sequence current is induced in the other as a result of mutual electromagnetic coupling by the zero sequence networks. This induced current can cause directional overcurrent relays, using residual quantities for polarization, on the unfaulted line to pickup and possibly operate as the polarization becomes ineffective. Mutual coupling can also cause

current reversals on the unfaulted line due to switching on the faulted line to clear a ground fault. The zero sequence mutual impedance can be as high as 50 to 70% of the self-impedance, while the positive and negative sequence mutual impedance of untransposed lines is less than 10%, usually less than 5 to 7%, of self-impedance. With transposition the values of the positive and negative sequence mutual impedance can be reduced by 50% or more. As a result, negative sequence induction is effectively negligible from a relaying standpoint. In many cases involving mutual coupling negative sequence directional sensing can provide correct indications of the direction of power flow, but it does not function accurately for all possible situations.

2.2.5. Pilot Protection With Directional Comparison Systems

Pilot protection is a type of differential protection where the relaying quantities at the protected line terminals are compared through a communication channel rather than a direct wire link. Directional comparison schemes compare the direction of the power flow at the different terminals and then decide if a fault condition exists. For internal faults the power flows into the line at the protected terminals, allowing simultaneous high-speed tripping. For external faults the information that current flows out at one end of the protected line is used to block the tripping of all other terminals. There are several schemes available for transmitting and decoding this information [3, 12].

2.3. Generator Protection

Generators are subject to a number of possible hazards for which protection is required. These hazards fall into two broad categories: internal faults within the zone of protection and abnormal operating/system conditions. Two situations where directional power or overcurrent relays can be applied are generator motoring and connecting generators out of synchronism. These cases are abnormal operating/system conditions.

2.3.1. Generator Motoring

The power system will drive a generator as a motor if the prime mover supply is removed and the unit is still connected to the system with the field excited. Serious damage can occur to the prime mover from its generator being driven as a motor, this is particularly critical for steam and hydro units. Motoring causes overheating in steam turbines possibly damaging the turbine and the turbine blades. Low water flow can cause cavitation of the turbine blades in hydro units. This can also happen when the steam or water flow valves are closed too rapidly during a load reduction phase or by tripping the turbine while not tripping the generator breaker. A reverse power relay is usually recommended for protection, this is a directional power relay connected to operate when power flows into the generator from the system.

2.3.2. Connecting Generators Out of Synchronism

Generators can experience severe damage if improperly connected to the power system. This can occur by incorrect closing of the circuit breaker while the unit is on turning gear, coasting to a stop, at standstill or by improper synchronization. In most cases the primary protection will function adequately but not necessarily for all situations. Additional protection is provided by three directional inverse-time overcurrent units, one in each phase, connected to operate for reverse power into the generator. The relay characteristics and connections should provide an operating zone from about 30° to 60° leading through 180° (reverse power into the generator) to 210° to 240° leading the UPF based on current normally flowing out of the generator into the power system. This replaces motoring protection and is more responsive to the conditions previously stated.

2.4. Transformer Protection

Power transformers experience a wide variety of faults and abnormal operating conditions, some of which directional overcurrent relays can provide effective protection against. Faults affecting transformers can be divided into two categories: through faults and internal faults [2]. Faults outside the protected zone of a transformer are designated as external faults, and faults inside the protected zone are designated as internal faults.

2.4.1. Parallel Transformer Units

Figure 2.11 shows parallel transformer units where the secondaries are connected together by a normally closed (NC) bus tie breaker. This arrangement is typical for large

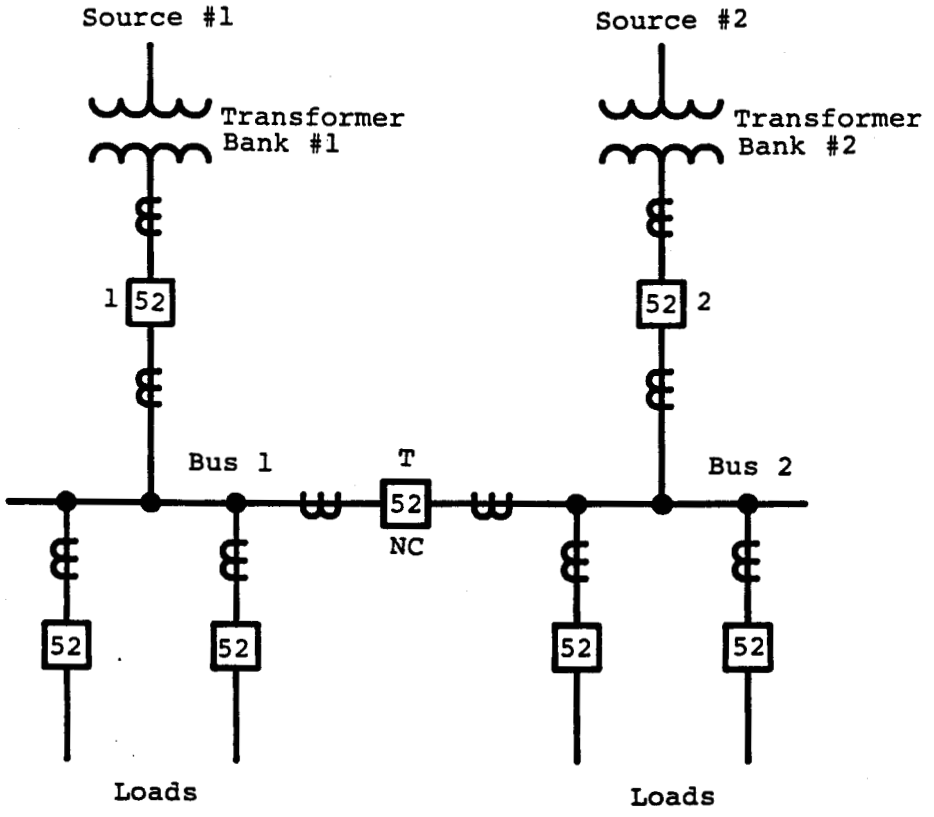

Figure 2.11: Parallel transformer units operating with a normally closed bus tie breaker [3].

or critical load substations. With the bus tie breaker operated as normally closed, there is the possibility for the interchange of power between the two sources; current would flow from one source through its transformer, the secondary buses and back through the other transformer to the second source. This is not a desirable or permissible state of operation and to prevent this directional overcurrent relays are applied to each transformer. They will operate only for fault current that flows into the transformer and then trip the secondary breaker, 52-1 or 52-2. Load current will flow through the relay but not in the

operating direction. Figure 2.12 shows the three-line connections for reverse phase protection of the parallel transformer units. The connections for partial differential protection of the bus are also shown in the figure.

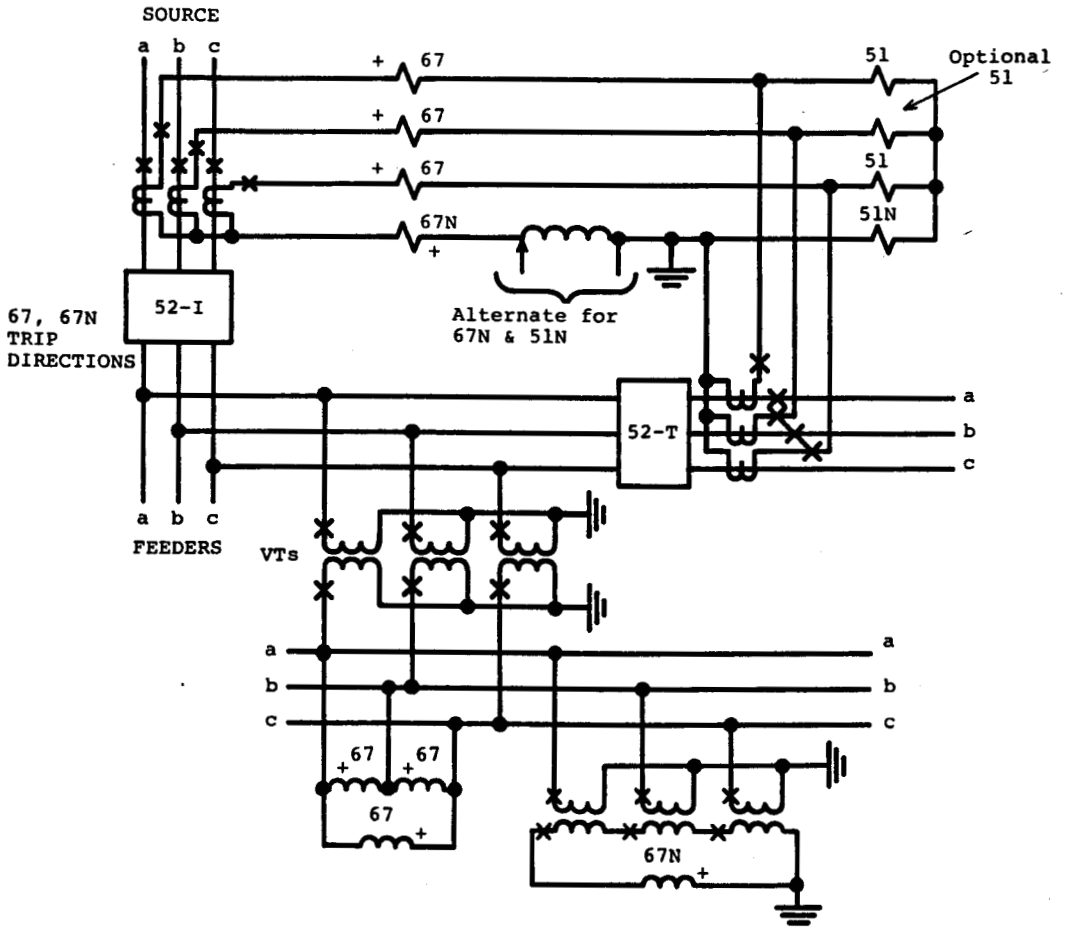

Figure 2.12: Three-line connections for reverse phase protection [3].

2.4.2. Ground Differential Protection With Directional Relays

The most common form of protection for transformers is differential. If the ct ratios and/or characteristics are not suitable for the application of conventional differential relays, a directional overcurrent relay can be used. The overcurrent unit is connected differentially and is torque controlled by the directional unit. The directional unit is connected in the same fashion as shown in Figure 2.6 where the relay is current polarized, one current coil is connected across the three line ct's and the other is across the neutral ct. This is particularly applicable when the ground-fault current is limited by a neutral impedance or where a low neutral ct is used for higher sensitivity for remote faults on distribution feeders. Relay torque is proportional to the product of the currents in the two coils multiplied by the cosine of the angle between them. The phase displacement between the two currents is set for 0° for an internal fault and 180° for an external fault; thus the relay will develop contact closing torque only for internal faults.

2.5. Summary

In summary, to determine the direction of power flow for phase faults either a single phase or polyphase configuration with one of the four commonly used directional sensing connections can be employed. Effective directional discrimination for ground faults can be provided by a single phase relay energized from residual voltages and currents or negative sequence quantities. The applications of directional and directional overcurrent relays to line, generator and transformer protection have also been reviewed.

3. DIGITAL RELAYING ALGORITHMS

In chapter two the basic theory and applications of directional relaying for phase and ground fault protection were presented. This chapter describes digital relaying algorithms used to estimate parameters of interest from instantaneous samples of system voltages and currents. Parameters of interest are quantities that a microprocessor-based relay evaluates in order to determine if a fault condition exists, for example peak values of current and voltage waveforms, the fundamental frequency of a periodic signal, or magnitudes of power system harmonics. Digital relaying algorithms are a set of mathematical equations describing either power system voltage and current waveforms or a model of the system itself. The solution of these equations yields numerical estimates of the parameters of interest. In order to obtain accurate estimates from these algorithms, the set of mathematical equations developed must adequately represent the power system waveforms or the system.

Digital relaying algorithms can be roughly divided into two classes, those using nonrecursive or recursive filters. Nonrecursive filters use a finite number of data samples to obtain estimates. The time period that contains these samples is called a data window. The output of these filters depends solely on the values of the samples in their data window. Recursive filters use feedback paths to introduce factors of the output into the input signal; thus the output of recursive filters are functions of present as well as all previous inputs.

3.1. Sampling and Data Windows

Sampling is the process by which instantaneous values of voltage and current are acquired for processing, there are several forms of sampling normally used. One of the most common methods is performed by taking a sample at every ΔT seconds and the required computations are then completed before the next sample becomes available. Another form of sampling consists of acquiring data samples at a relatively high rate for part of a signal's cycle, stopping and processing the acquired data, and then resume sampling. A further alternative is to sample the signals at a comparatively low rate during normal conditions until an abnormal state occurs and then switch to a faster sampling rate.

Data samples can be collected into a data window designating the time period of the data. Figure 3.1 shows a data window and its progression through time. Assume an

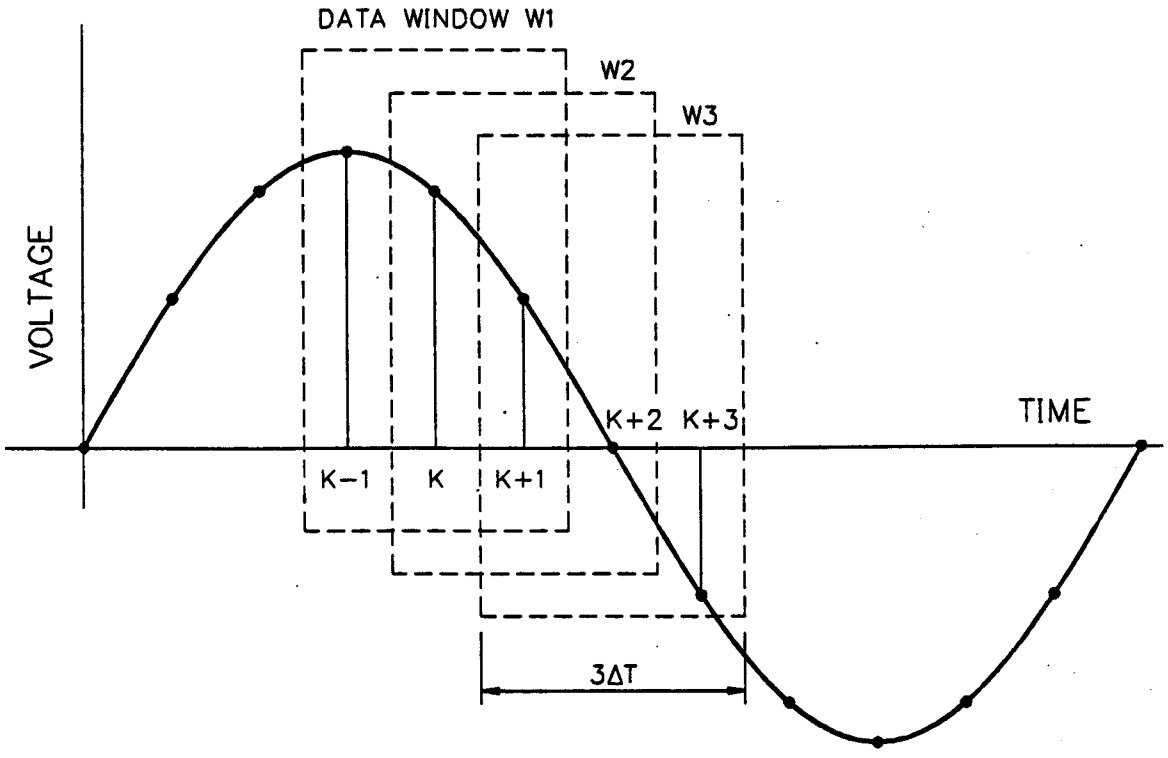

Figure 3.1: A data window and its progression through time.

algorithm uses three consecutive data points to estimate a parameter of interest, the

$(k-1)^{th}$, k^{th} and the $(k+1)^{th}$ samples. The data window is $3\Delta T$ seconds long and is represented by W_1. One sampling interval later a new sample is available and W_1 becomes W_2; the $(k-1)^{th}$ sample is discarded and the $(k+2)^{th}$ sample is added to the data window. This is the process of updating a data window.

3.2. Nonrecursive Algorithms for Estimating Phasors

Nonrecursive relaying algorithms can be grouped into two further categories based on their window size; short window algorithms and long window algorithms. Short window algorithms use fewer samples, typically in the range of two to six. The computation time of short window algorithms is shorter than that of long window algorithms but results are less accurate because of it. Long window algorithms use a larger number of samples, usually spanning one cycle or more; since more samples are used results are more accurate but the computation time is longer.

3.2.1. Trigonometric Algorithms

Trigonometric algorithms assume that input voltages and currents are sinusoids of a single frequency only and that the power system continues to operate at its nominal frequency. However, harmonics and noise are present in these signals when faults and other transient conditions occur; front end analog devices are then required to suppress noise and non-fundamental frequency components. With the previous assumptions, the instantaneous voltage of a sinusoid at the fundamental frequency can be expressed as:

$$v = V_p \sin(\omega_0 t + \theta_v), \tag{3.1}$$

where:

v	is the instantaneous value,
V_p	is the peak value,
θ_v	is the phase angle,
ω_0	is the nominal frequency and
t	is the time.

The peak value of the voltage phasor and its phase angle can be determined from the following equations.

$$V_p^2 = (V_p \cos(\omega_0 t + \theta_v))^2 + (V_p \sin(\omega_0 t + \theta_v))^2. \tag{3.2}$$

$$\omega_0 t + \theta_v = \text{arctg} \frac{V_p \sin(\omega_0 t + \theta_v)}{V_p \cos(\omega_0 t + \theta_v)}. \tag{3.3}$$

Equations 3.1, 3.2 and 3.3, form the basis for trigonometric algorithms. Taking the first derivative of the instantaneous voltage, Equation 3.1, with respect to time results in the following equation.

$$v' = \omega_0 V_p \cos(\omega_0 t + \theta_v). \tag{3.4}$$

Dividing both sides of the preceding equation with ω_0 results in:

$$\frac{v'}{\omega_0} = V_p \cos(\omega_0 t + \theta_v). \tag{3.5}$$

The peak value and phase angle of the voltage signal can be obtained from Equations 3.1, 3.2, 3.3 and 3.5.

$$V_p^2 = v^2 + \left(\frac{v'}{\omega_0}\right)^2. \tag{3.6}$$

$$\omega_0 t + \theta_v = \text{arctg}\left(\omega_0 \frac{v}{v'}\right). \tag{3.7}$$

Mann and Morrison [18] estimated the first derivative v' from three consecutive samples. The sampling of the waveforms is done after every sampling interval of ΔT seconds. If the actual sampling times are $(k-1)\Delta T$, $k\Delta T$ and $(k+1)\Delta T$ seconds then the estimate of the first derivative at time $k\Delta T$ using Newton's central formula is mathematically expressed as:

$$v_k' = \frac{v_{k+1} - v_{k-1}}{2\Delta T}. \tag{3.8}$$

Gilcrest, Rockefeller and Udren [5] used the first and second derivatives of the

voltage equation to estimate its peak value and phase angle. The second derivative of the voltage equation is:

$$v'' = -\omega_0^2 V_p \sin(\omega_0 t + \theta_v). \tag{3.9}$$

Rearranging Equation 3.9 to isolate $V_p \sin(\omega_0 t + \theta_v)$ and substituting the result into Equation 3.2 along with Equation 3.5 produces an equation to estimate the peak value. References [5] and [19] use the following equations to estimate the peak values and phase angles.

$$V_p^2 = \left(\frac{v'}{\omega_0}\right)^2 + \left(\frac{v''}{-\omega_0^2}\right)^2. \tag{3.10}$$

$$\omega_0 t + \theta_v = \operatorname{arctg}\frac{-v''}{\omega_0 v'}. \tag{3.11}$$

Using Newton's central difference approach, the second derivative of the voltage equation is given as:

$$v_k'' = \frac{v_{k+1} - 2v_k + v_{k-1}}{\Delta T^2}. \tag{3.12}$$

Makino and Miki [20] derived expressions from the voltage equation without the use of derivatives. Using only two samples, $(k-1)\Delta T$ and $k\Delta T$, and the following equations they determined the peak value and phase angle of a sinusoid.

$$V_p \cos\theta_v = \frac{v_k \cos\omega_0 \Delta T - v_{k-1}}{\sin\omega_0 \Delta T}. \tag{3.13}$$

$$V_p \sin\theta_v = v_k. \tag{3.14}$$

3.2.2. Correlation Algorithms

A signal can be correlated with itself, other signals or other functions. This can be used to extract the real and imaginary parts of the fundamental frequency component. Ramamoorty [21] suggested that the information concerning the fundamental frequency voltage and current phasors can be extracted from fault transients by correlating one cycle of data samples with samples of sine and cosine waves of that frequency. This is more commonly known as the Fourier technique and can be mathematically expressed as:

$$V_r(k) = \frac{2}{m}\sum_{n=0}^{m-1} v_{k+n-m+1} \sin\frac{2\pi n}{m}, \tag{3.15}$$

$$V_i(k) = \frac{2}{m}\sum_{n=0}^{m-1} v_{k+n-m+1} \cos\frac{2\pi n}{m}, \tag{3.16}$$

where:

m	is the number of samples per second,
V_r	is the real part of the fundamental frequency component of the signal and
V_i	is the imaginary part of the fundamental frequency component of the signal.

After evaluating Equations 3.15 and 3.16 the peak value and phase angle of the voltage signal can be determined from the following equations.

$$V_p = \sqrt{V_r^2 + V_i^2}. \tag{3.17}$$

$$\theta_v = \text{arctg}\,\frac{V_i}{V_r}. \tag{3.18}$$

Implementing the correlation approach, Phadke et al. [22] used a data window of half a cycle plus one sample.

Another group of functions that use correlation algorithms are even and odd rectangular waves [23], shown in Figure 3.2; mathematically they are expressed as:

$$W_r(t) = signum(\sin \omega_0 t), \tag{3.19}$$

$$W_i(t) = signum(\cos \omega_0 t), \tag{3.20}$$

where:

signum(x)	= -1 for $x < 0$,
	= 0 for $x = 0$,
	= 1 for $x > 0$,
$W_r(t)$	is the odd rectangular wave and
$W_i(t)$	is the even rectangular wave.

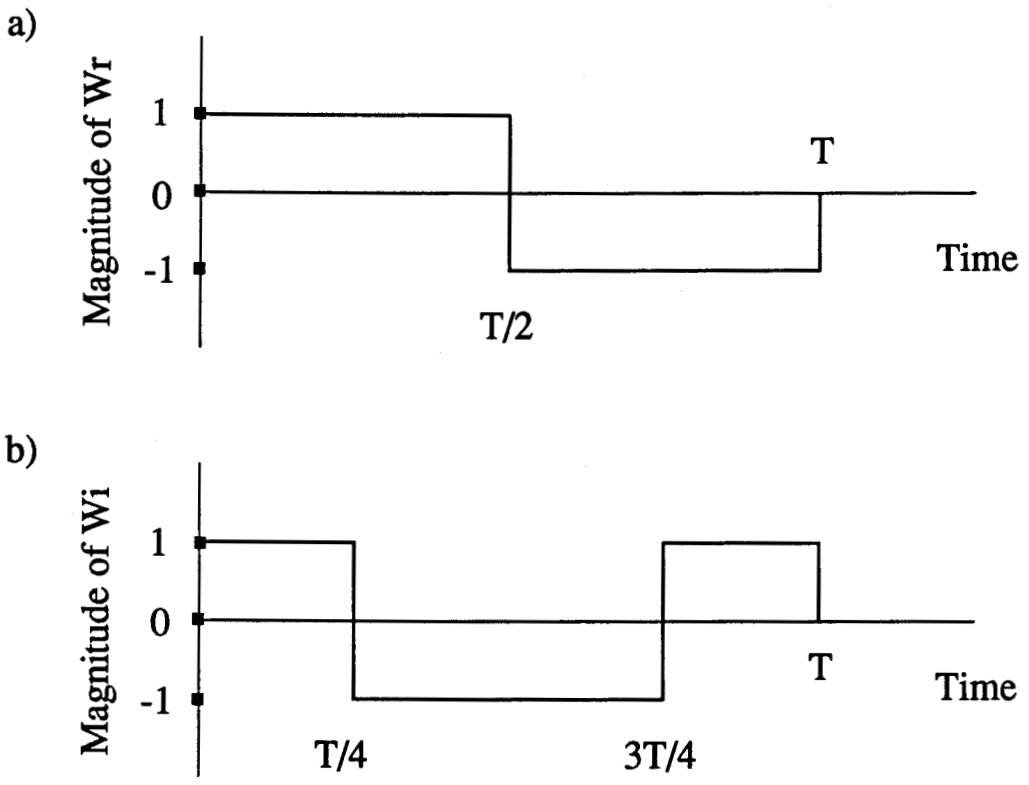

Figure 3.2: The a) odd and b) even rectangular signals of the fundamental frequency.

The real and imaginary components of the fundamental frequency voltage phasor can then be represented by the following equations.

$$V_r(k) = \frac{1}{A}\sum_{n=0}^{m-1} v_{k+n-m+1}\, signum(\sin\frac{2\pi n}{m}), \tag{3.21}$$

$$V_i(k) = \frac{1}{A}\sum_{n=0}^{m-1} v_{k+n-m+1}\, signum(\cos\frac{2\pi n}{m}), \tag{3.22}$$

where:

A is a scaling factor.

The computations involved in these equations are only additions and subtractions; therefore, it becomes advantageous to use this technique. Schweitzer et al. [24] used this approach to calculate the fundamental and harmonic frequency components of signals.

3.2.3. Least Error Squares Technique

Luckett et al. [25] proposed the use of least error squares (LES) curve fitting for estimating the peak value and phase angle of voltage and current phasors. Brooks [26] then used it in a distance relay scheme. Sachdev and Baribeau [27] further developed the LES technique to include the decay rate of the dc component. They also showed that the on-line computation time can be reduced by computing the filter coefficients off-line. This technique is briefly described below.

Fault voltages and currents contain not only fundamental frequency components but components of harmonic frequencies, non-harmonic high frequency components and decaying dc components as well. The non-harmonic high frequency components can be suppressed by using front end anti-aliasing/low-pass filters. Therefore, the assumption can be made that the power system voltages and currents to which the digital relay will be subjected are composed of decaying dc components, the fundamental frequency component and harmonic frequency components. The voltage signal from a coupling capacitance voltage transformer or voltage transformer can be mathematically modeled as:

$$v(t) = k_0 e^{-t/\tau} + \sum_{n=1}^{N} k_n \sin(n\omega_0 t + \theta_n), \tag{3.23}$$

where:

$v(t)$	is the instantaneous voltage at some measurement location,
τ	is the time constant of the decaying dc component,
N	is the order of the highest harmonic present,
ω_0	is the fundamental frequency of the system,
k_0	is the magnitude of the dc offset at $t=0$,
k_n	is the peak value of the n^{th} harmonic component and
θ_n	is the phase angle of the n^{th} harmonic.

Equation 3.23 can be expanded using the trigonometric identity $\sin(\alpha \pm \beta) = \sin\alpha\cos\beta \pm \cos\alpha\sin\beta$ and by approximating the decaying dc component by the first two terms of its Taylor's series expansion; this approximation is adequate as long as the data window is not too wide.

$$v(t) = k_0 - (k_0/\tau)t + \sum_{n=1}^{N} k_n(\sin(n\omega_0 t)\cos\theta_n + \cos(n\omega_0 t)\sin\theta_n). \tag{3.24}$$

With $t=t_1$ and assuming that harmonics greater than three are prefiltered out Equation 3.23 can be rearranged into the following format.

$$v(t) = k_0 - (k_0/\tau)t_1 + k_1\sin(\omega_0 t_1 + \theta_1) + k_2\sin(2\omega_0 t_1 + \theta_2) + k_3\sin(3\omega_0 t_1 + \theta_3). \tag{3.25}$$

$$\begin{aligned} v(t) = {} & k_0 - (k_0/\tau)t_1 + (k_1\cos\theta_1)\sin(\omega_0 t_1) + (k_1\sin\theta_1)\cos(\omega_0 t_1) \\ & + (k_2\cos\theta_2)\sin(2\omega_0 t_1) + (k_2\sin\theta_2)\cos(2\omega_0 t_1) \\ & + (k_3\cos\theta_3)\sin(3\omega_0 t_1) + (k_3\sin\theta_3)\cos(3\omega_0 t_1). \end{aligned} \tag{3.26}$$

$$v(t) = a_{11}x_1 + a_{12}x_2 + a_{13}x_3 + a_{14}x_4 + a_{15}x_5 + a_{16}x_6, \tag{3.27}$$

where:

$$x_1 = k_0 \qquad a_{11} = 1$$

$x_2 = -k_0/\tau$ $\quad a_{12} = t_1$

$x_3 = k_1\cos\theta_1$ $\quad a_{13} = \sin(\omega_0 t_1)$

$x_4 = k_1\sin\theta_1$ $\quad a_{14} = \cos(\omega_0 t_1)$

$x_5 = k_2\cos\theta_2$ $\quad a_{15} = \sin(2\omega_0 t_1)$

$x_6 = k_2\sin\theta_2$ $\quad a_{16} = \cos(2\omega_0 t_1)$

$x_7 = k_3\cos\theta_3$ $\quad a_{17} = \sin(3\omega_0 t_1)$

$x_8 = k_3\sin\theta_3$ $\quad a_{18} = \cos(3\omega_0 t_1)$

Since the voltage is being sampled at intervals of ΔT seconds, t_1 in the a coefficients can be replaced by $m\Delta T$; therefore:

$a_{11} = 1$ $\quad a_{15} = \sin(2\omega_0 m\Delta T)$

$a_{12} = m\Delta T$ $\quad a_{16} = \cos(2\omega_0 m\Delta T)$

$a_{13} = \sin(\omega_0 m\Delta T)$ $\quad a_{17} = \sin(3\omega_0 m\Delta T)$

$a_{14} = \cos(\omega_0 m\Delta T)$ $\quad a_{18} = \cos(3\omega_0 m\Delta T)$

The following equation can now be obtained.

$$v(m\Delta T) = a_{m1}x_1 + a_{m2}x_2 + a_{m3}x_3 + a_{m4}x_4 + a_{m5}x_5 + a_{m6}x_6 + a_{m7}x_7 + a_{m8}x_8, \qquad (3.28)$$

where:

m represents the voltage sample referenced from the center of the window.

Assuming there are n samples and $n > 8$ the matrix equations are:

$$\underset{n\times 8}{[A]}\ \underset{8\times 1}{[x]} = \underset{n\times 1}{[v]}, \qquad (3.29)$$

$$\underset{8\times1}{[x]} = \underset{8\times n}{[A]^{+}}\ \underset{n\times1}{[v]}, \tag{3.30}$$

where:

$[A]^{+}$ is the left pseudo-inverse of $[A]$.

$$[x] = [[A^T][A]]^{-1}[A^T][v]. \tag{3.31}$$

From Equation 3.31 it can be seen that the modelled components of the signal can be determined from their corresponding row elements in the left psuedo-inverse matrix of $[A]$ and the acquired data samples. This technique can be applied to a current signal represented by voltage as well.

3.3. Recursive Algorithms for Estimating Phasors

For nonrecursive filters to achieve a sharp transition from pass-band to stop-band they require large data windows. Recursive filters have this characteristic inherently due to their inclusion of previous outputs. Thus recursive filters can achieve sharper roll-offs with fewer coefficients. This section describes two of the most important recursive filters: the recursive discrete Fourier transform (DFT) and the Kalman filter.

3.3.1. Recursive Discrete Fourier Transform

Phadke, Thorp and Adamiak [28] designed a recursive discrete Fourier transform (DFT) algorithm to estimate voltage phasors. Using their notation, the DFT of a voltage signal can be expressed as:

$$V_H = \frac{2}{N}\sum_{k=0}^{N-1} v_k\, e^{-j\frac{2\pi}{N}kH}, \tag{3.32}$$

where:

H is the harmonic number,
k is the sample number and
N is the number of samples in the data window being used.

Letting the harmonic number equal one, which produces the fundamental frequency component and using the following trigonometric identity, $e^{-j\phi} = \cos\phi - j\sin\phi$, it can be shown that:

$$V_{Real} = \frac{2}{N}\sum_{k=0}^{N-1} v_k \sin\frac{2\pi}{N}k; \tag{3.33}$$

$$V_{Imag} = \frac{2}{N}\sum_{k=0}^{N-1} v_k \cos\frac{2\pi}{N}k. \tag{3.34}$$

When a new sample is acquired, the oldest one is discarded and new estimates of the real and imaginary components are calculated.

$$V_{Real} = \frac{2}{N}\sum_{k=0}^{N-1} v_{k+1} \sin\frac{2\pi}{N}(k+1), \tag{3.35}$$

$$V_{Imag} = \frac{2}{N}\sum_{k=0}^{N-1} v_{k+1} \cos\frac{2\pi}{N}(k+1). \tag{3.36}$$

These equations can be written recursively as:

$$V_{Real} = \frac{2}{N}(v_N - v_0)\sin\frac{2\pi}{N}k + \frac{2}{N}\sum_{k=0}^{N-1} v_k \sin\frac{2\pi}{N}k, \tag{3.37}$$

$$V_{Imag} = \frac{2}{N}(v_N - v_0)\cos\frac{2\pi}{N}k + \frac{2}{N}\sum_{k=0}^{N-1} v_k \cos\frac{2\pi}{N}k, \tag{3.38}$$

or

$$V_{Real} = \frac{2}{N}(v_N - v_0)\sin\frac{2\pi}{N}k + V_{Real,old}, \tag{3.39}$$

$$V_{Imag} = \frac{2}{N}(v_N - v_0)\cos\frac{2\pi}{N}k + V_{Imag,old}. \tag{3.40}$$

3.3.2. Kalman Filtering

Kalman filters are statistical or optimal filters that use the statistical properties of the signal that is being processed in order to produce estimates with greater accuracy. They are based on least squares theory and provide optimal results if the statistical properties of the signal are known and used in the design process; otherwise suboptimal results are produced. Girgis and Brown [29] and later Dasgupta, Malik and Hope [30] applied Kalman filtering to power system protection. Sachdev, Wood and Johnson [31] explained this technique in power system terminology and illustrated its use for power system measurement. As well, they described a procedure for designing Kalman filters taking into account harmonic and decaying dc signals. They demonstrated that each frequency component can be considered to be a phasor composed of a real and an imaginary part, which requires two states of the Kalman filter's state vector. Modelling the decaying dc component required one additional state.

To design a Kalman filter a state space model of the signal is required. The model should include any changes that are expected due to changes in system operating states and the statistical properties of the signal must be determined. The model includes a state transition equation and an output equation. In the following example, current is used as the output equation.

$$[x(n+1)] = [P][x(n)]+[Q][\Delta x(n)], \text{ and} \tag{3.41}$$

$$[i(n)] = [C][x(n)]+[b(n)], \tag{3.42}$$

where:

$[x(n)]$	is the state vector at time $t = n\Delta T$,
$[\Delta x(n)]$	are the changes in the state vector from $t = (n-1)\Delta T$ to $t = n\Delta T$,
$[P]$	is the state transition matrix,
$[Q]$	is the driving function matrix,
$[i(n)]$	is the instantaneous value of the current at $t = n\Delta T$,
$[C]$	defines the relationship between the instantaneous value of the current and its phasor representation and
$[b(n)]$	is the noise and measurement error at $t = n\Delta T$.

The state vector, $[x(n)]$, comprises the real and imaginary components of the fundamental and harmonic frequencies that are assumed to exist in the signal. The state transition matrix, $[P]$, advances the state vector by one sampling interval, and the driving function matrix, $[Q]$, will advance the change in the state vector, $[\Delta x]$, by one sampling interval.

The Kalman gains, which are the filter coefficients, are time varying and are calculated to minimize the square of the expected errors between the values of the actual and estimated system states. Using statistical information about the signal the Kalman gains are calculated by recursively solving the following equations.

$$[K(n)] = [M(n)][C]^T [\,[C][M(n)][C]^T+[B]\,]^{-1}, \tag{3.43}$$

$$[Z(n)] = [\,[I]-[K(n)][C]\,][M(n)], \text{ and} \tag{3.44}$$

$$[M(n+1)] = [P][Z(n)][P]^T + [Q][U][Q]^T, \tag{3.45}$$

where:

$[K(n)]$	are the Kalman gains at $t = n\Delta T$,
$[M(n)]$	is the covariance matrix of the single step transformation,
$[B]$	is the covariance matrix of the noise inputs $[b(n)]$,
$[Z(n)]$	is the state estimation error covariance matrix,
$[I]$	is an identity matrix and
$[U]$	is the covariance matrix of the $[\Delta x]$ inputs.

The resulting Kalman filter equation estimates new values of the state variables, the real and imaginary components of the phasors, and is given in Equation 3.46. This equation gives the estimate for the state vector based on the predicted values adjusted by the product of the Kalman gains and the difference between the measured and estimated currents.

$$[\bar{x}(n)] = [P][\bar{x}(n-1)] + [K(n)][\,[i(n)]-[C][P][\bar{x}(n-1)]\,], \tag{3.46}$$

where:

$[\overline{x}(n)]$ are the estimates of the state vector $[x(n)]$.

Equation 3.47 shows the state transition matrix, $[P]$, and the driving function matrix, $[Q]$, developed by Sachdev, Wood and Johnson [31] for an 11 state Kalman filter. During fault conditions the current waveforms are assumed to be composed of a decaying dc component and components of the fundamental, second, third, fourth and fifth harmonic frequencies.

$$[Q] = [P] = \begin{bmatrix} [F(1)] & [0] & [0] & [0] & [0] & [0] \\ [0] & [F(2)] & [0] & [0] & [0] & [0] \\ [0] & [0] & [F(3)] & [0] & [0] & [0] \\ [0] & [0] & [0] & [F(4)] & [0] & [0] \\ [0] & [0] & [0] & [0] & [F(5)] & [0] \\ 0 & 0 & 0 & 0 & 0 & e^{-\lambda \Delta T} \end{bmatrix} \quad (3.47)$$

where:

$$[F(n)] = \begin{bmatrix} \cos(n\omega_0 \Delta T) & -\sin(n\omega_0 \Delta T) \\ \sin(n\omega_0 \Delta T) & \cos(n\omega_0 \Delta T) \end{bmatrix}$$

$$[0] = \begin{bmatrix} 0 & 0 \\ 0 & 0 \end{bmatrix}$$

3.4. Summary

In summary this chapter has briefly discussed methods for sampling data and the structure of data windows. It has also described the underlining mathematical equations and assumptions of several digital relaying algorithms. The nonrecursive group of algorithms reviewed were trigonometric, correlation and least error squared. The recursive algorithms discussed were the recursive DFT and Kalman filter.

The relaying algorithm chosen for use in this work is the non-recursive Least Error Squares filter. This technique was chosen because it does not require any statistical information about the signal being processed, it can effectively reject the decaying dc component of a signal and for its ease of implementation. The complete design and implementation of this filter is discussed in Chapter four.

4. DESIGN OF A MICROPROCESSOR-BASED DIRECTIONAL OVERCURRENT RELAY

Chapter three discussed various digital relaying algorithms available for estimating the parameters of interest. In this chapter, the design of a microprocessor-based directional overcurrent relay is presented. Directional overcurrent relays are basically composed of two main elements, an overcurrent element and a directional element. The design can be further broken into seven general blocks, shown in Figure 4.1.

The initialization block accepts input at the time of commissioning, describing the desired relay characteristics such as configuration, MTA's, torque offsets, and pickup settings, and then initializes the relay. The data acquisition block acquires digitized samples of the voltages and currents, needed by the signal processing block, from the power system. The signal processing block estimates the parameters of interest which are the fundamental frequency components of the sampled voltages and currents acquired from the power system. The directional element block evaluates the connection voltages and currents required and calculates the torque produced by a particular directional unit. If the calculated torque is greater than a pre-specified value, the power flow is to the line side, forward/tripping direction, of the relay, and the overcurrent element block is activated. The overcurrent element block determines the multiples of pickup current seen by the relay and implements a time delay based on that current, the time multiplier setting and the type of current-time characteristic selected. A trip logic block then decides if a trip signal should be generated. The resetting block is needed to reset the relay after tripping and in case the current in one of the protected phases drops below pickup or changes direction.

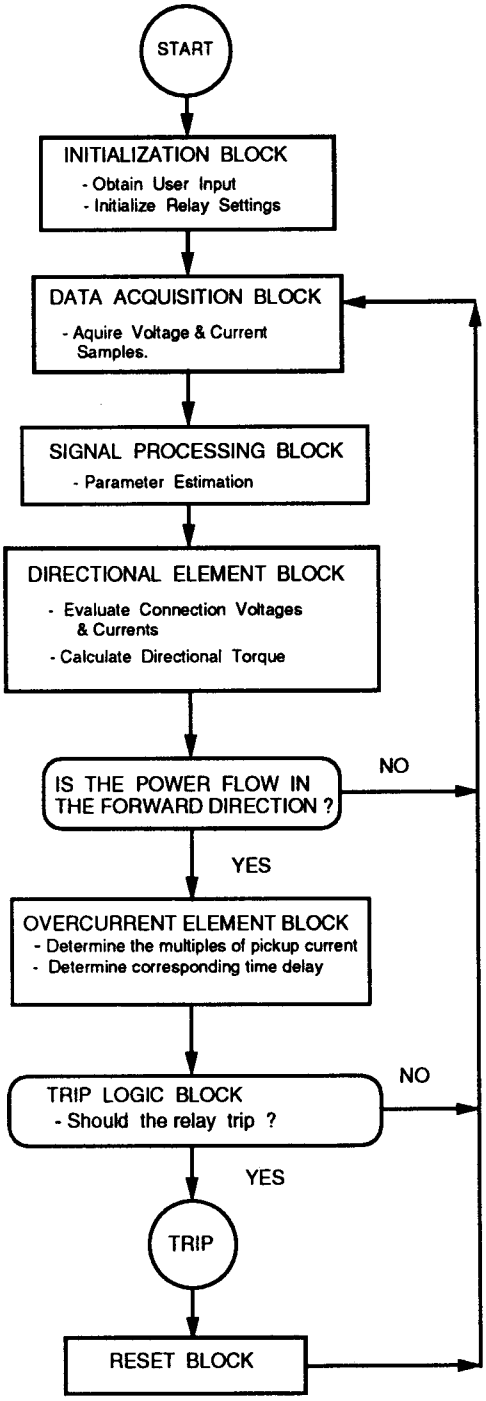

Figure 4.1: A general block diagram of a microprocessor-based directional overcurrent relay.

4.1. Modelling the Directional Element

The directional element consists of three directional phase units and one directional ground unit. Any of the four connections for directional phase units, listed in Table 2.1, can be derived from sampled values of V_a, V_b, V_c, I_a, I_b and I_c. As well, the connection inputs for a directional ground unit, $3V_0$, $3I_0$ or V_2, I_2, can be determined in the same manner using symmetrical component equations. In this design the negative sequence quantities are left at three times their magnitude, $3V_2$ and $3I_2$, to reduce calculation time and increase their magnitude for polarization purposes. The connection voltages and currents can then be used to calculate the torque produced by each phase unit and the ground unit. A decision about the direction of power flow in the protected zone can then be made.

4.1.1. Implementing the Directional Torque Equation

Using the mathematical technique of projections [32] Equation 2.1 can be rearranged into a form that requires only the real and imaginary components of the voltage and current inputs [10]; thus the microprocessor does not have to perform any complex transcendental calculations to evaluate the various torques. As a result the directional algorithm is more efficient as the phase voltages and currents can be estimated in a rectangular format.

Taking into consideration that voltages and currents can be interpreted as vectors the torque produced by a single phase directional relay is:

$$T = K_1|\mathbf{V}_{pol}||\mathbf{I}|\cos(\theta-\tau) - K_2, \tag{4.1}$$

where:

$\mathbf{V}_{pol}$ is the polarizing quantity.

The operating characteristic is shown in Figure 4.2. Let $\theta-\tau=\beta$ and consider only the first term of Equation 4.1.

$$1^{st}\ term = K_1|\mathbf{V}_{pol}||\mathbf{I}|\cos\beta. \tag{4.2}$$

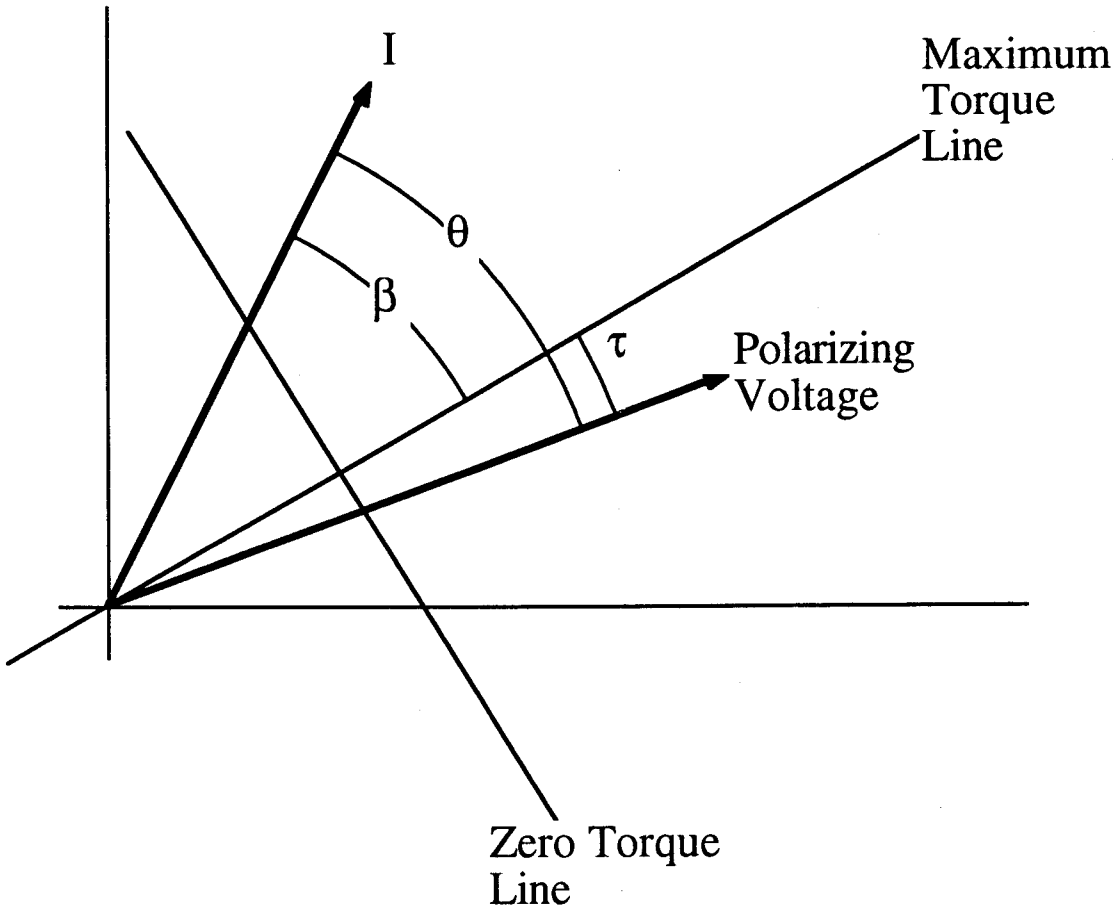

Figure 4.2: The operating characteristic for a single phase relay demonstrating the implementation of the torque equation.

If the maximum torque line is considered to represent a unit vector **MTL**, signifying a direction $\tau°$ from the voltage reference, projections can be used to modify Equation 4.2 thereby removing the cosine term. A projection p is defined as:

$$p = |\mathbf{a}|\cos\gamma = \frac{\mathbf{a}\cdot\mathbf{b}}{|\mathbf{b}|}. \tag{4.3}$$

The projection p of vector **a** onto vector **b** is equal to the dot product of the two vectors

divided by the magnitude of vector **b**. If **b** is a unit vector Equation 4.3 reduces to $p = \mathbf{a} \cdot \mathbf{b}$. Applying this to Equation 4.2:

$$K_1 |\mathbf{V}_{pol}||\mathbf{I}|\cos\beta = K_1 |\mathbf{V}_{pol}|\mathbf{I} \cdot \mathbf{MTL}. \tag{4.4}$$

Because the maximum torque line is not known in absolute terms but only in relation to $\mathbf{V}_{pol}$, the unit vector **MTL** can be written in terms of the reference voltage. Let $\mathbf{V}_{pol}$ and τ be defined in terms of their real and imaginary components; then transform $\mathbf{V}_{pol}$ into a unit vector and rotate it by $\tau°$. The resulting equation, Equation 4.9, can then be substituted into Equation 4.4.

$$\mathbf{V}_{pol} = V_{pol,Real} + jV_{pol,Imaginary}. \tag{4.5}$$

$$\textbf{Unit Vector} = \frac{Real + jImaginary}{\sqrt{Real^2 + Imaginary^2}}. \tag{4.6}$$

$$\mathbf{MTL} = \frac{V_{pol,Real} + jV_{pol,Imaginary}}{|\mathbf{V}_{pol}|} \; 1\angle\tau. \tag{4.7}$$

$$1\angle\tau = \cos\tau + j\sin\tau. \tag{4.8}$$

$$\mathbf{MTL} = \frac{(V_{pol,Real}\cos\tau - V_{pol,Imag}\sin\tau) + j(V_{pol,Real}\sin\tau - V_{pol,Imag}\cos\tau)}{|\mathbf{V}_{pol}|}. \tag{4.9}$$

If the current vector **I** is also defined in terms of its real and imaginary components the dot product between **I** and **MTL** can be expressed as follows.

$$\mathbf{I} = I_{Real} + jI_{Imaginary}. \tag{4.10}$$

$$\mathbf{I} \cdot \mathbf{MTL} = \frac{I_{Real}(V_{pol,Real}\cos\tau - V_{pol,Imag}\sin\tau) + I_{Imag}(V_{pol,Real}\sin\tau - V_{pol,Imag}\cos\tau)}{|\mathbf{V}_{pol}|}. \tag{4.11}$$

Substituting Equation 4.11 into Equation 4.4 results in Equation 4.12 which is defined solely in terms of real and imaginary components.

$$K_1|\mathbf{V}_{pol}||\mathbf{I}|\cos\beta = K_1\{I_{Real}(V_{pol,Real}\cos\tau - V_{pol,Imag}\sin\tau) + I_{Imag}(V_{pol,Real}\sin\tau + V_{pol,Imag}\cos\tau)\}. \quad (4.12)$$

The rectangular components of the MTA can be input directly to the relay or it can determine them off-line before commissioning. The voltage and current inputs in Equation 2.1 are assumed to be rms but most filters estimate only peak values. To change the voltage and current inputs from peak values to rms, their real and imaginary components in Equation 4.12 should be divided by $\sqrt{2}$. These divisors can be collected outside the main brackets to give a multiplication factor of 0.5 which can then be included in Equation 4.12 to calculate torque from peak voltages and currents.

$$K_1|\mathbf{V}_{pol}||\mathbf{I}|\cos(\theta-\tau) = 0.5K_1\{I_{Real}(V_{pol,Real}\cos\tau - V_{pol,Imag}\sin\tau) + I_{Imag}(V_{pol,Real}\sin\tau + V_{pol,Imag}\cos\tau)\}. \quad (4.13)$$

4.2. Mathematical Models of Current-Time Characteristics

Several mathematical equations exist that express overcurrent relay operating times as functions of relay currents. These equations can be divided into two categories, polynomial and exponential [33].

4.2.1. Exponential Equations

Equation 4.14 was proposed by A.R. van Warrington to relate contact closing time of an inverse-time overcurrent relay to its operating current [2]. It provides a good model of the operating characteristics of European inverse-time overcurrent relays and the coefficients are easily found.

$$t_r = c_0 + \frac{c_1 TDS}{I^{\beta}-1}, \quad (4.14)$$

where:

t_r	is the trip contact closing time,
TDS	is the time dial setting,
I	is the relay current in multiples of tap setting and
c_0, c_1 and β	are relay constants.

Equation 4.15 is an empirical formula proposed by J.E. Hieber [34]; the relay constants are determined at the maximum and minimum time dial settings. Relay characteristics at intermediate time dial settings can be obtained by nonlinear interpolation of the characteristics determined from the maximum and minimum time dial settings. Even though an adequate model is provided, the calculation of the required coefficients can be quite complex.

$$t_r = c_0 + \frac{c_1}{(I-h+wI^{-2I})^q} - b\frac{I}{50}^{\beta}, \tag{4.15}$$

where:

b,h,q and w	are constants.

The International Electrotechnical Commission (IEC) Standard 255.4 [35] for modelling inverse-time overcurrent relays is given in Equation 4.16.

$$t_r = \frac{k}{I(t)^{\alpha} - 1}, \tag{4.16}$$

where:

k	is a constant characterizing the relay,
α	is an index characterizing the algebraic function and
$I(t)$	is the current signal, in multiples of pickup, observed at time t.

There are three defined curves, standard inverse, very inverse, and extremely inverse, which are listed in Table 4.1 and shown in Figure 4.3.

Table 4.1: IEC Standard 255.4 constants for modelling inverse-time overcurrent relay operating characteristics

Relay Characteristic	k	α
Standard Inverse	0.14	0.02
Very Inverse	13.5	1.0
Extremely Inverse	80.0	2.0

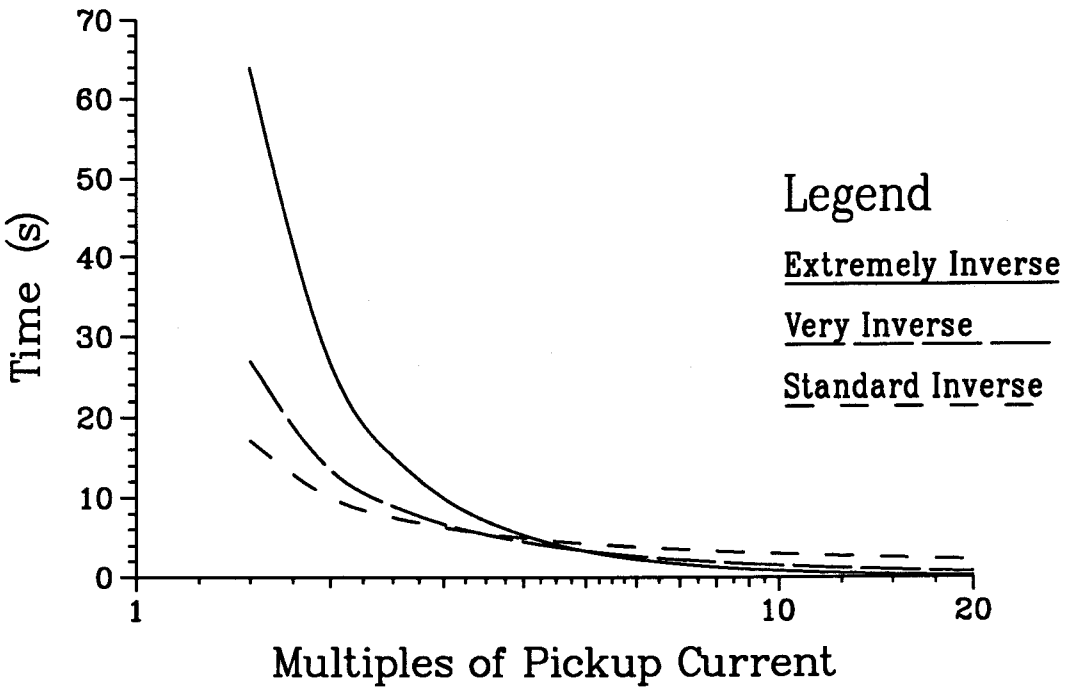

Figure 4.3: IEC Standard 255.4 current-time characteristics.

4.2.2. Polynomial Equations

Several researchers have suggested the use of polynomial equations to model the current-time characteristics of overcurrent relays. Albrecht et al. [36] expressed the operating time of an overcurrent relay as a polynomial in two variables, current and time dial setting.

$$t_r = \{\sum_{j=1}^{m}\sum_{i=1}^{n} c_{ji}\, TDS^j\, I^i\}^{\gamma}, \tag{4.17}$$

where:

c_{ji}, m, n and γ are constants.

G.E. Radke [37] expressed the operating time as a polynomial in logarithms of the relay current.

$$log(t_r - d_c) = c_0 + c_1(\log I) + c_2(\log I)^2 + c_3(\log I)^3 + c_4(\log I)^4, \tag{4.18}$$

where:

d_c, c_0, c_1, c_2, c_3 and c_4 are constants.

By assigning an appropriate value to c_0 each time dial setting can be modelled. Both of the suggested models, defined by Equations 4.17 and 4.18, can provide an accurate representation of inverse-time characteristics. However, the operating curves are not asymptotic to the pickup current and the operating time does not decrease monotonically with increasing current.

Sachdev, Singh and Fleming [38, 10] examined the following polynomials for their suitability to represent overcurrent relay characteristics. These polynomial equations also effectively reproduce inverse-time characteristics and are asymptotic to the pickup current and minimum operating time. For selected time dial settings they can be used to model inverse-time characteristics.

$$\log(t_r) = c_0 + \frac{c_1}{\log I} + \frac{c_2}{(\log I)^2} + \frac{c_3}{(\log I)^3} + \cdots \tag{4.19}$$

$$t_r = c_0 + \frac{c_1}{I-1} + \frac{c_2}{(I-1)^2} + \frac{c_3}{(I-1)^3} + \cdots \tag{4.20}$$

$$t_r = c_0 + \frac{c_1}{I-1} + \frac{c_2}{I^2-1} + \frac{c_3}{I^3-1} + \cdots \tag{4.21}$$

$$t_r = c_0 + \frac{c_1}{I-1} + \frac{c_2 I}{(I-1)^2} + \frac{c_3 I^2}{(I-1)^3} + \cdots \tag{4.22}$$

$$t_r = c_0 + \frac{c_1}{I-1} + \frac{c_2 I}{I^2-1} + \frac{c_3 I^2}{I^3-1} + \cdots \tag{4.23}$$

Composite models have also been suggested for obtaining relay operating curves at other time dial settings [38]. This approach consists of three steps.

1. Develop a model of the operating characteristic with the time as a function of current at a specific *TDS*.
2. Develop a polynomial model for the relay operating time versus time dial settings for a selected multiple of pickup current. The following is an example equation.

$$t_r = b_0 + b_1(TDS) + b_2(TDS)^2 + b_3(TDS)^3. \tag{4.24}$$

3. Combine the two models for calculating the relay operating time for selected relay operating currents and time dial settings.

Damborg et al. [39] combined Equations 4.24 and 4.21 into the following equation:

$$t_r = c_1 + c_2 TDS + \frac{c_3 TDS}{(I-1)^2} + \frac{c_4(TDS)^2}{I-1} + \frac{c_5(TDS)^2}{(I-1)^2} + \frac{c_6 TDS}{(I-1)^3} + \frac{c_7(TDS)^2}{(I-1)^4}. \tag{4.25}$$

The coefficients c_1 to c_7 are calculated with the least squares technique [27] using all operating times for the time dial settings.

Any of the models previously listed could be used in a microprocessor-based overcurrent relay to accurately represent an inverse-time characteristic. Three main criteria were considered while selecting an appropriate model for this application.

1. The accuracy of the model's representation of an operating characteristic.
2. The ease of implementation on a microprocessor.
3. The adherence to a common standard for operating characteristics.

Implementing polynomial equations on a microprocessor is cumbersome due to the complexity of the required computations to represent a characteristic. The IEC model was used in this project because it is relatively easy to implement and provides an accurate standard that has begun to be adopted in the North American market.

4.3. Implementing the Overcurrent Element

The overcurrent element consists of four units for inverse-time overcurrent operation, one for each phase and one for the ground path. Current levels during a fault fluctuate with time, and the overcurrent element's operating time must reflect these changes. These time varying current levels are accounted for by integrating a weighting function, $w_r(t)$, that depends on the observed rms current [10, 40]. If a current is greater than the pickup value, the weight is determined from Equation 4.26; the larger the current multiple, the larger is the weight assigned to it. For currents less than or equal to the pickup value, the function value is zero. This weighting function is based on the inverse of the IEC time characteristic given in Equation 4.16.

$$w_r(t) = T_{num}\frac{I(t)^{\alpha} - 1}{k} = \frac{T_{num}}{t_r(t)}, \tag{4.26}$$

where:

$I(t)$ is the observed current in multiples of pickup at time t,
$w_r(t)$ is the weight corresponding to $I(t)$ at time t and
T_{num} is a target number.

Ideally, the integration of Equation 4.26 would start after the inception of a fault when the estimated rms current exceeds the pickup value, $I(t) \geq 1$. When the integration exceeds the target number, which is mathematically expressed in Equation 4.27, a trip command is issued. If the estimated rms current falls below the pickup setting a resetting process is undertaken by altering the integrand to achieve a desired reset characteristic.

$$\int_0^t w_r(t)\,dt \;>\; T_{num}\,. \tag{4.27}$$

Using the rectangular rule for integration and the fact that the currents are sampled at intervals of ΔT, Equation 4.27 can be rewritten as:

$$\sum_{n=0}^{N} w_r(n)\Delta T \;>\; T_{num}\,, \tag{4.28}$$

where:

n is the n^{th} sample after the inception of a fault.

Equation 4.28 can also be expressed as:

$$\sum_{n=0}^{N} W_r(n) \;>\; T_{num}\,, \tag{4.29}$$

where:

$W_r(n) = 0$ when the estimated current is less than pickup and

$W_r(n) = \frac{T_{num}\Delta T}{t_r(n)}$ when the current is greater than the pickup setting.

To account for a TMS, the target number in Equation 4.29 is simply multiplied with the chosen TMS. The operating time of the relay $N\Delta T$, where N is the number of sampling intervals required to implement the necessary time delay, is unknown. It is determined by calculating the value of $W_r(n)$ at each sampling instance and evaluating Equation 4.29 for a positive answer.

Figure 4.4 displays a graphical representation of Equation 4.29, with $W_r(n)$ normalized using the target number. At each sampling instance when the current is greater than an overcurrent unit's pickup setting and the directional element determines that the power flow is in the tripping direction, the weight is evaluated and added to the appropriate trip counter. If the current is less than the pickup value or its direction

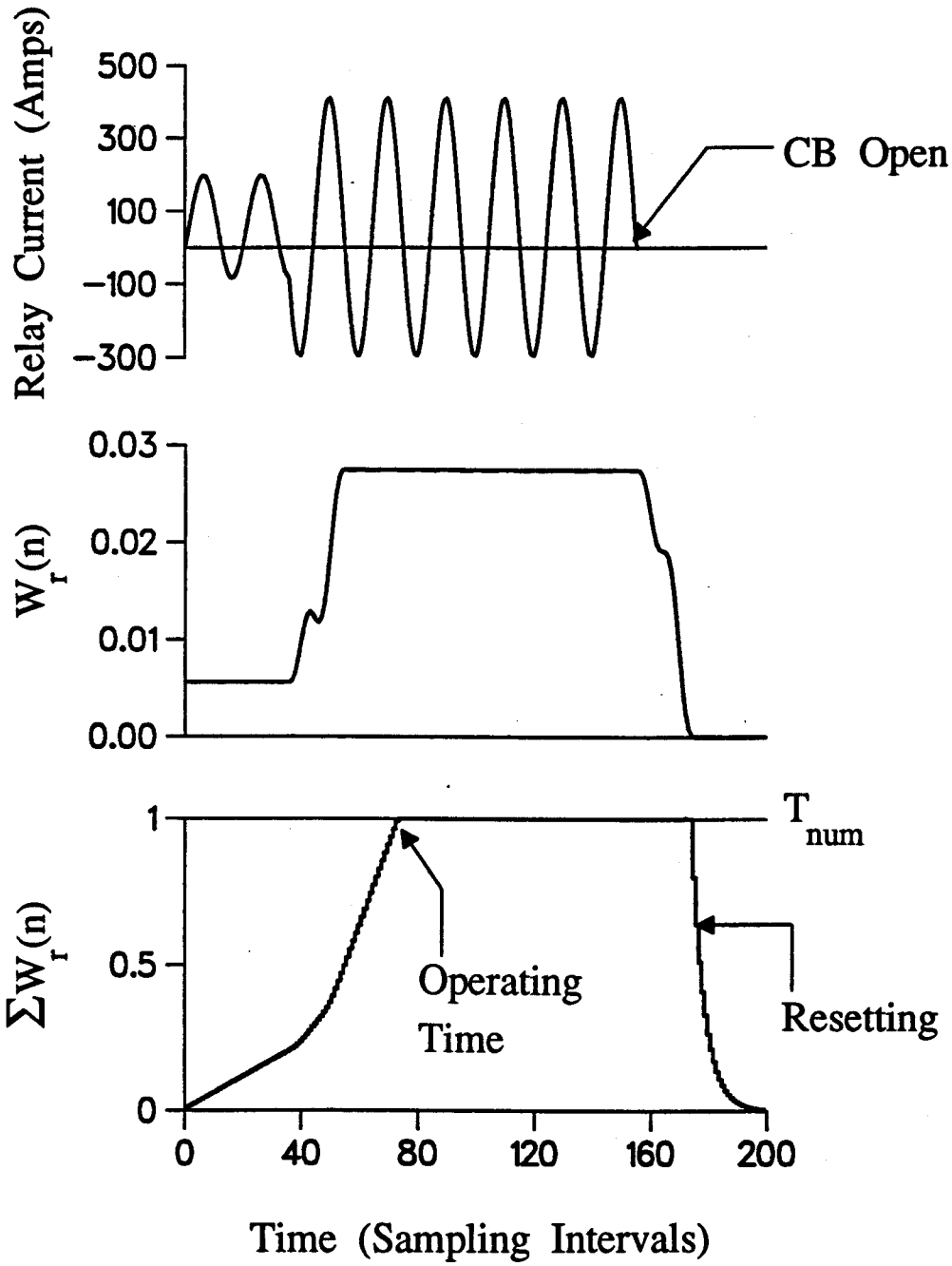

Figure 4.4: The graphical representation of Equation 4.29 [41].

changes, resetting of the trip counter is initiated. When the summation defined in Equation 4.29 reaches the target number, a trip command is issued, and resetting of the relay may begin. The figure also shows that an increase in fault current results in a larger $W_r(n)$ being added to the trip counter, decreasing the operating time of the relay. Instead of evaluating the weights on-line, a lookup table is calculated off-line by the relay and then the weights are determined using linear interpolation.

4.3.1. Selection of the Target Number

Most microprocessors process data in a fixed point format resulting in truncation errors. This can seriously affect the implementation of the required time delays by the microprocessor; although it is possible to select the target number, T_{num}, such that the implemented time delays are within one sampling interval of the desired characteristic [42]. In this design single precision floating point was used to implement the time delays, thus abrogating the need for determining an acceptable target number. It was set to a default value of one.

4.3.2. Lookup Table

The weighting factor W_r, defined in Equation 4.29, can be determined from w_r which is defined in Equation 4.26. The multiples of pickup current are substituted into Equation 4.26 and the result is multiplied by ΔT. On-line calculations of the weighting factors would require an excessive amount of computations to be performed in one sampling interval. A more computationally efficient method is to have a look-up table of the multiples of pickup current and their corresponding weights. The weighting factors, at a time multiplier setting of one and a specified current-time characteristic, for the integer multiples of pickup current up to 25, were calculated off-line and stored in a look-up table. Different TMS's were accounted for when the target number was multiplied with the selected TMS. For estimated currents listed, the corresponding weighting values were read from the table. To determine the weights for non-listed currents, linear interpolation was used, using Equation 4.30.

$$W_r(n) = W_L + \frac{(W_G - W_L)(I_n - I_L)}{I_G - I_L} \tag{4.30}$$

where:

I_n	is the estimated current in multiples of pickup,
$W_r(n)$	is corresponding weight for I_n,
I_L, I_G	are the currents, in multiples of pickup, that are lesser and greater than the estimated current and
W_L, W_G	are the weights in the look-up table corresponding to currents I_L and I_G respectively.

Figure 4.5 shows the weighting curves for the three IEC current-time characteristics up to a current multiple of 20. From this figure it is evident that the very inverse curve has the best characteristics for implementation because it is linear and there will be little error with linear interpolation. The extremely and standard inverse curves are nonlinear which will create large errors for linear interpolation in the low current multiple range. To partially alleviate this problem weights were also calculated at half multiples between the range of one to four. If the estimated current is greater than 25 multiples of pickup the weight assigned to it is the value determined at 25 multiples. There are separate look-up tables for the phase units and the ground unit enabling them to use different current-time characteristics instead of the same one.

4.3.3. Resetting

After issuing a trip signal or if any of the estimated currents reduce to levels below pickup or their direction changes, resetting of the affected trip counters should be undertaken. Electromechanical overcurrent relays reset gradually due to the force of a restraining spring. Solid state relays reset either gradually or without any intentional delay, i.e., instantaneously. Microprocessor-based relays can have a variety of resetting characteristics because they are software controlled. There are three resetting characteristics available, instantaneous, linear and exponential. It is assumed that the overcurrent phase units and the ground unit will have the same resetting characteristic.

The instantaneous reset characteristic sets the trip counter sum $\sum W_r(n)$ to zero.

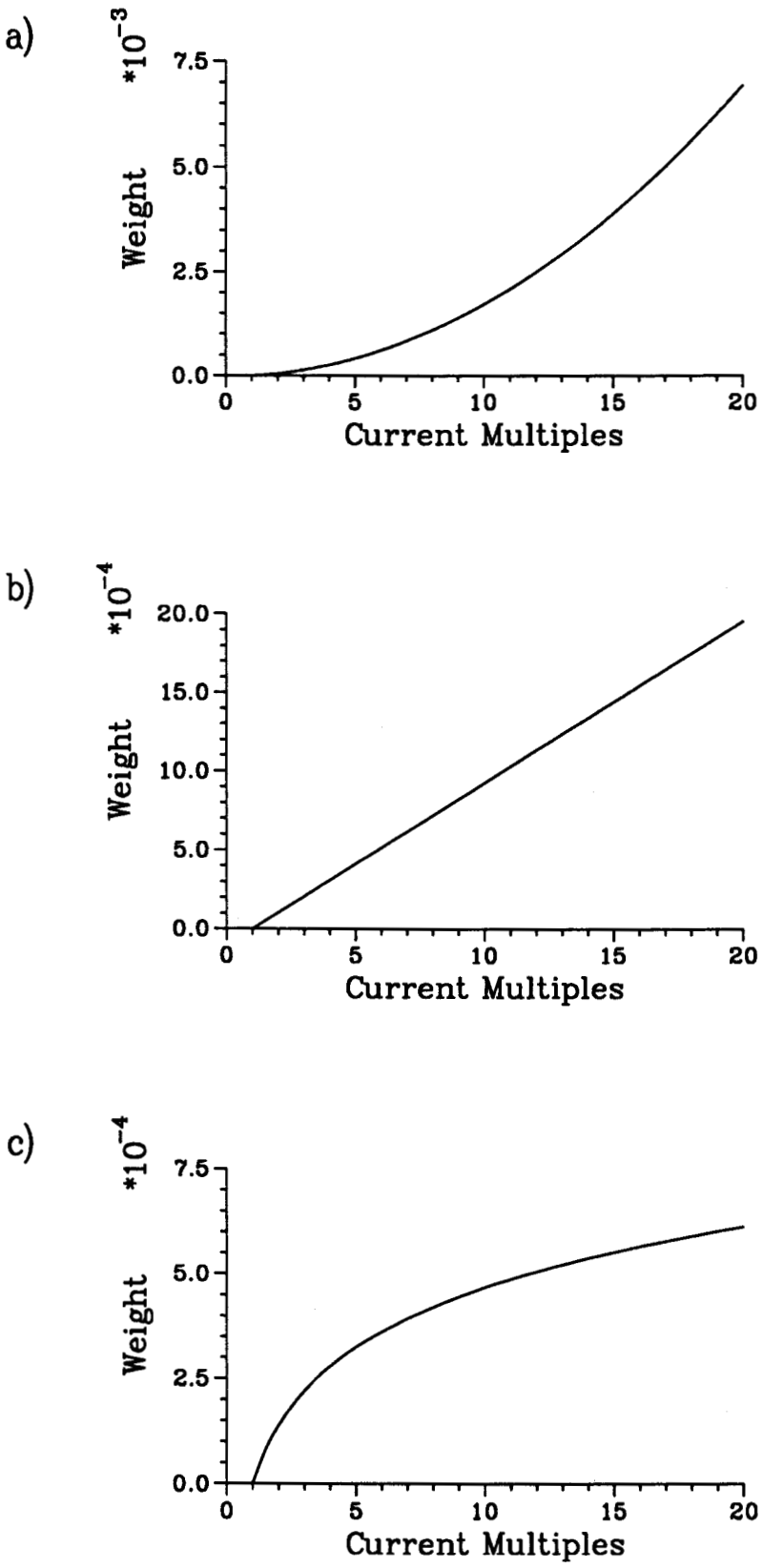

Figure 4.5: The weighting curves for the IEC current-time characteristics determined for a target number of one: a) extremely inverse, b) very inverse and c) standard inverse.

The linear reset characteristic gradually resets the relay with time. It modifies $\sum W_r(n)$ using Equation 4.31. Figure 4.6 shows resetting the sum with different values of L.

$$\sum W_r(n+1) = \{ \sum W_r(n) \} - L, \tag{4.31}$$

where:

L is an integer number used for resetting the relay.

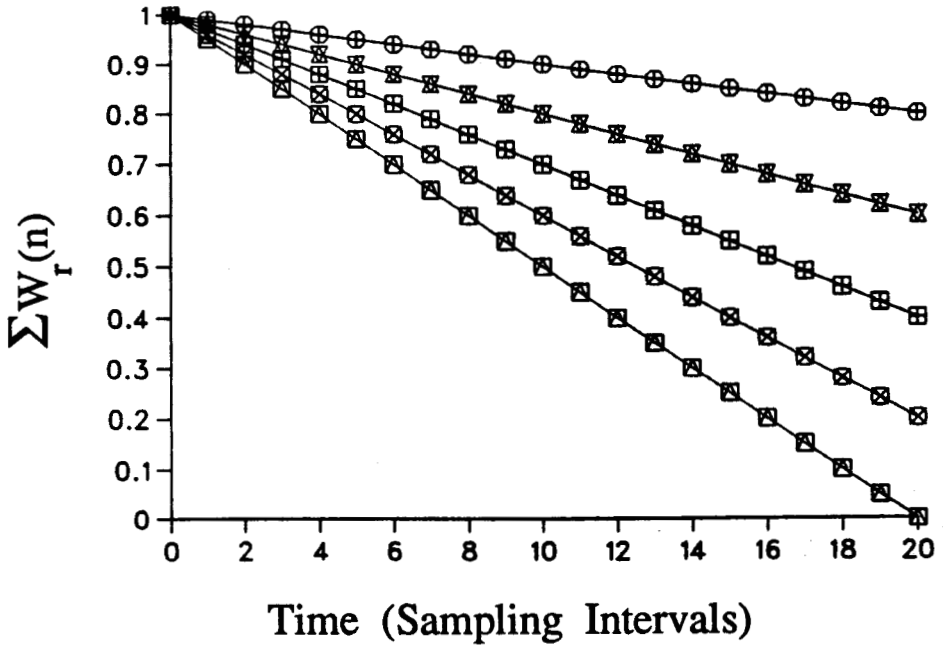

Figure 4.6: Linear reset characteristics for L equalling 0.01, 0.02, 0.03, 0.04 and 0.05 respectively [43].

The exponential reset characteristic resets $\sum W_r(n)$ exponentially with time. Figure 4.7 shows resetting the sum with different values of E.

$$\sum W_r(n+1) = E \sum W_r(n), \tag{4.32}$$

where:

E is a fractional number used for resetting the relay.

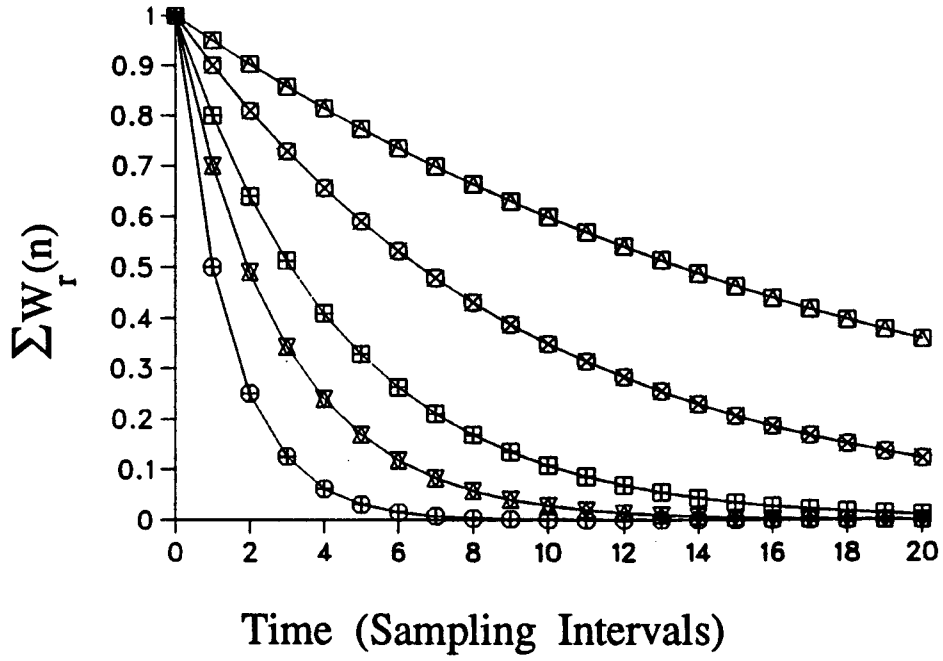

Figure 4.7: Exponential reset characteristics for E equalling 0.95, 0.90, 0.80, 0.70 and 0.50 respectively [43].

4.4. Implementing Directional Instantaneous Overcurrent Units

Instantaneous overcurrent units can be integrated into the general overcurrent algorithm by the calculation of an instantaneous weighting value, W_{IT}, and an instantaneous pickup setting, one pair of settings for the phase units and one pair for the ground unit. At any instance when the estimated phase or residual current is greater than its instantaneous pickup setting, the instantaneous weight would be added to the appropriate trip counter instead of the inverse-time characteristic weight.

The operating time for instantaneous units can be defined as:

$$t_{IT} = IT_{op}(I), \tag{4.33}$$

where:

t_{IT} is the instantaneous unit's operating time and

$IT_{op}(I)$ equals a constant for currents greater than the instantaneous pickup value and infinity for currents less than that value.

The process of determining the required W_{IT} for the desired instantaneous tripping time can be accomplished in the same manner as was done for the inverse current-time characteristics. Rectangular integration is applied to a weighting function based on a straight line current-time characteristic as opposed to an inverse one which produces the following criterion for W_{IT}.

$$W_{IT} = \frac{T_{num}\Delta T}{IT_{op}}, \tag{4.34}$$

where:

IT_{op} is the operating time for the instantaneous unit.

The overcurrent criterion, stated in Equation 4.29, is then modified to include W_{IT}.

$$\sum_{n=0}^{N} W_r(n) > T_{num}, \tag{4.35}$$

where:

n is the n^{th} sample after the inception of the fault and

$W_r(n) = W_{IT}$ when the current is greater than the instantaneous pickup.

4.5. Phasor Estimation Technique: LES

The signal processing algorithm used by the directional overcurrent relay is the parameter estimation technique of least error squares. It is a curve fitting algorithm that assumes the composition of the voltage and current signals are known in advance. Most computations are performed off-line and therefore the computational requirements are not substantially greater than other large data window algorithms. The strengths and weaknesses of LES algorithms are as follows [44]:

- They effectively reject high frequency components.
- They attenuate noise.
- They effectively reject the decaying dc components.
- They require no statistical information about the signals.
- Their transient response is slower than short window techniques but is comparable to the Fourier analysis approach.
- They might require more multiplications than the Fourier or Kalman approach.

The signals seen by the relay were modelled as being composed of the first two terms of the Taylor's series expansion of a decaying dc component, a fundamental component and the 2^{nd}, 3^{rd}, 4^{th} and 5^{th} harmonics. These harmonics are modeled so the relay may function in harmonic rich environments where generators and/or transformers are located. A 13 point data window, centered in the middle, with a sampling frequency of 720 Hz was chosen as the best trade-off between the speed/size of the window versus the accuracy of its estimates and variance in its noise. This is a $1\frac{1}{12}$ full cycle window 18.1 ms long with approximately 1.4 ms between data samples to do the necessary calculations and perform any other duties that are required. Table 4.2 lists the LES filter coefficients. Running the sampled voltages and currents through these filters will produce estimates of their real and imaginary components. From the filter coefficients in Table 4.2, it can be shown that the noise introduced by the cosine and sine filters is $0.3601\ \sigma_n^2$ and $0.1522\ \sigma_n^2$ respectively, where σ_n^2 is the variance of the input noise. Therefore, both filters will suppress noise quite effectively with the noise suppression of the sine filter best, 57.74% less noise is transmitted by it.

Figure 4.8 shows the frequency response of the LES filters. From this figure it is evident that the sine filter's frequency response is quite good and all harmonics except for the sixth are suppressed to zero; the magnitude of the sixth harmonic is 8.70% of its original value. The cosine filter's frequency response is also good except that its lobes are larger and its main lobe is offset from the fundamental frequency by approximately 18.5 Hz. All harmonics in the frequency range considered are suppressed to zero in the cosine filter.

Table 4.2: The filter coefficients for a 13 point LES filter.

Coefficient Number	Cosine Coefficients	Sine Coefficients
x[-6]	0.3110042	-0.0869565
x[-5]	-0.0833333	-0.1370912
x[-4]	-0.1443376	-0.0905797
x[-3]	-0.1666667	0.0072464
x[-2]	-0.1443376	0.0760870
x[-1]	-0.0833333	0.1515839
x[0]	0.0000000	0.1594203
x[1]	0.0833333	0.1515839
x[2]	0.1443376	0.0760870
x[3]	0.1666667	0.0072464
x[4]	0.1443376	-0.0905797
x[5]	0.0833333	-0.1370912
x[6]	-0.3110042	-0.0869565

Since the LES filter is nonrecursive the estimated phasors will rotate counter clockwise by 30° in the pre- and post-fault regions and by some unknown angle in the fault region. This rotation will not affect the relay because it only needs to know the relative position of the phasors with respect to each other and all MTA's are referenced from the connection voltage. As well, the point in time which the estimates are actually evaluated at is represented by the center of the data window; therefore an additional phase shift of 180° has to be added to these estimates to have them tied to the positive time edge of the window. The 180° phase shift represents the six data points between the center of the window and its edge, with a phase shift of 30° per data point. This phase

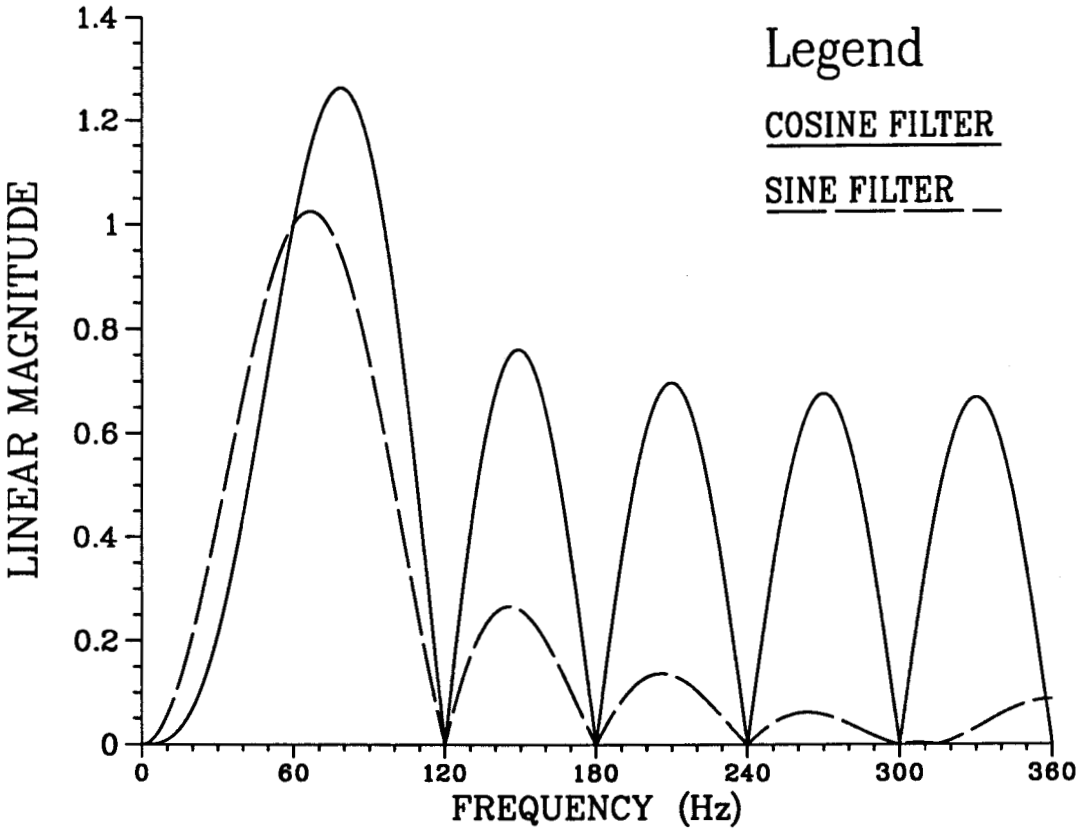

Figure 4.8: The frequency response of the 13 point LES filters.

shift is easily accomplished by multiplying the estimates of the real and imaginary components by −1 or by pre-multiplying the filter coefficients by −1, which is the same as evaluating the filter coefficients with the newest sample at time zero. Noise coefficients and frequency response will remain unchanged.

Because of the sampling rate chosen, the anti-aliasing filter in the data acquisition block must have a cut-off frequency (f_c) of less than 360 Hz, $f_c \leq \frac{1}{2} f_s$. A 2nd order Butterworth low-pass filter with a f_c of 270 Hz was designed to accomplish this task. The low-pass filter also reduces the sixth harmonic component of any input signal by

approximately 49.0%; this improves the suppression of the sixth harmonic in the LES sine filter to 4.26% of its original value. The complete design and frequency response of this filter is described in Appendix A.

4.5.1. Amplitude Estimation of Current

The rms value of the fundamental frequency current is used to determine the weight corresponding to the fault currents. A piecewise linear approximation technique is employed to determine the rms value from the real and imaginary components estimated by the LES filter [40]. With these components and Equation 4.36, I_{rms} can be determined.

$$I_{rms} = Lx + Sy, \tag{4.36}$$

where:

L	represents the larger of the two values, $\lvert I_{real} \rvert$ and $\lvert I_{imaginary} \rvert$,
S	represents the smaller of the two values, $\lvert I_{real} \rvert$ and $\lvert I_{imaginary} \rvert$,
x and y	are coefficients for the region in which the fraction S/L lies.

The fraction S/L is evaluated and the appropriate coefficients are used from Table 4.3 to calculate the rms value; a four region approximation was used in this design. A more complete mathematical description of this technique is given in Appendix B.

Table 4.3: Coefficients for calculating the rms value of the fundamental frequency current using a four region approximation.

Region	x	y
$0.00 = S/L \leq 0.25$	0.7036	0.0873
$0.25 < S/L \leq 0.50$	0.6641	0.2473
$0.50 < S/L \leq 0.75$	0.6015	0.3738
$0.75 < S/L \leq 1.0$	0.5337	0.4649

4.6. Memory Polarization for Close-In Faults

For close-in three-phase or three-phase-to-ground faults, the system voltage levels at the relay location will collapse almost to zero which makes directional discrimination difficult even with existing polarization. This is also applicable to when grounding wires are inadvertently left on a power line. To overcome this problem, memory polarization using the pre-fault voltages can be applied to ensure that sufficient signal levels will exist. Memory polarization cannot be used for other types of close-in faults because it interferes with existing polarization and either produces no benefit or is a detriment to directional discrimination.

Memory polarization is implemented in the following fashion. The relay checks the acquired phase voltages against a threshold, memory polarization setting, to see if they have collapsed. If all three have collapsed, then the newly acquired voltage samples are discarded and the value of the corresponding 13^{th} sample, the oldest one and part of the previous cycle, is used in its place. This process of discarding new samples and replacing them with their pre-fault value can continue ad infinitum through the data windows.

4.7. Software Implementation

The software for the directional overcurrent relay was first implemented in C [45, 46] on a Sun SPARC workstation. This program was then used to model new functions, debug code and for comparison purposes with later microprocessor-based versions. These were implemented in TMS320C25 C [47] and assembly language [48, 49] on a DSP-C25 board, which contains a Texas Instruments (TI) TMS320C25 digital signal processing (DSP) microprocessor, from the Ariel Corporation [50, 51] that is mounted on a host personal computer (PC). TMS320C25 C is based on the Unix System V C language written by Brian W. Kernighan and Dennis M. Ritchie and is compatible with ANSI standard C. An interface program, written in Lattice C, was used to download the program, relay settings and input data to the DSP-C25 board from the host computer and upload output data back to the host for inspection.

The first microprocessor-based version of the relay implemented on the DSP-C25

board used the previously written C code which was then cross-compiled into TMS assembly language. Other ancillary functions were also written to interface with the host PC. Floating point arithmetic was used where applicable, and this was done by a custom set of floating point routines developed by TI for the TMS320C25 DSP chip. In the second microprocessor-based version of the relay existing time critical code was rewritten from floating point to fixed point functions, to reduce the calculation time required during one sampling interval.

Figure 4.9 shows a simplified flowchart describing the operation and structure of the relay software. The relay first goes through an initialization function where user defined relay settings are acquired and processed. At each sampling interval data is acquired and stored in six 13-point data windows, one for each phase voltage and current, from these the real and imaginary components of the voltages and currents can be estimated by the LES filter. The relay then determines if all three instantaneous phase voltages have dropped below the memory polarization setting (MPS); if they have memory polarization is invoked.

The rms currents in the lines and ground circuit are calculated, using the LES filter and linear piece-wise approximation, and compared against the pickup setting for their particular overcurrent unit; this process acts as a fault detecting element. If any of the rms currents exceed pickup, the relay proceeds to estimate the phase voltages and then to evaluate the connection voltages and currents necessary for determining directionality. If all four overcurrent units do not exceed their pickup settings, their trip counters are checked for resetting and another set of data will be acquired. Having a fault detecting element allows the relay to avoid performing unnecessary calculations; there is no need to estimate phase voltages, evaluate connection voltages and currents and determine the direction of power flow if none of the currents are large enough to operate their overcurrent unit.

The torques, ground, phase or polyphase, are then determined by the directional units; which torques are calculated depends on the configuration chosen at the time of commissioning. These torques are then compared against their offsets and based on these

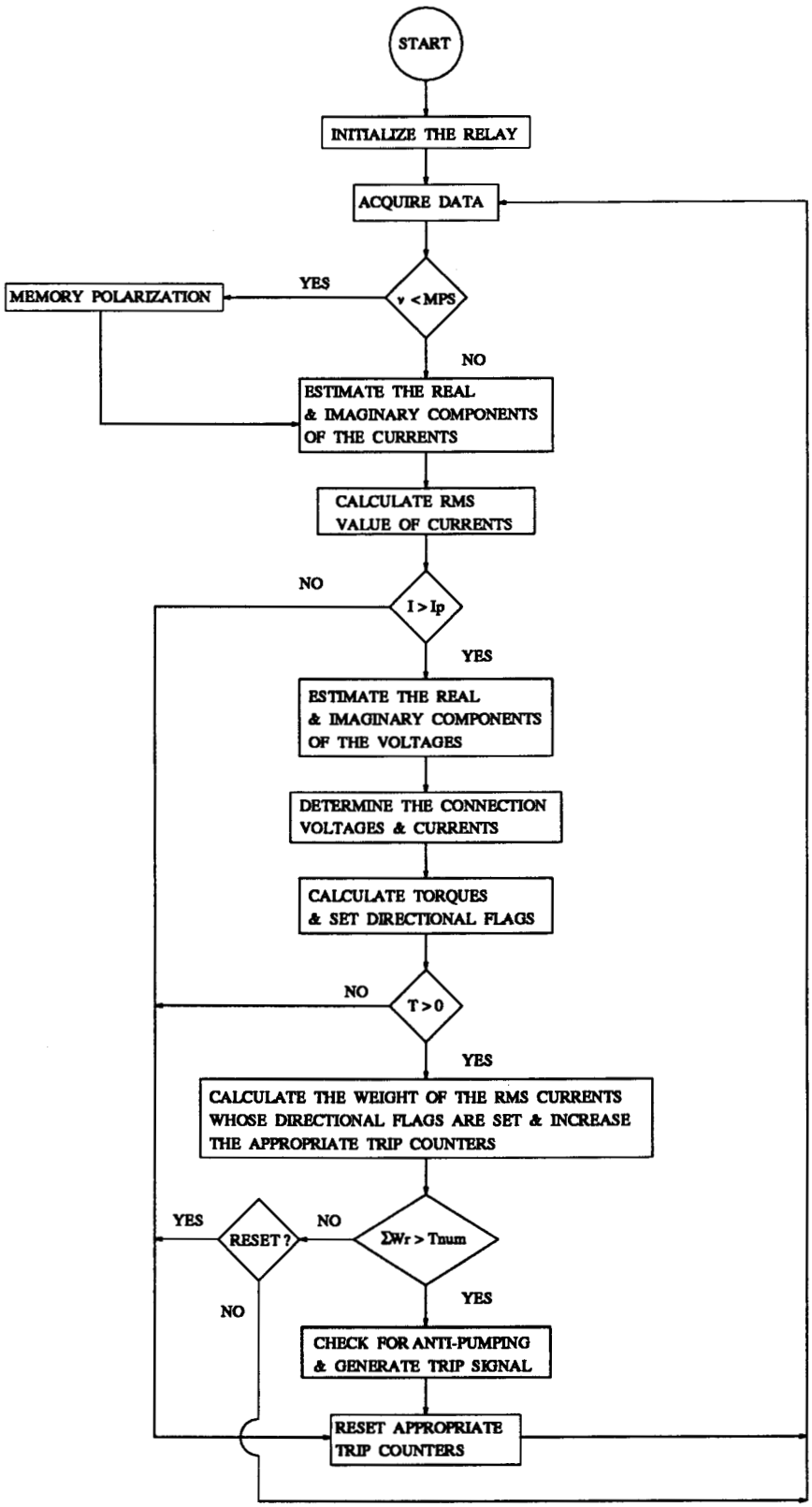

Figure 4.9: A simplified flowchart of the directional overcurrent relay software.

comparisons directional flags are set; if a torque minus its offset is greater than zero the power flow is in the forward direction. The flags indicate the direction of power flow for the overcurrent phase and ground units, allowing individual units to increment their trip counters. If none of the directional units indicate power flow in the tripping direction, the trip counters are checked for resetting, and a new set of data is acquired. When an overcurrent unit's pickup setting has been exceeded and its directional flag is on, it can then determine an appropriate weighting value and increment its trip counter. There are four trip counters (a, b, c and g) representing the four overcurrent inverse-time and instantaneous units.

The tripping logic then determines if the tripping criterion has been met; if it has, a trip signal is generated. There are basically two kinds of tripping that can be implemented: three pole and single pole. Three pole tripping is where all three circuit breakers are tripped for a fault, while single pole tripping is where only the faulted phase's circuit breaker is tripped. The advantage of using single pole tripping is that a higher stability limit can be attained and, therefore there is less shock to the system. In this design three pole tripping was used for all ground faults. Three or single pole tripping were available for both phase fault configurations. Resetting of the relay is then begun after this.

4.8. Summary

In summary this chapter has described the basic design and implementation of a versatile microprocessor-based directional overcurrent relay. It has been shown how the directional element is modelled and torque controls the overcurrent element. A brief review of existing mathematical models for current-time characteristics has been presented leading to the development of an overcurrent element. The implementation of directional instantaneous units and memory polarization for close-in faults have also been discussed. As well, the design of a LES filter used to estimate phasors, and an amplitude estimation technique have been described. Finally, an overall review of the relay's software structure and operation is presented.

5. TESTING AND SYSTEM STUDIES

Chapter four outlined the basic design and structure of the directional overcurrent relay. This chapter describes the testing done to verify the operation of the relay's directional and overcurrent elements. As well, system studies applying the microprocessor-based relay to a model of a transmission network are presented.

5.1. Testing the Directional Element

Typical pre-fault and post-fault waveforms were generated, with a C program on a Sun SPARC workstation, to verify the operation and response of the relay's directional element to known waveforms. The occurrence of a fault when a voltage signal passes through its peak will cause maximum harmonics in its post-fault waveform. Faults occurring near the voltage zero generate maximum dc offsets in the post-fault current signal. Harmonics and dc offsets can be present in both signals and are of a decaying nature, usually dying down to a steady state response a few cycles after the start of the fault. The following equations list the pre- and post-fault waveforms used to generate data for normal steady state operation and for a three-phase fault near a voltage zero. In addition to the fundamental frequency components, decaying harmonics are included in the post-fault waveforms; decaying dc is also present in the current waveform. The data was generated at 720 Hz, quantized using the A/D model described in Appendix C and then processed by the relay, no prefiltering is done on the data.

Pre-fault Waveforms:

$$v(t) = \sin(\omega t), \tag{5.1}$$

$$i(t) = \sin(\omega t - 20°). \tag{5.2}$$

Post-fault Waveforms:

$$v(t) = 0.8\sin(\omega t) + (0.2\sin(3\omega t) + 0.1\sin(5\omega t))\, e^{-t/0.025}, \tag{5.3}$$

$$i(t) = 10\sin(\omega t - 70°) + 2.6e^{-t/0.020} + 0.2\sin(3\omega t - \frac{70°}{3})\, e^{-t/0.025}. \tag{5.4}$$

Figures 5.1(a) and (b) show the torques generated by the relay under pre-fault and post-fault conditions. The plots start at time zero to highlight the transient region due to start up or a fault. In both cases, after the transient region is passed, the relay torques reach steady state values closely approximating the theoretical values for the pre- and post-fault cases of 0.66 pu and 6.82 pu respectively. The small variations in post-fault torques are due to decaying dc, as the LES filter has modeled only two terms for it.

5.2. Testing the Overcurrent Element

The overcurrent element was tested by generating, in software, a constant multiple of rms current and recording the number of sampling intervals required to issue a trip signal based on this current. All three current-time characteristics were tested at TMS's of 0.1 and 1.0, and the results are presented in Tables 5.1 to 5.6. Results do not include errors caused by A/D conversion, peak value estimation and rms magnitude approximation of the fundamental frequency current. However, the values will include errors due to the single precision floating point arithmetic functions used. Further results are included in Appendix F for TMS's of 0.5 and 1.6. The tables list the relay operating time in seconds calculated from the number of sampling intervals required to generate a trip signal, theoretical IEC time determined from Equation 4.16 and constants listed in Table 4.1, percentage difference and the difference in cycles of 60 Hz. The tables show that the relay can effectively emulate the selected IEC current-time characteristics; differences are all within ± 5% or 3 cycles of 60 Hz. As well, the addition to the lookup table of current multiples 1.5, 2.5 and 3.5 has decreased the error in those regions for the extremely and standard inverse curves. As the TMS increases from 0.1 to 1.6 the errors rise slightly due to truncation of the mantissa in single precision floating point arithmeti; however, the normal maximum TMS is 1.6 and the error is within acceptable limits at this setting.

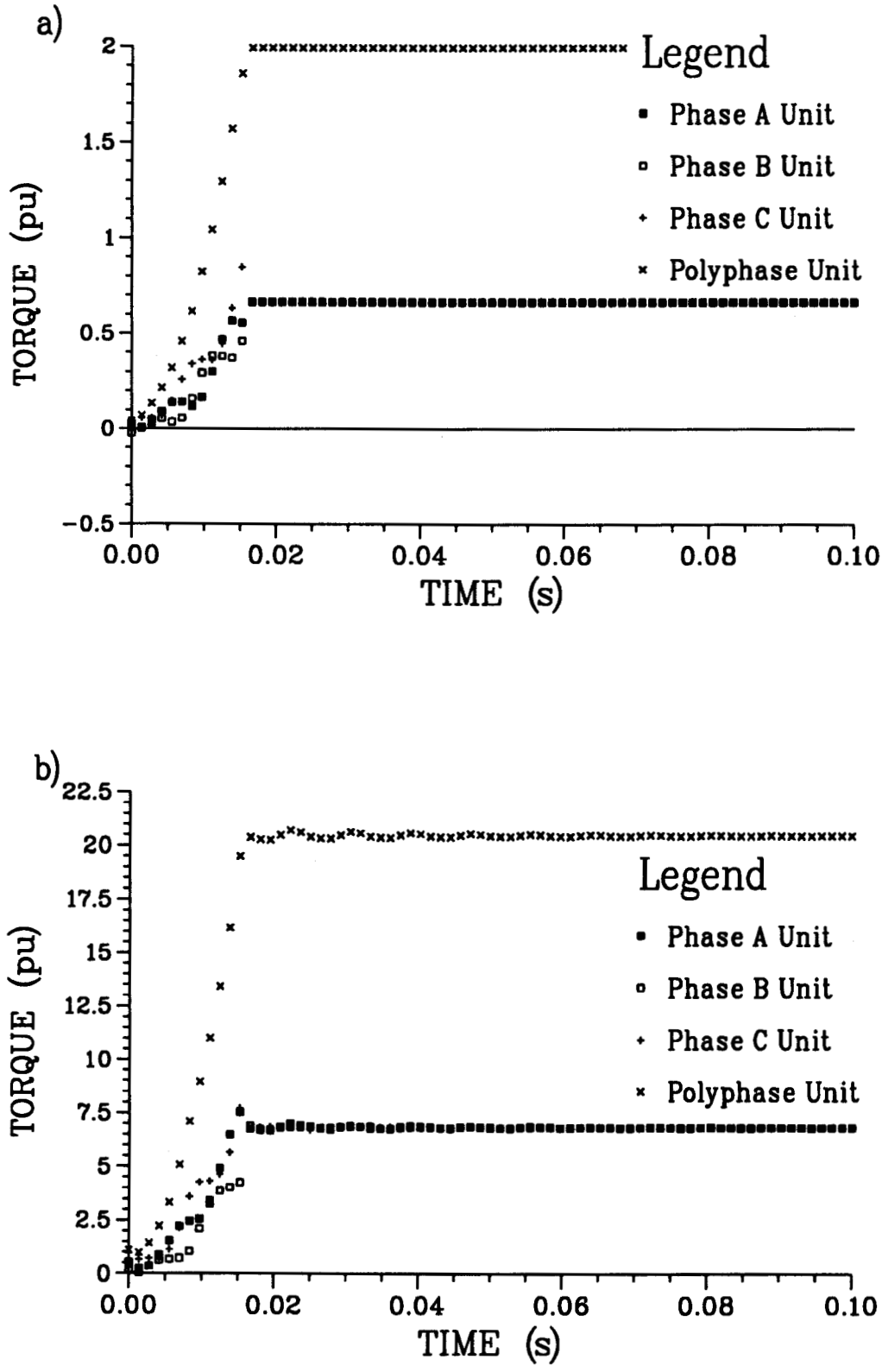

Figure 5.1: Torques generated by the relay under a) pre-fault and b) post-fault conditions with a MTA of 30° for the directional phase units.

Table 5.1: The performance of the extremely inverse current-time characteristic at TMS=1.0.

Current Multiple	Relay Time (s)	IEC Time (s)	Percent Difference	Cycle Difference
1.5	64.015278	64.000000	0.023872	0.916667
2.0	26.681944	26.666667	0.057292	0.916667
2.5	15.240278	15.238095	0.014323	0.130952
3.0	10.001389	10.000000	0.013889	0.083333
3.5	7.112500	7.111111	0.019531	0.083333
4.0	5.334722	5.333333	0.026042	0.083333
4.5	4.104167	4.155844	-1.243490	-3.100649
5.0	3.334722	3.333333	0.041667	0.083333
5.5	2.712500	2.735043	-0.824219	-1.352564
6.0	2.286111	2.285714	0.017361	0.023810
6.5	1.929167	1.939394	-0.527344	-0.613636
7.0	1.668056	1.666667	0.083333	0.083333
7.5	1.441667	1.447964	-0.434896	-0.377828
8.0	1.270833	1.269841	0.078125	0.059524
8.5	1.119444	1.122807	-0.299479	-0.201754
9.0	1.001389	1.000000	0.138889	0.083333
9.5	0.894444	0.896359	-0.213542	-0.114846
10.0	0.808333	0.808081	0.031250	0.015152
12.5	0.515278	0.515298	-0.003906	-0.001208
15.0	0.358333	0.357143	0.333333	0.071429
17.5	0.262500	0.262080	0.160156	0.025184
20.0	0.201389	0.200501	0.442708	0.053258

Table 5.2: The performance of the extremely inverse current-time characteristic at TMS=0.1.

Current Multiple	Relay Time (s)	IEC Time (s)	Percent Difference	Cycle Difference
1.5	6.401389	6.400000	0.021701	0.083333
2.0	2.668056	2.666667	0.052083	0.083333
2.5	1.525000	1.523810	0.078125	0.071429
3.0	1.001389	1.000000	0.138889	0.083333
3.5	0.712500	0.711111	0.195312	0.083333
4.0	0.534722	0.533333	0.260417	0.083333
4.5	0.411111	0.415584	-1.076389	-0.268398
5.0	0.334722	0.333333	0.416667	0.083333
5.5	0.272222	0.273504	-0.468750	-0.076923
6.0	0.229167	0.228571	0.260417	0.035714
6.5	0.193056	0.193939	-0.455729	-0.053030
7.0	0.168056	0.166667	0.833333	0.083333
7.5	0.144444	0.144796	-0.243056	-0.021116
8.0	0.127778	0.126984	0.625000	0.047619
8.5	0.112500	0.112281	0.195313	0.013158
9.0	0.101389	0.100000	1.388889	0.083333
9.5	0.090278	0.089636	0.716146	0.038515
10.0	0.081944	0.080808	1.406250	0.068182
12.5	0.052778	0.051530	2.421875	0.074879
15.0	0.036111	0.035714	1.111111	0.023810
17.5	0.026389	0.026208	0.690104	0.010852
20.0	0.020833	0.020050	3.906250	0.046992

Table 5.3: The performance of the very inverse current-time characteristic at TMS=1.0.

Current Multiple	Relay Time (s)	IEC Time (s)	Percent Difference	Cycle Difference
1.5	27.001389	27.000000	0.005144	0.083333
2.0	13.501389	13.500000	0.010288	0.083333
2.5	9.001389	9.000000	0.015432	0.083333
3.0	6.751389	6.750000	0.020576	0.083333
3.5	5.401389	5.400000	0.025720	0.083333
4.0	4.501389	4.500000	0.030864	0.083333
4.5	3.858333	3.857143	0.030864	0.071429
5.0	3.376389	3.375000	0.041152	0.083333
5.5	3.001389	3.000000	0.046296	0.083333
6.0	2.701389	2.700000	0.051440	0.083333
6.5	2.455556	2.454545	0.041152	0.060606
7.0	2.251389	2.250000	0.061728	0.083333
7.5	2.077778	2.076923	0.041152	0.051282
8.0	1.929167	1.928571	0.030864	0.035714
8.5	1.801389	1.800000	0.077160	0.083333
9.0	1.688889	1.687500	0.082305	0.083333
9.5	1.588889	1.588235	0.041152	0.039216
10.0	1.501389	1.500000	0.092593	0.083333
12.5	1.175000	1.173913	0.092593	0.065217
15.0	0.965278	0.964286	0.102881	0.059524
17.5	0.819444	0.818182	0.154321	0.075758
20.0	0.711111	0.710526	0.082305	0.035088

Table 5.4: The performance of the very inverse current-time characteristic at TMS=0.1.

Current Multiple	Relay Time (s)	IEC Time (s)	Percent Difference	Cycle Difference
1.5	2.701389	2.700000	0.051440	0.083333
2.0	1.351389	1.350000	0.102881	0.083333
2.5	0.901389	0.900000	0.154321	0.083333
3.0	0.676389	0.675000	0.205761	0.083333
3.5	0.540278	0.540000	0.051440	0.016667
4.0	0.451389	0.450000	0.308642	0.083333
4.5	0.386111	0.385714	0.102881	0.023810
5.0	0.338889	0.337500	0.411523	0.083333
5.5	0.301389	0.300000	0.462963	0.083333
6.0	0.270833	0.270000	0.308642	0.050000
6.5	0.245833	0.245455	0.154321	0.022727
7.0	0.226389	0.225000	0.617284	0.083333
7.5	0.208333	0.207692	0.308642	0.038462
8.0	0.193056	0.192857	0.102881	0.011905
8.5	0.180556	0.180000	0.308642	0.033333
9.0	0.169444	0.168750	0.411523	0.041667
9.5	0.159722	0.158824	0.565844	0.053922
10.0	0.151389	0.150000	0.925926	0.083333
12.5	0.118056	0.117391	0.565844	0.039855
15.0	0.097222	0.096429	0.823045	0.047619
17.5	0.081944	0.081818	0.154321	0.007576
20.0	0.072222	0.071053	1.646091	0.070175

Table 5.5: The performance of the standard inverse current-time characteristic at TMS=1.0.

Current Multiple	Relay Time (s)	IEC Time (s)	Percent Difference	Cycle Difference
1.5	17.197222	17.194219	0.017467	0.180203
2.0	10.030556	10.029027	0.015241	0.091712
2.5	7.570833	7.569710	0.014834	0.067371
3.0	6.302778	6.301931	0.013438	0.050811
3.5	5.519444	5.517942	0.027237	0.090176
4.0	4.980556	4.979756	0.016054	0.047967
4.5	4.604167	4.584367	0.431900	1.187994
5.0	4.280556	4.279720	0.019522	0.050129
5.5	4.047222	4.036576	0.263737	0.638756
6.0	3.837500	3.837192	0.008015	0.018453
6.5	3.676389	3.670148	0.170040	0.374443
7.0	3.529167	3.527742	0.040372	0.085454
7.5	3.409722	3.404583	0.150958	0.308369
8.0	3.297222	3.296774	0.013607	0.026916
8.5	3.205556	3.201426	0.128984	0.247759
9.0	3.116667	3.116350	0.010163	0.019002
9.5	3.043056	3.039851	0.105411	0.192260
10.0	2.970833	2.970599	0.007901	0.014083
12.5	2.704167	2.702067	0.077715	0.125994
15.0	2.516667	2.515517	0.045685	0.068952
17.5	2.377778	2.376338	0.060579	0.086373
20.0	2.268056	2.267356	0.030837	0.041951

Table 5.6: The performance of the standard inverse current-time characteristic at TMS=0.1.

Current Multiple	Relay Time (s)	IEC Time (s)	Percent Difference	Cycle Difference
1.5	1.720833	1.719422	0.082089	0.084687
2.0	1.004167	1.002903	0.126031	0.075838
2.5	0.758333	0.756971	0.179965	0.081737
3.0	0.630556	0.630193	0.057516	0.021748
3.5	0.552778	0.551794	0.178260	0.059018
4.0	0.498611	0.497976	0.127617	0.038130
4.5	0.461111	0.458437	0.583381	0.160466
5.0	0.429167	0.427972	0.279144	0.071680
5.5	0.405556	0.403658	0.470182	0.113876
6.0	0.384722	0.383719	0.261383	0.060179
6.5	0.368056	0.367015	0.283568	0.062444
7.0	0.352778	0.352774	0.001002	0.000212
7.5	0.341667	0.340458	0.354931	0.072504
8.0	0.330556	0.329677	0.266380	0.052692
8.5	0.320833	0.320143	0.215750	0.041443
9.0	0.312500	0.311635	0.277570	0.051900
9.5	0.305556	0.303985	0.516615	0.094226
10.0	0.297222	0.297060	0.054656	0.009742
12.5	0.270833	0.270207	0.231917	0.037599
15.0	0.252778	0.251552	0.487388	0.073562
17.5	0.238889	0.237634	0.528152	0.075304
20.0	0.227778	0.226736	0.459628	0.062528

5.3. System Studies Using EMTP

The performance of the microprocessor-based relay was also evaluated using data obtained from simulating faults with the Electro-Magnetic Transients Program (EMTP) on a six-bus model of the Saskatchewan Power Corporation's (SPC) transmission network, both of which are described in Appendices D and E. Figure 5.2 shows the one line diagram of the six-bus test system.

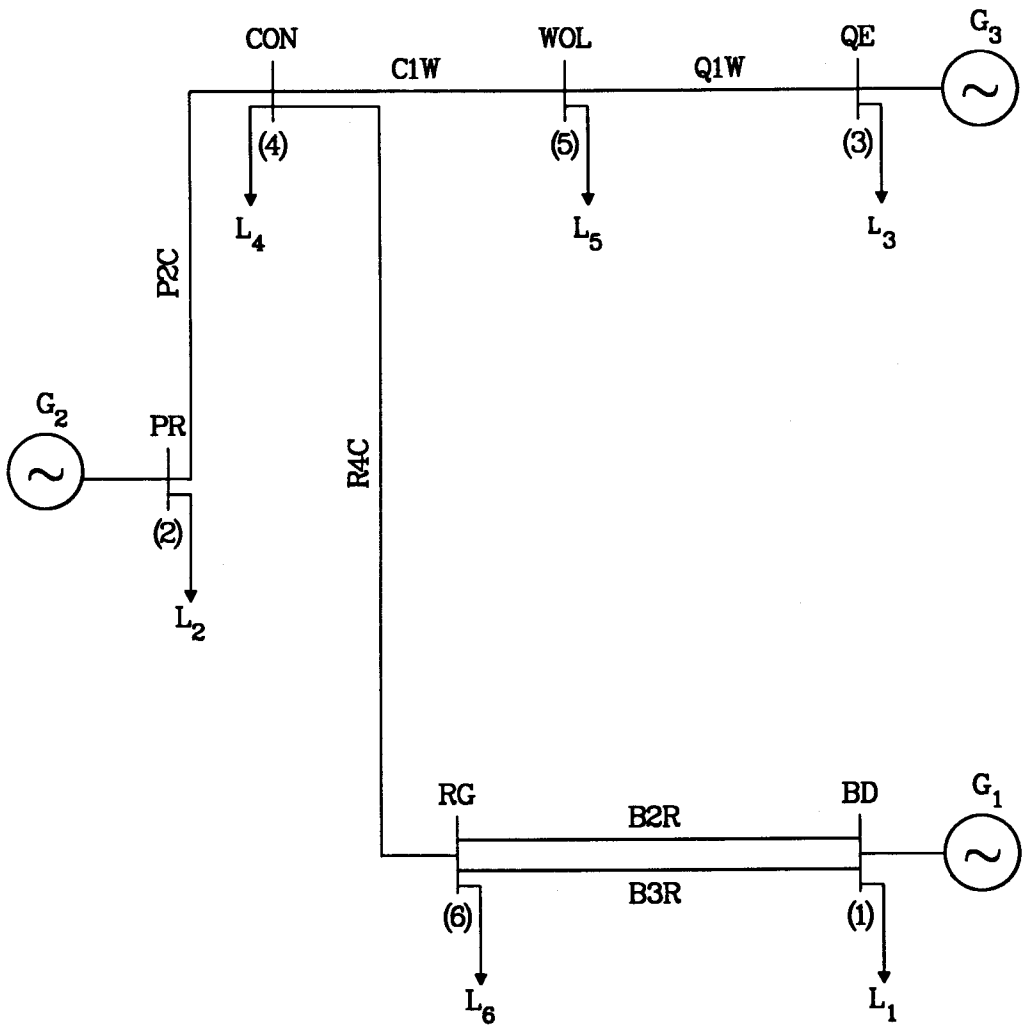

Figure 5.2: One line diagram of the SPC six-bus test system.

The following types of faults were simulated at the midpoint of line P2C.

1. Single-phase-to-ground fault.
2. Three-phase fault.
3. Two-phase fault.
4. Two-phase-to-ground fault.

In the following simulations a directional sensing connection of 90° was used with the directional phase units, and both residual and negative sequence quantities were used with the ground unit, with MTA's of $-60°$ and 90° respectively. Appendix F lists further results using different directional sensing connections with the phase units. The sampling frequency used by EMTP to generate fault data was set high, f_s=23040 Hz, so that it could approximate a continuous signal along with its high frequency components, frequency components up to $\frac{1}{2}f_s$ are present in the EMTP output. The EMTP output data was then pre-processed by a digital anti-aliasing filter implemented in Fortran on a Sun SPARC workstation. This filter is described in Appendix A. The data was then resampled to change the sampling rate, f_s, to 720 Hz, scaled and quantized using the A/D model described in Appendix C. The data was then ready to be downloaded to the Ariel DSP-C25 board by the Lattice C interface program.

5.3.1. Single-Phase-To-Ground Faults

A single-phase-to-ground fault was simulated at the midpoint of line P2C for a relay at bus Poplar River (PR) whose tripping direction is towards bus Condie (CON). Figure 5.3 shows the voltage and current waveforms at bus PR for an *A* phase-to-ground fault on line P2C; Figure 5.4 shows these waveforms after they have been filtered and resampled at 720 Hz, demonstrating the effect of the anti-aliasing filter designed in Appendix A.

The torque produced by each directional phase unit, with a MTA of 30°, and the resulting polyphase torque is displayed in Figure 5.5(a). All pre-fault torques are constant and positive indicating that the power flow is away from bus PR and in the tripping direction. In the fault region the torque produced by the phase A unit begins to increase in response to the rise in phase *A* current. The unfaulted phases *B* and *C*

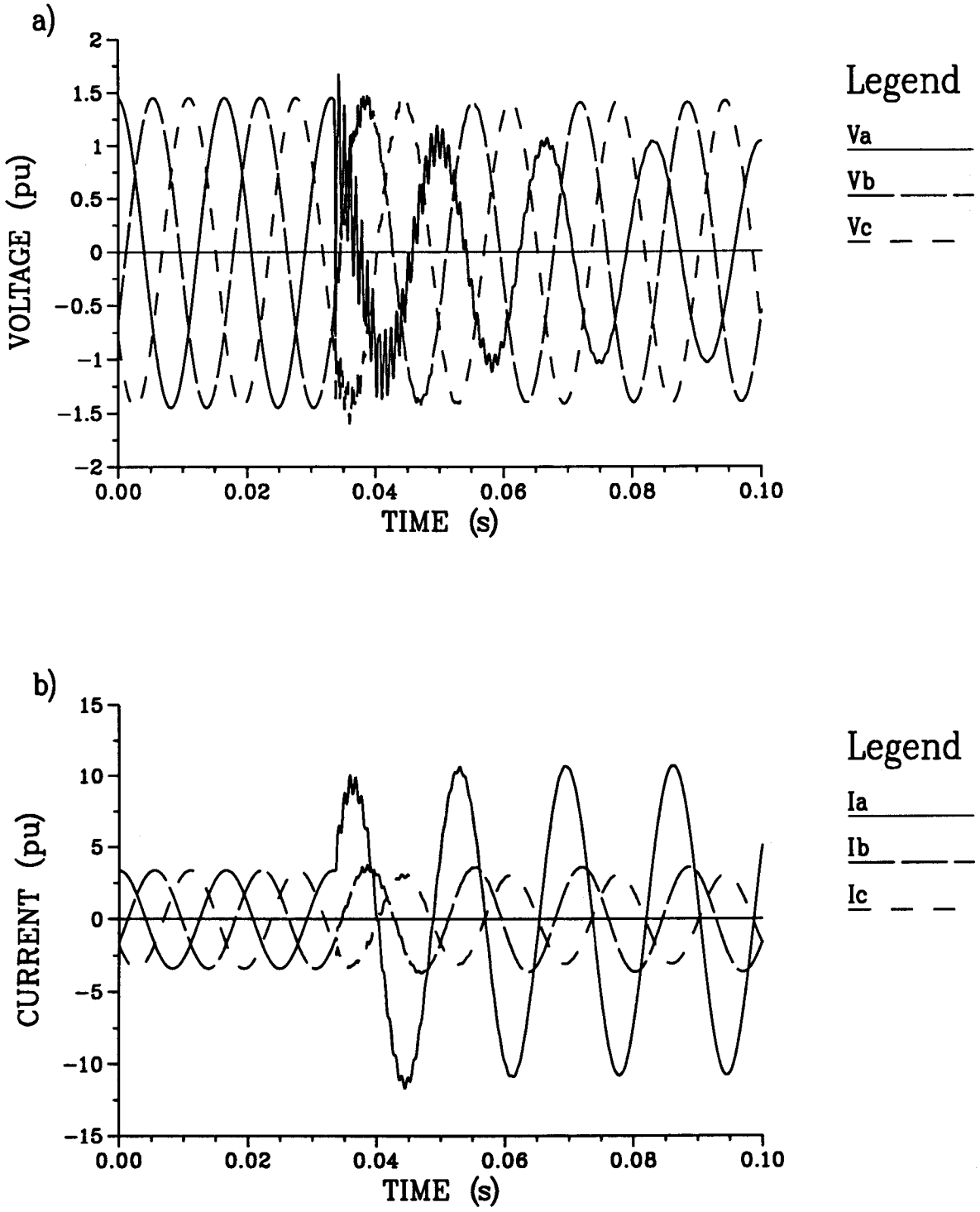

Figure 5.3: The a) voltage and b) current waveforms at the relay for line P2C at bus PR for a single-phase-to-ground fault.

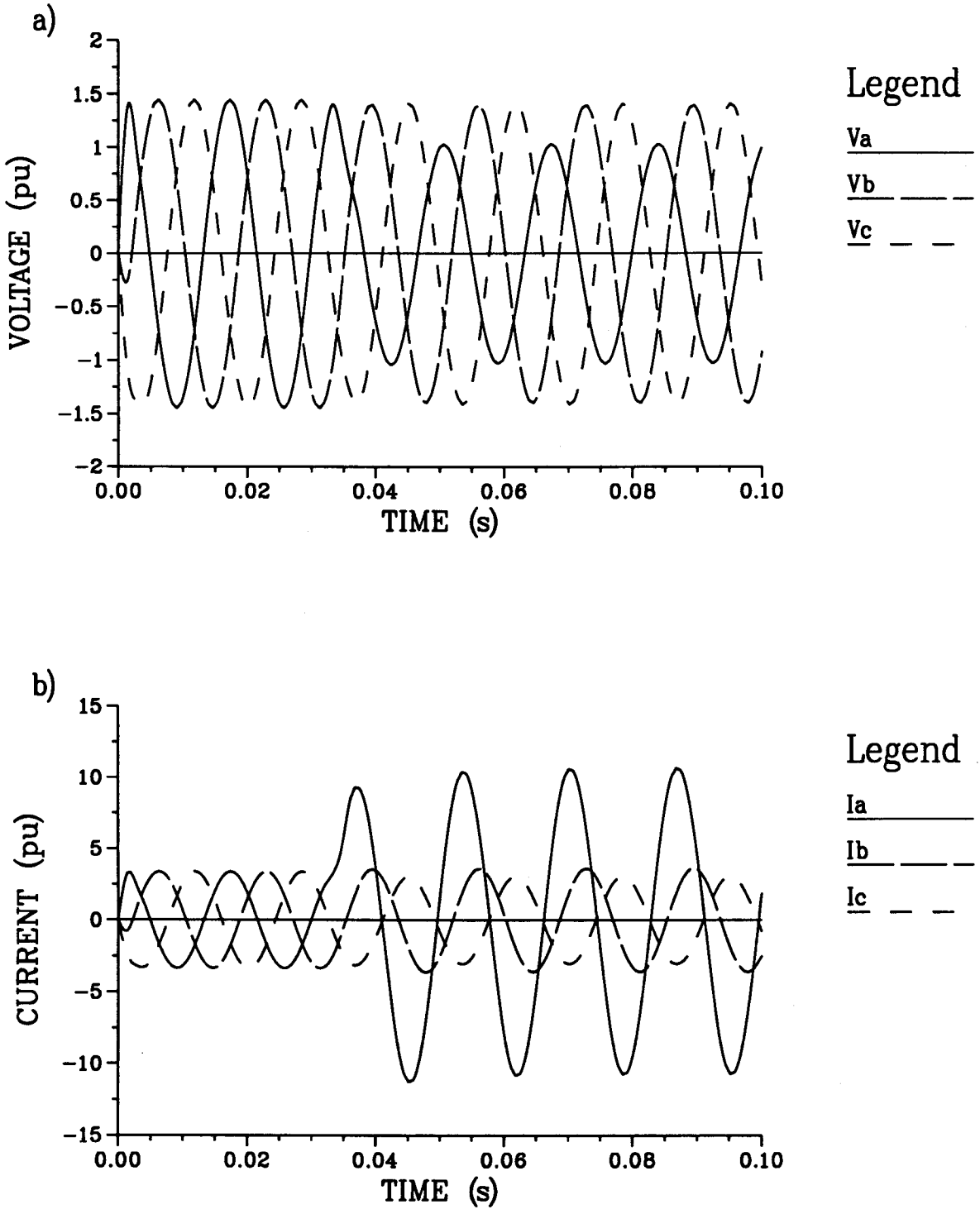

Figure 5.4: Filtered and resampled a) voltage and b) current waveforms at the relay for line P2C at bus PR for a single-phase-to-ground fault.

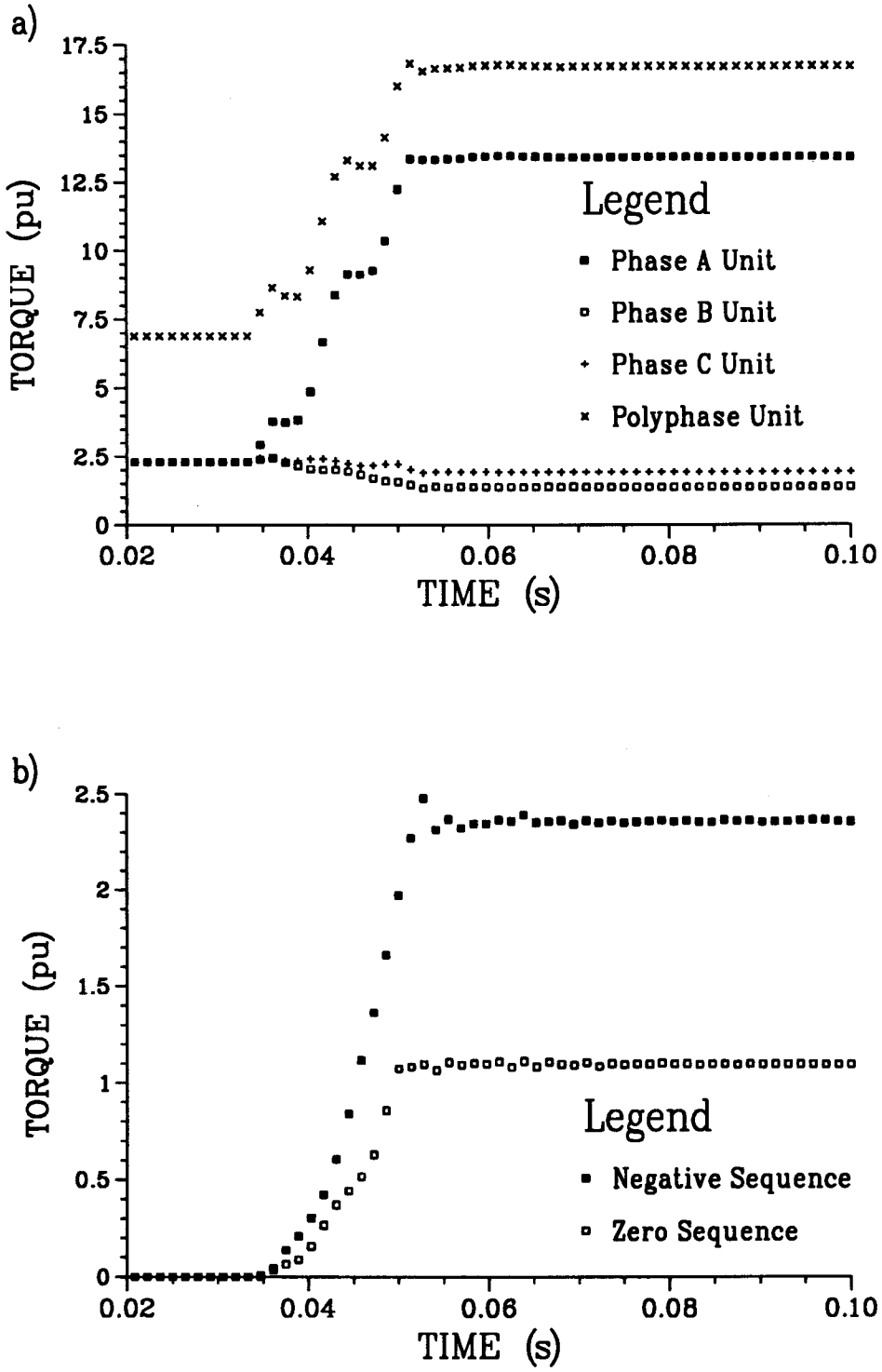

Figure 5.5: Torques developed by the relay for line P2C at bus PR for a single-phase-to-ground fault with a) a MTA of 30° for the directional phase units and b) MTA's of –60° and 90° for the directional ground unit when polarized with zero and negative sequence quantities respectively.

experience an increase in phase angle between the relay inputs and a drop in current respectively; thus resulting in a reduction of generated torque. The polyphase torque shown in the figure is dominated by the production of torque from the phase A unit. Figure 5.5(b) shows the torque generated by the ground unit using zero and negative sequence polarization. From this figure it is evident that a greater amount of negative sequence torque is produced than zero sequence and this is in part due to the use of $3V_2$ and $3I_2$. However, both torques increase from zero after the inception of the fault, and their magnitudes are not as large as the polyphase torque. Because zero sequence torque is normally zero and only generated when there is an imbalance, the ground unit is better than the phase unit in determining the direction of ground faults. Negative sequence polarization is also shown to be a valid alternative; even though torque is generated during phase faults the ground overcurrent unit will not increment its trip counter because no zero sequence current is present. The torques change one sampling interval after the occurrence of the fault demonstrating the sensitivity of the relay to a change in system conditions. Part of this delay is attributable to the time delay of the anti-aliasing filter used to prefilter the data.

Figure 5.6 shows the incrementing of the trip counters for the phase and ground overcurrent units using an extremely inverse current-time characteristic, a TMS of 1.0, pickup settings of 1.5 times pre-fault load current and 0.707 pu respectively and a default target number of one. This figure demonstrates that that the ground unit is much more effective due to its lower pickup setting and only the faulted phase unit is operating among the phase units.

Figure 5.7 shows the torque produced when a MTA of 45° is used with the directional phase units. The results are similar to those shown in Figure 5.5(a) except that all pre-fault torques and the post-fault torques of the B and C units are higher while the phase A unit's post-fault torque is less. This is due to the change in phase angle between the relay inputs and the MTA because the maximum torque line is closer to the pre-fault current and farther away from the faulted current. So, while the 45° MTA generates higher pre-fault and unfaulted post-fault torque, it does not generate as much torque in the faulted phase which is highly desirable.

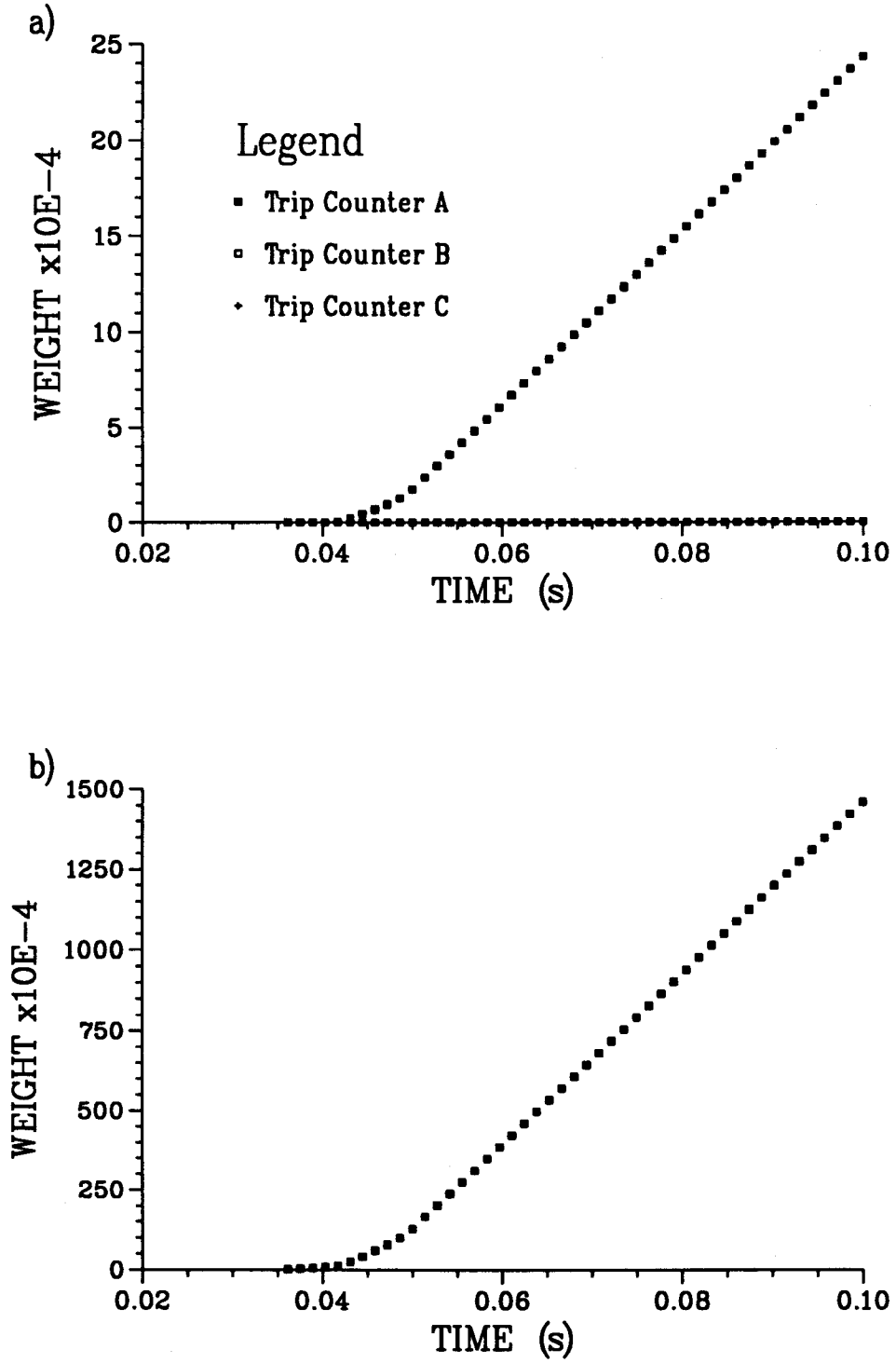

Figure 5.6: The incrementing of the trip counters of the overcurrent a) phase units and b) ground unit for line P2C at bus PR for a single-phase-to-ground fault.

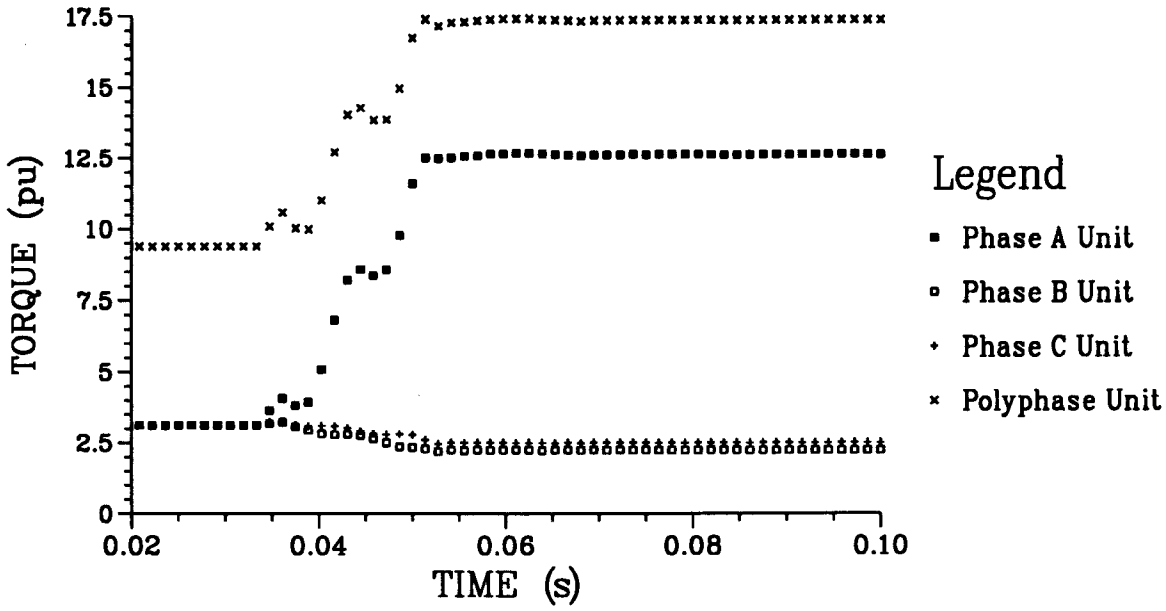

Figure 5.7: Torques developed by the relay for line P2C at bus PR for a single-phase-to-ground fault with a MTA of 45° for the directional phase units.

Due to the window size of the LES filters, the estimated voltages and currents take some time to transit from the pre-fault to the post-fault region. This causes a similar time lag in the estimated torque as it moves from its pre-fault to its fault level. For the directional phase units, if the normal direction of power flow and the fault direction are the same, the delay is minimal as the torque is normally positive and in this case is just increasing to its during-fault level. But if the normal direction of power flow and the fault direction are opposite to each other, the sign of the estimated torque will take a number of samples to change from negative to positive in the faulted phase. As is the case for a fault at the midpoint of line P2C with a relay located at bus CON whose tripping direction is towards bus PR.

Figure 5.8 shows the voltage and current waveforms at the relay for line P2C located at bus CON for a single-phase-to-ground fault. Figure 5.9(a) displays the torques generated by the directional phase units, with a MTA of 30°, and the polyphase torque.

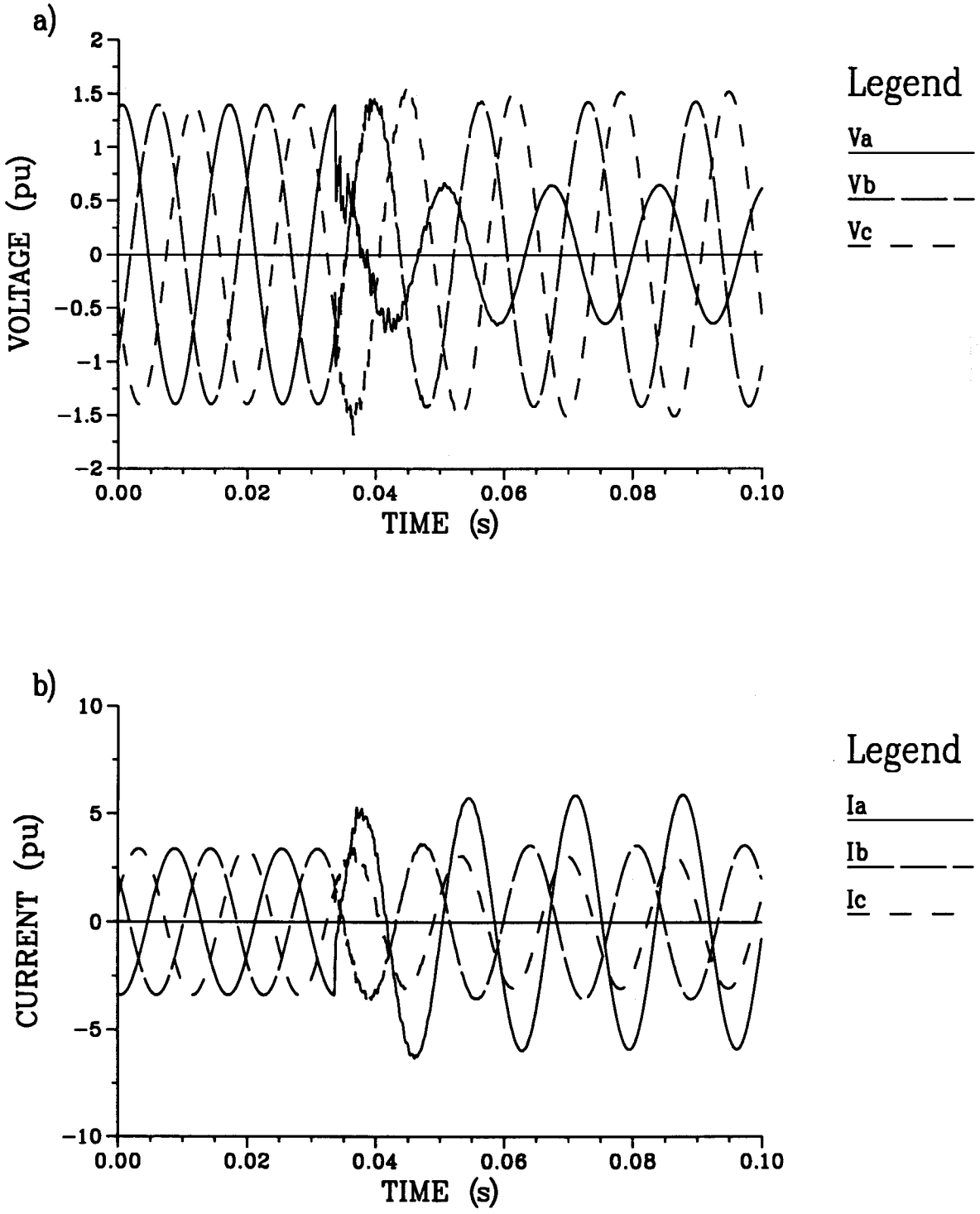

Figure 5.8: The a) voltage and b) current waveforms at the relay for line P2C at bus CON for a single-phase-to-ground fault.

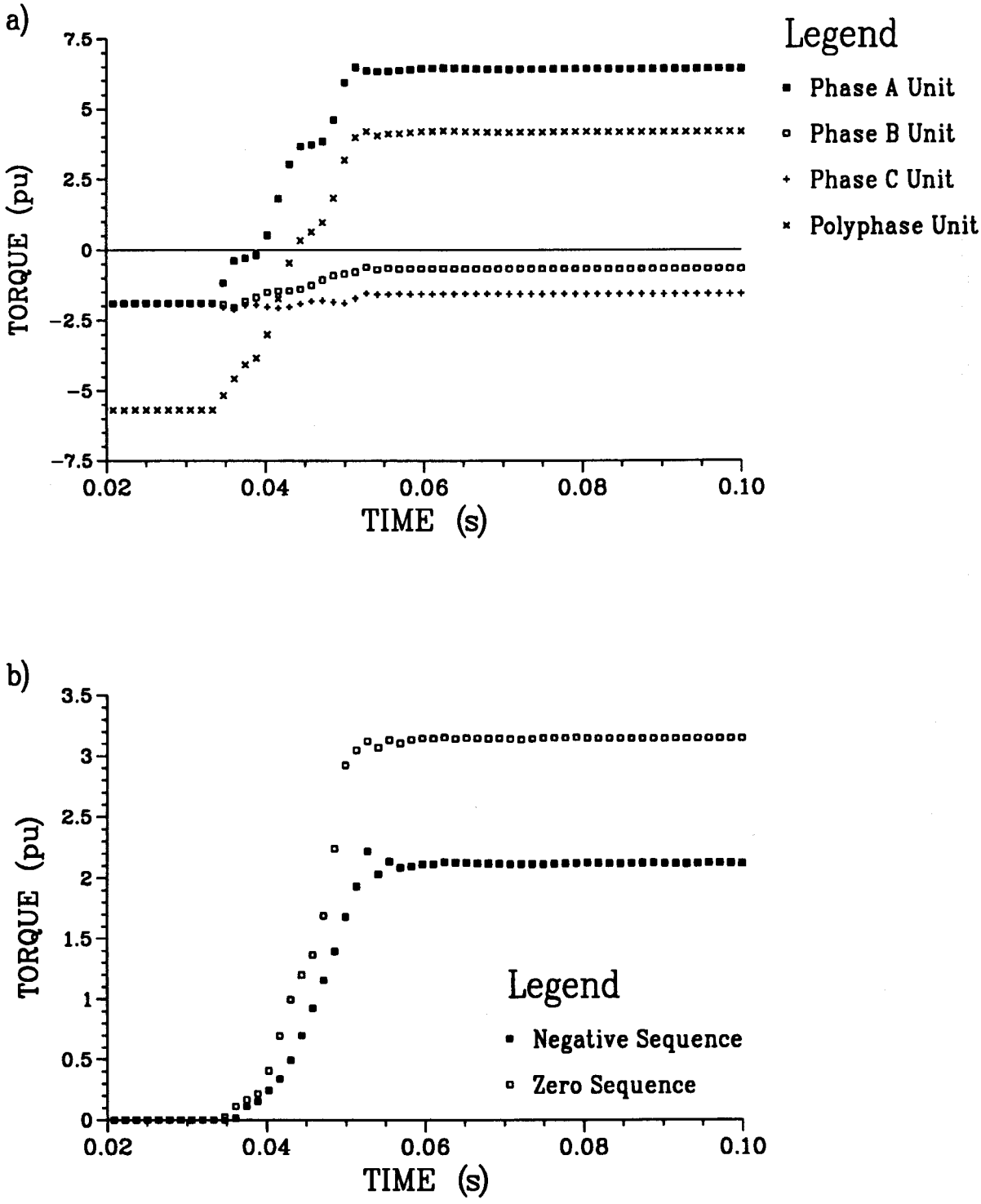

Figure 5.9: Torques developed by the relay for line P2C at bus CON for a single-phase-to-ground fault with a) a MTA of 30° for the directional phase units and b) MTA's of –60° and 90° for the directional ground unit when polarized with zero and negative sequence quantities respectively.

Figure 5.9(b) shows the torques generated by the ground unit with MTA's of –60° and 90° using zero and negative sequence polarization respectively. The torques produced by the directional units in the pre-fault region are negative because the power flow is towards bus CON while the relay's tripping direction is away from bus CON towards bus PR. In the fault region the phase A unit torque begins to increase, eventually attaining a positive value indicating a reversal in power flow. The torque generated by the B and C units remains negative indicating that the power in these two phases is still flowing towards bus CON. This can also be seen in Figure 5.8 where there is no major phase shift in the unfaulted phases as opposed to phase *A*.

Five samples are needed for the phase A unit torque and eight samples are needed by the polyphase torque to change polarity. Even though the case discussed is a single-phase-to-ground fault and the ground unit would be expected to process it, the scenario holds true for phase faults. For a fault in either the tripping or non-tripping direction this did not affect the directional ground unit as its normal torque value is zero. As shown in Figure 5.9(b) the ground unit is quite sensitive to the onset of a ground fault; its pickup and decision about the direction of power flow would be quicker than the phase units regardless of configuration. Figure 5.10 shows the phase unit and polyphase torque generated with a MTA of 45°. It is apparent that the torques are less than that shown in Figure 5.9(a).

5.3.2. Three-Phase Fault

The voltage and current waveforms at bus PR for a three-phase fault on line P2C are shown in Figure 5.11. Figure 5.12(a) shows the torques generated by the directional phase units, with a MTA of 30°, and the resulting polyphase torque. In the pre-fault region, the torques are stable and positive; at the onset of the fault, they begin to increase in response to the fault current. Since there is no phase imbalance the torque produced by the ground unit, shown in Figure 5.12(b), remains at zero; there is a small amount produced with negative sequence polarization but this passes as the data window moves over the fault point. The torques generated when a MTA of 45° is used with the directional phase units, shown in Figure 5.13, are similar to those of Figure 5.12(a) but are larger in the pre-fault region and smaller in the post-fault region.

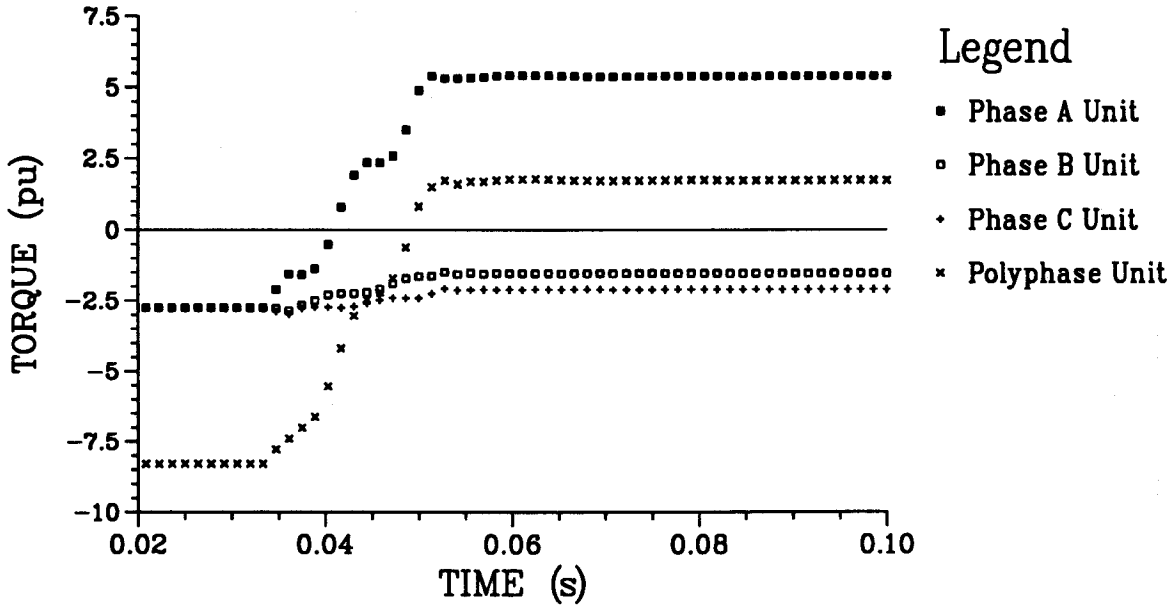

Figure 5.10: Torques developed by the relay for line P2C at bus CON for a single-phase-to-ground fault with a MTA of 45° for the directional phase units.

In both figures there is some ripple in the post-fault phase B and C unit torques, which quickly decays, due to the decaying dc component of their fault currents. The decay rate of the dc current is so large, evident in the faulted current waveforms, that the first two terms of the Taylor's series expansion of an exponential does not completely suppress this effect in the LES filter. This effect will vary depending on the phase angle of the voltage at the time of the inception of the fault, as evidenced by the phase A unit torque which does not exhibit any noticeable ripple.

5.3.2.1. Close-In Three-Phase Fault

The voltage and current waveforms at bus PR for a close-in three-phase fault, 2.4 km from bus PR, on line P2C are shown in Figure 5.14. Figure 5.15(a) shows the torques generated by the directional phase units, with a MTA of 30°, using memory polarization. Figure 5.16(a) shows the torques generated by the directional phase units, with a MTA of 30°, without memory polarization. From these two figures it is evident that the torque produced with memory polarization is superior to that produced without; thus, with memory polarization directional discrimination can be maintained. In either figure the ground unit torque is not greatly affected by the absence or presence of memory polarization, except to remove the transient negative sequence torque.

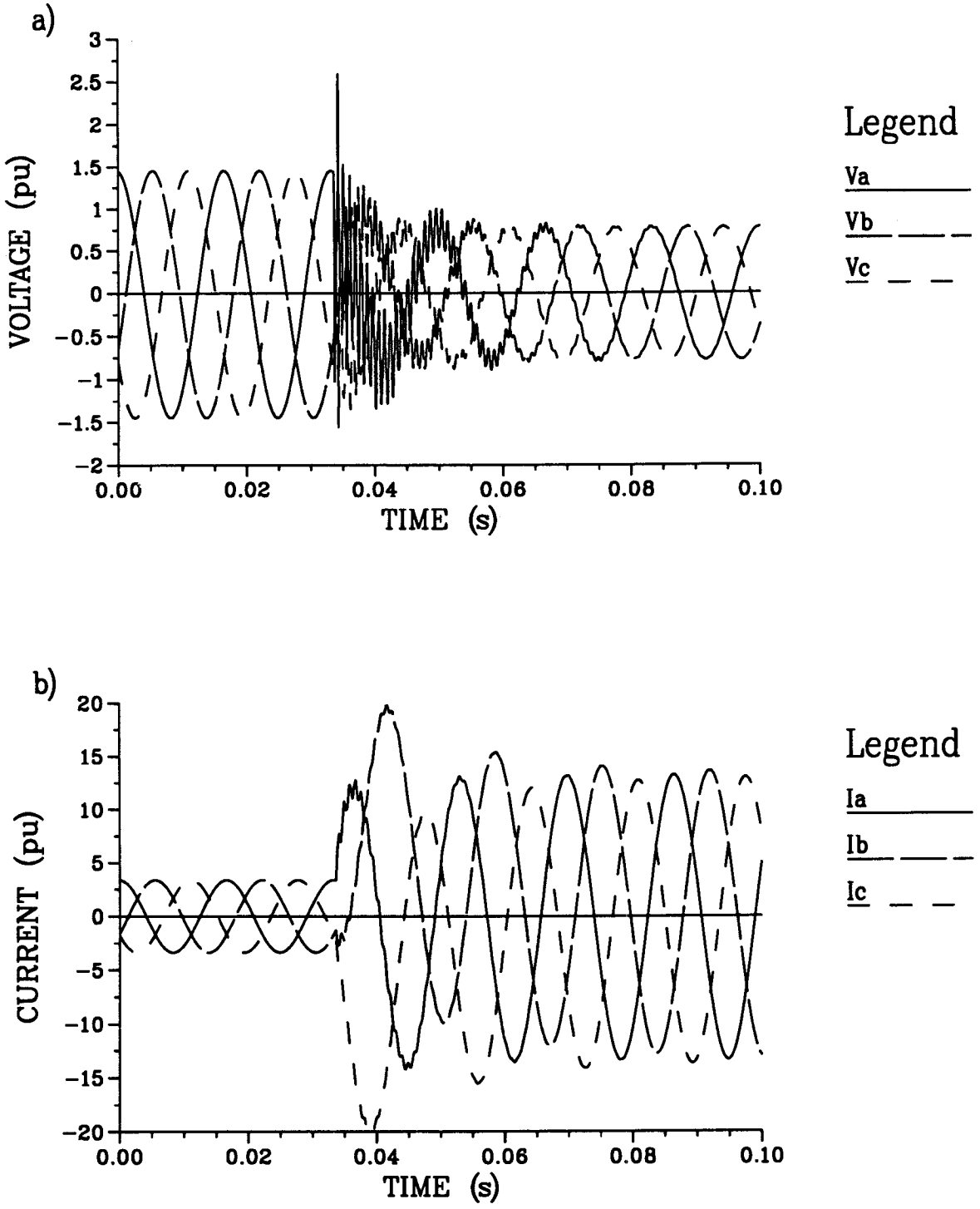

Figure 5.11: The a) voltage and b) current waveforms at the relay for line P2C at bus PR for a three-phase fault.

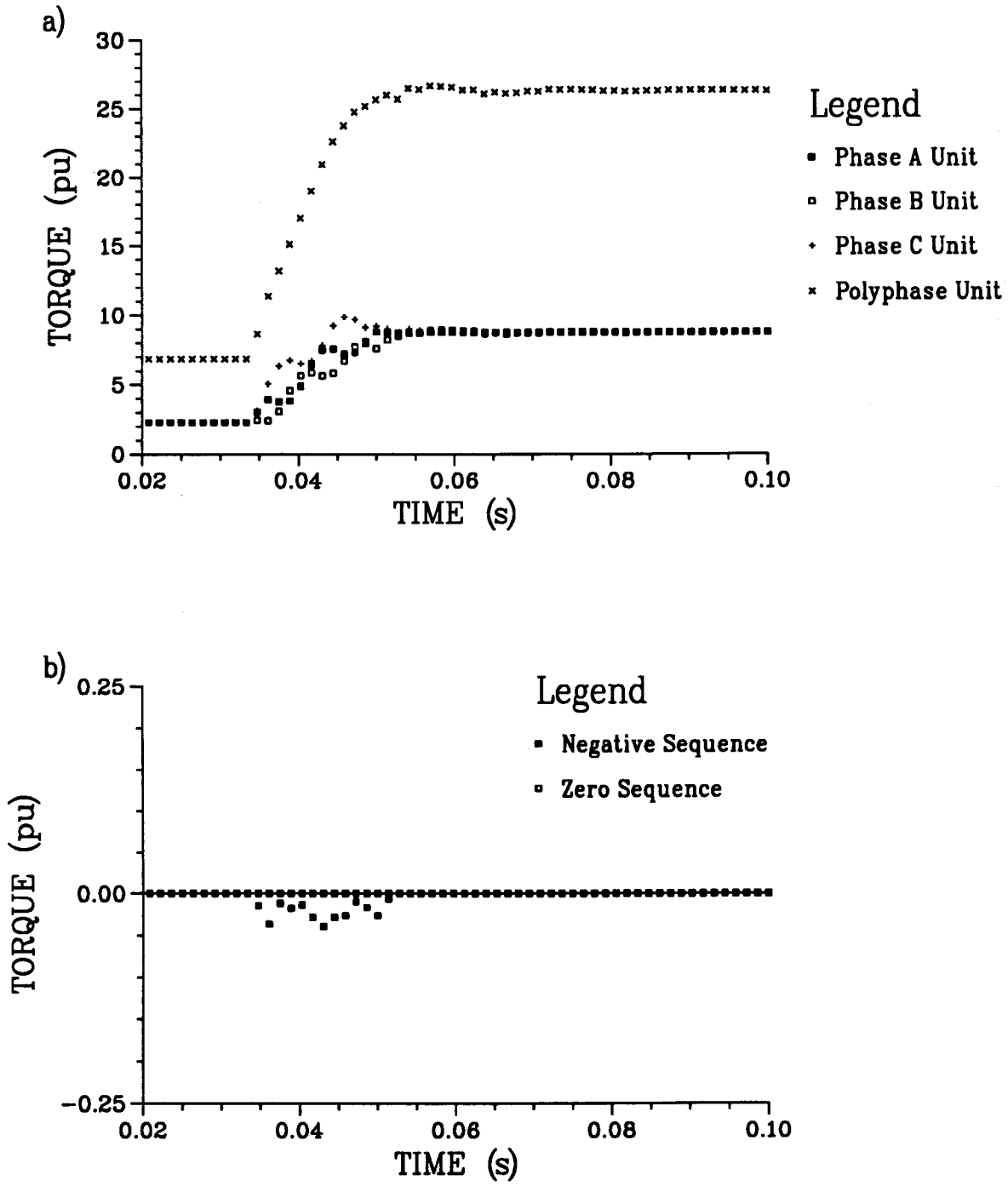

Figure 5.12: Torques developed by the relay for line P2C at bus PR for a three-phase fault with a) a MTA of 30° for the directional phase units and b) MTA's of –60° and 90° for the directional ground unit when polarized with zero and negative sequence quantities respectively.

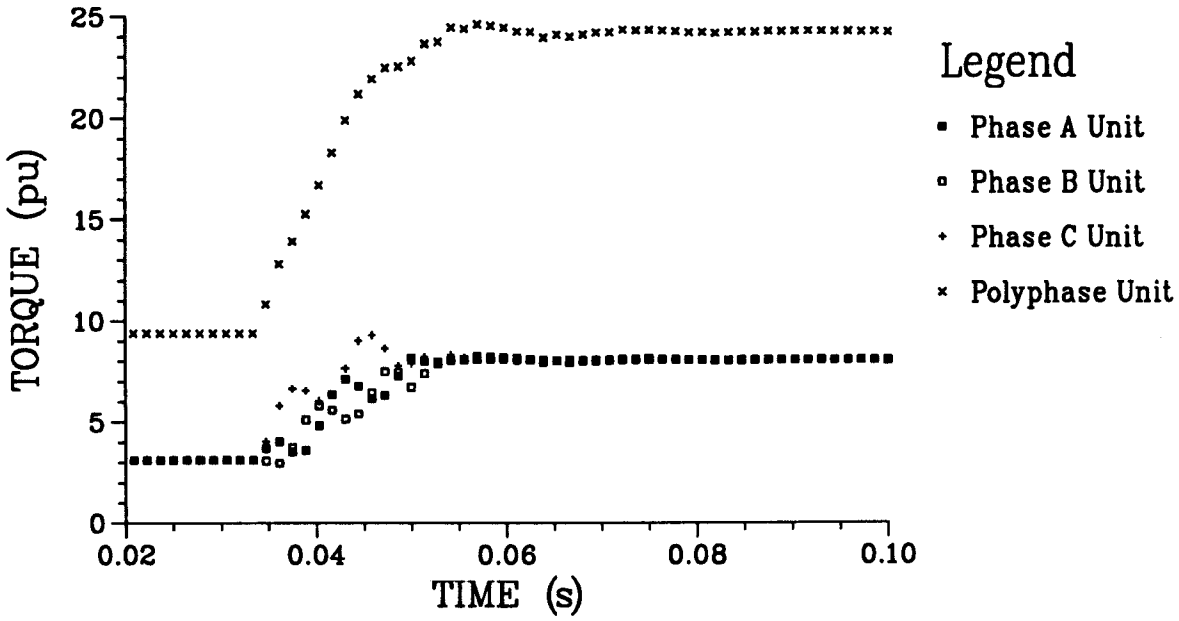

Figure 5.13: Torques developed by the relay for line P2C at bus PR for a three-phase fault with a MTA of 45° for the directional phase units.

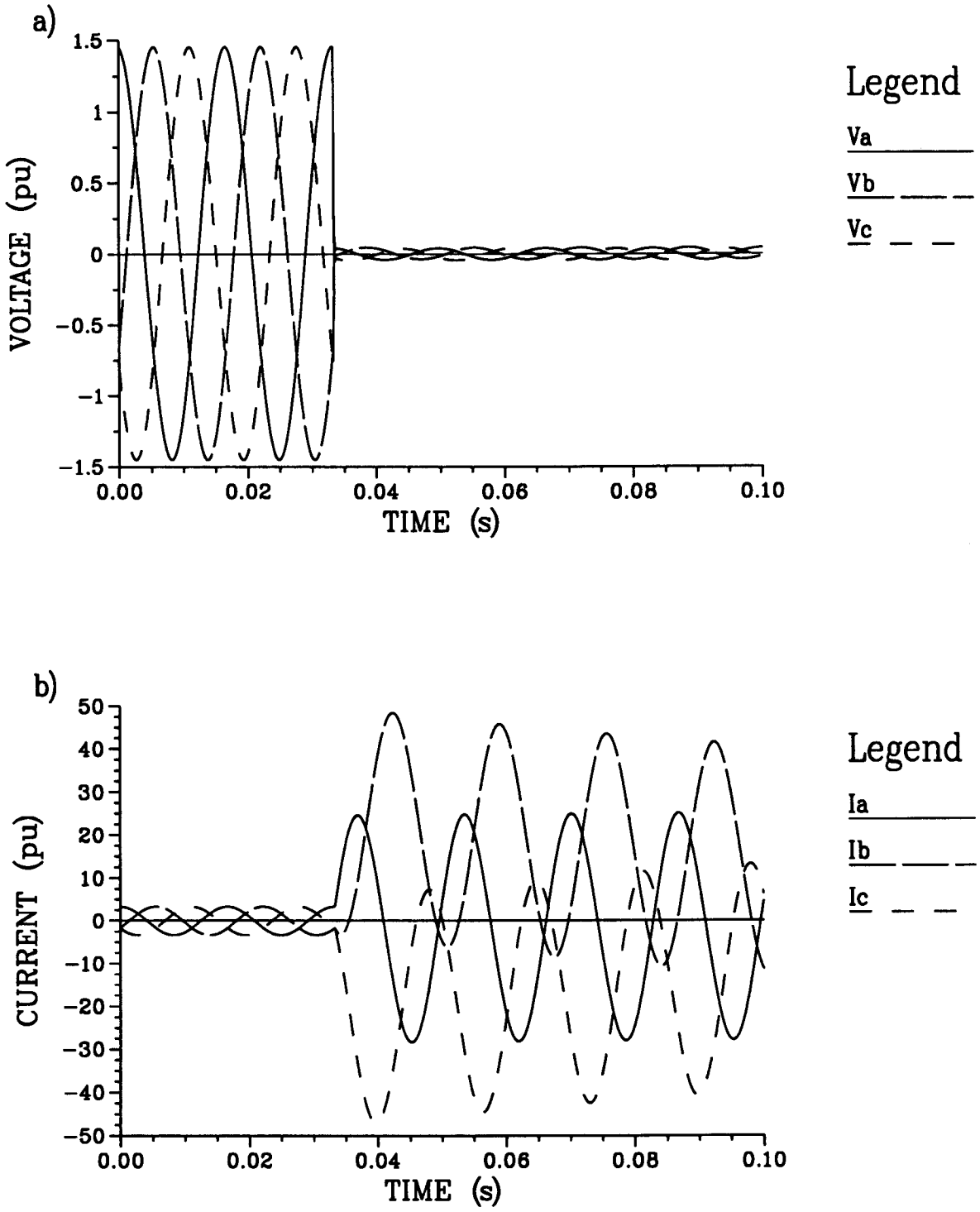

Figure 5.14: The a) voltage and b) current waveforms at the relay for line P2C at bus PR for a close-in three-phase fault.

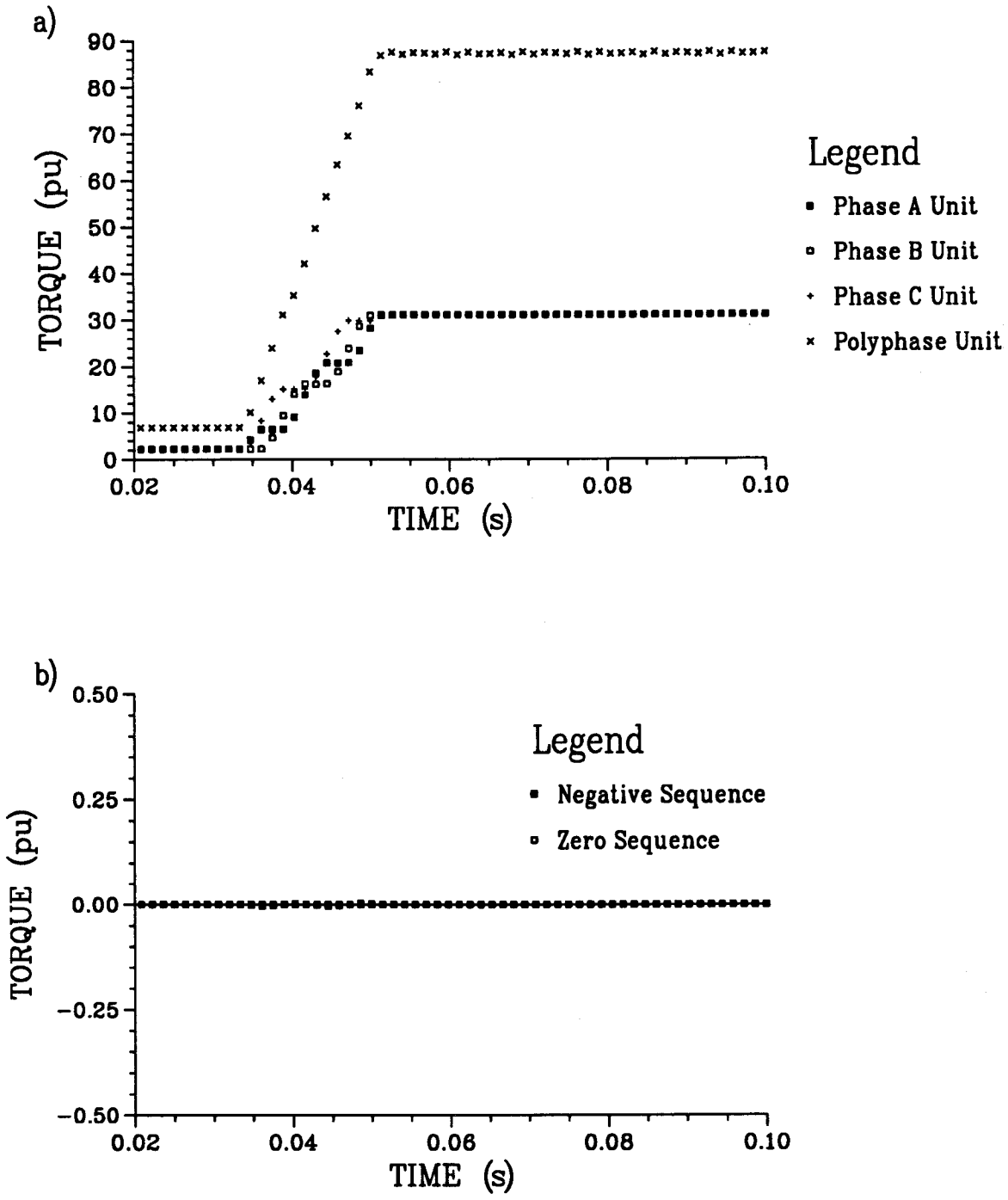

Figure 5.15: Torques developed by the relay with memory polarization for line P2C at bus PR for a close-in three-phase fault with a) a MTA of 30° for the directional phase units and b) MTA's of −60° and 90° for the directional ground unit when polarized with zero and negative sequence quantities respectively.

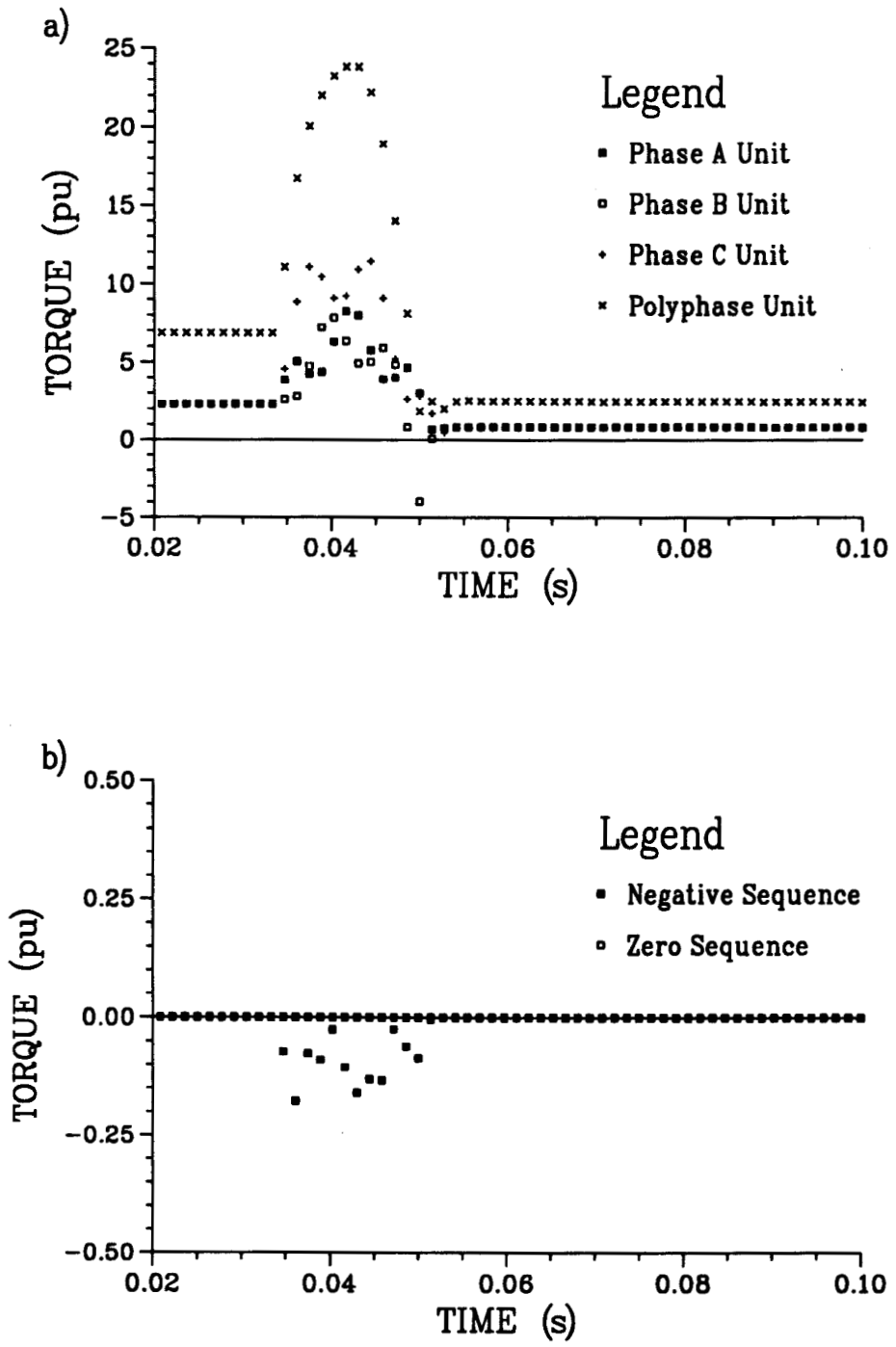

Figure 5.16: Torques developed by the relay without memory polarization for line P2C at bus PR for a close-in three-phase fault with a) a MTA of 30° for the directional phase units and b) MTA's of −60° and 90° for the directional ground unit when polarized with zero and negative sequence quantities respectively.

5.3.3. Two-Phase Fault

Figure 5.17 shows the voltage and current waveforms at bus PR for a two-phase fault on line P2C. The torques generated by the directional overcurrent relay located at bus PR, using MTA's of 30° and 45° for the directional phase units are shown in Figures 5.18(a) and 5.19 respectively. The curves are similar except for minor differences. Phase units with a MTA of 30° generate more torque in the post-fault region than with a MTA of 45° and as a result the post-fault polyphase torque is also larger. There is some ripple in the first 15 ms of the post-fault phase B and C unit torques due to the large decay rate of the dc component in the faulted phases.

The torque produced by the ground unit is shown in Figure 5.18(b). The zero sequence torque is zero as there is no ground fault, but there is negative sequence torque produced indicating a two-phase or ground fault in the tripping direction. However, as there is no zero sequence current present the ground overcurrent unit will not pickup.

5.3.4. Two-Phase-To-Ground Fault

Figure 5.20 shows the voltage and current waveforms at bus PR for a two-phase-to-ground fault on line P2C. The torques generated by the directional phase units with MTA's of 30° and 45° are shown in Figures 5.21(a) and 5.22 respectively; torque output is similar in both cases except for minor differences. The phase units with a MTA of 30° generate more torque in the post-fault region than with a MTA of 45° and as a result the post-fault polyphase torque is also larger. Again there is some ripple in the first 15 ms of the post-fault phase B and C unit torques due to the large decay rate of the decaying dc component present.

Since there is also a ground fault involved the directional ground unit generates torque, as shown in Figure 5.21(b), zero and negative sequence torque is generated soon after the fault occurs with the negative sequence torque being much larger in part due to the use of $3V_2$ and $3I_2$. If the pre-fault power flow was in the opposite direction the directional ground unit would pickup quicker than the directional phase units with either polarization.

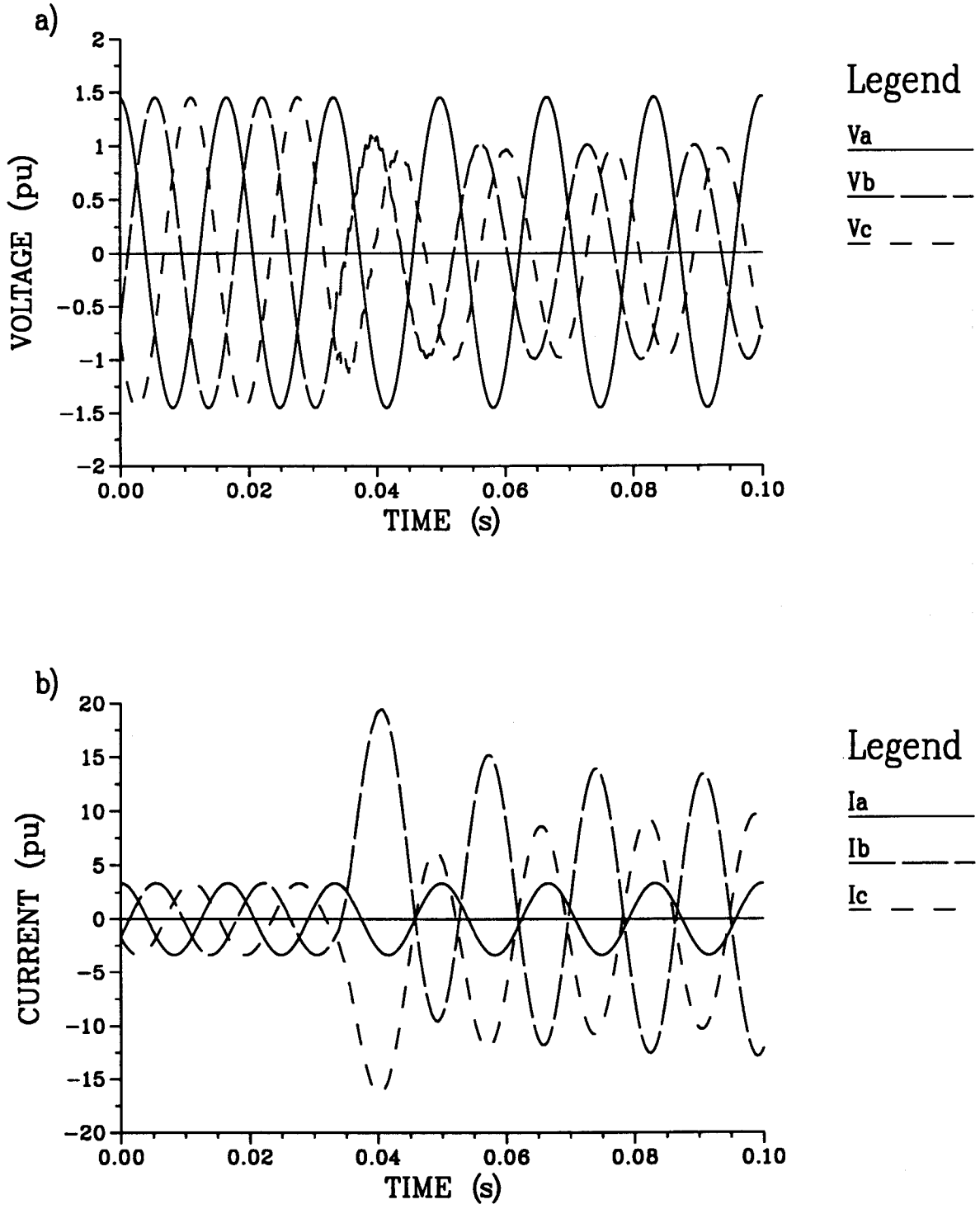

Figure 5.17: The a) voltage and b) current waveforms at the relay for line P2C at bus PR for a two-phase fault.

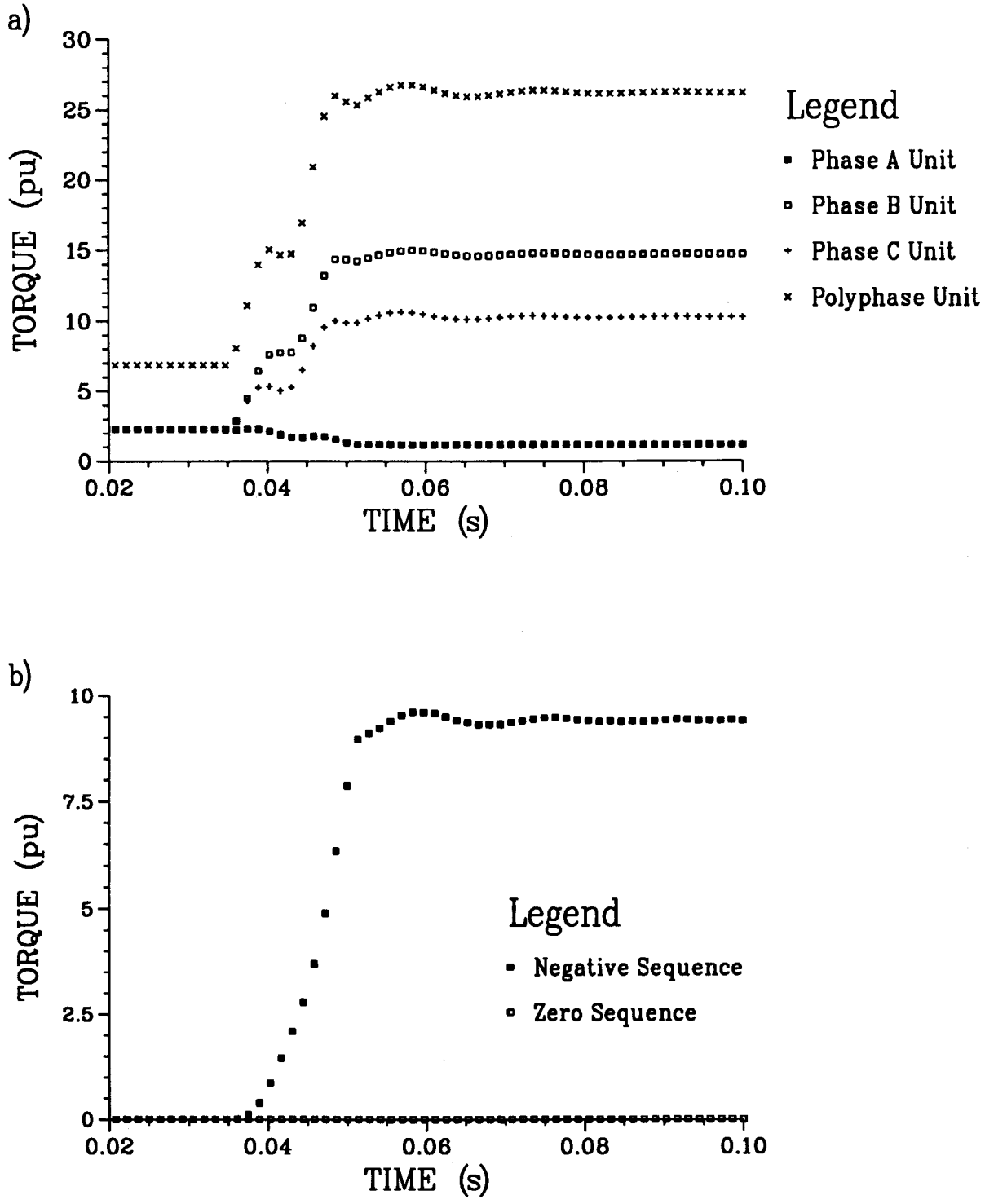

Figure 5.18: Torques developed by the relay for line P2C at bus PR for a two-phase fault with a) a MTA of 30° for the directional phase units and b) MTA's of –60° and 90° for the directional ground unit when polarized with zero and negative sequence quantities respectively.

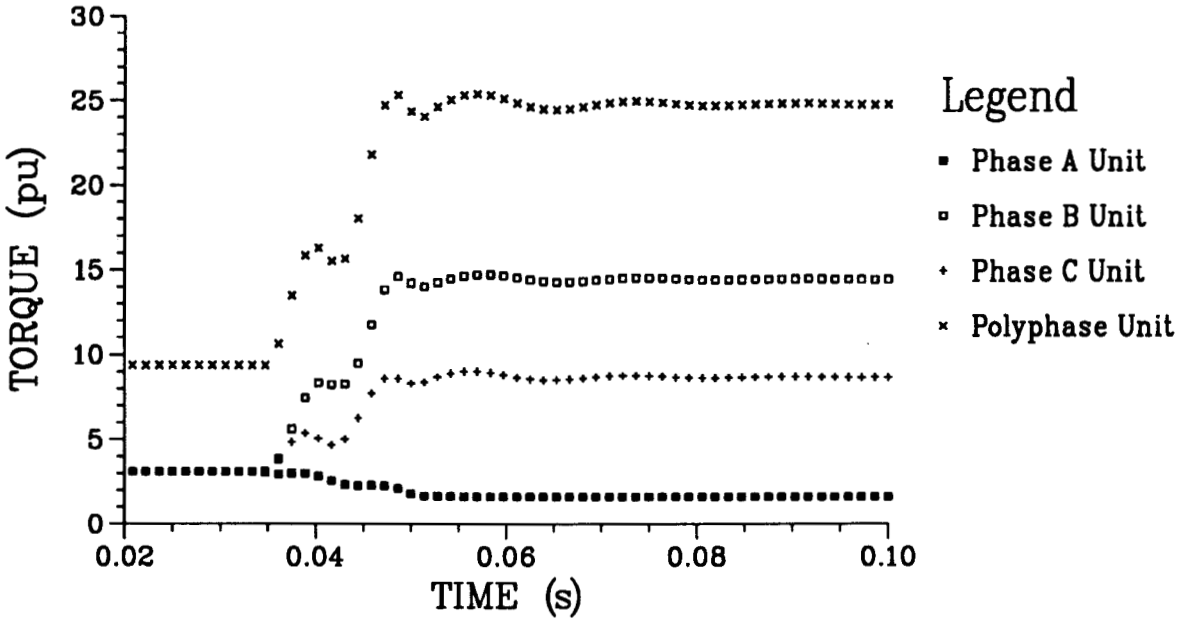

Figure 5.19: Torques developed by the relay for line P2C at bus PR for a two-phase fault with a MTA of 45° for the directional phase units.

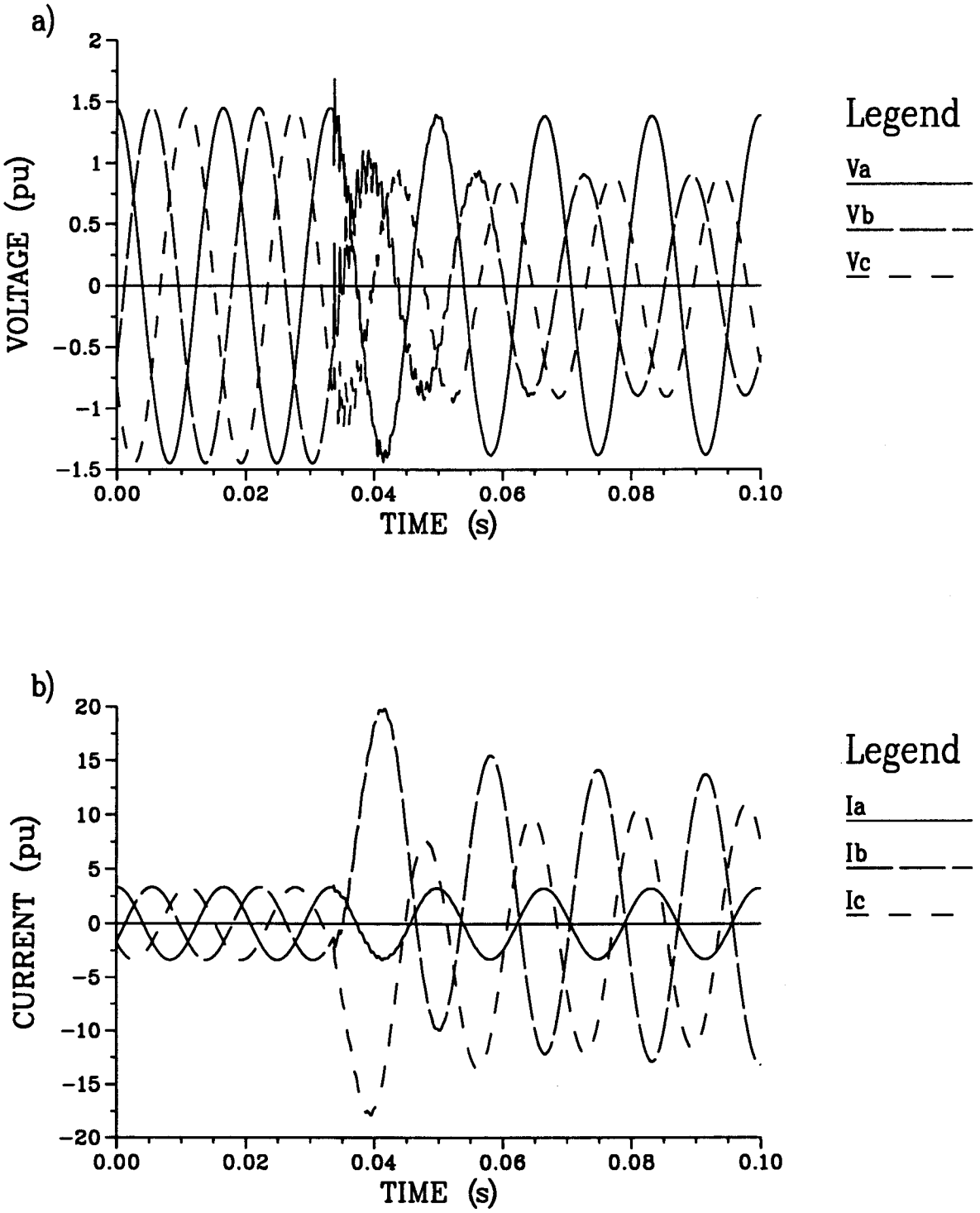

Figure 5.20: The a) voltage and b) current waveforms at the relay for line P2C at bus PR for a two-phase-to-ground fault.

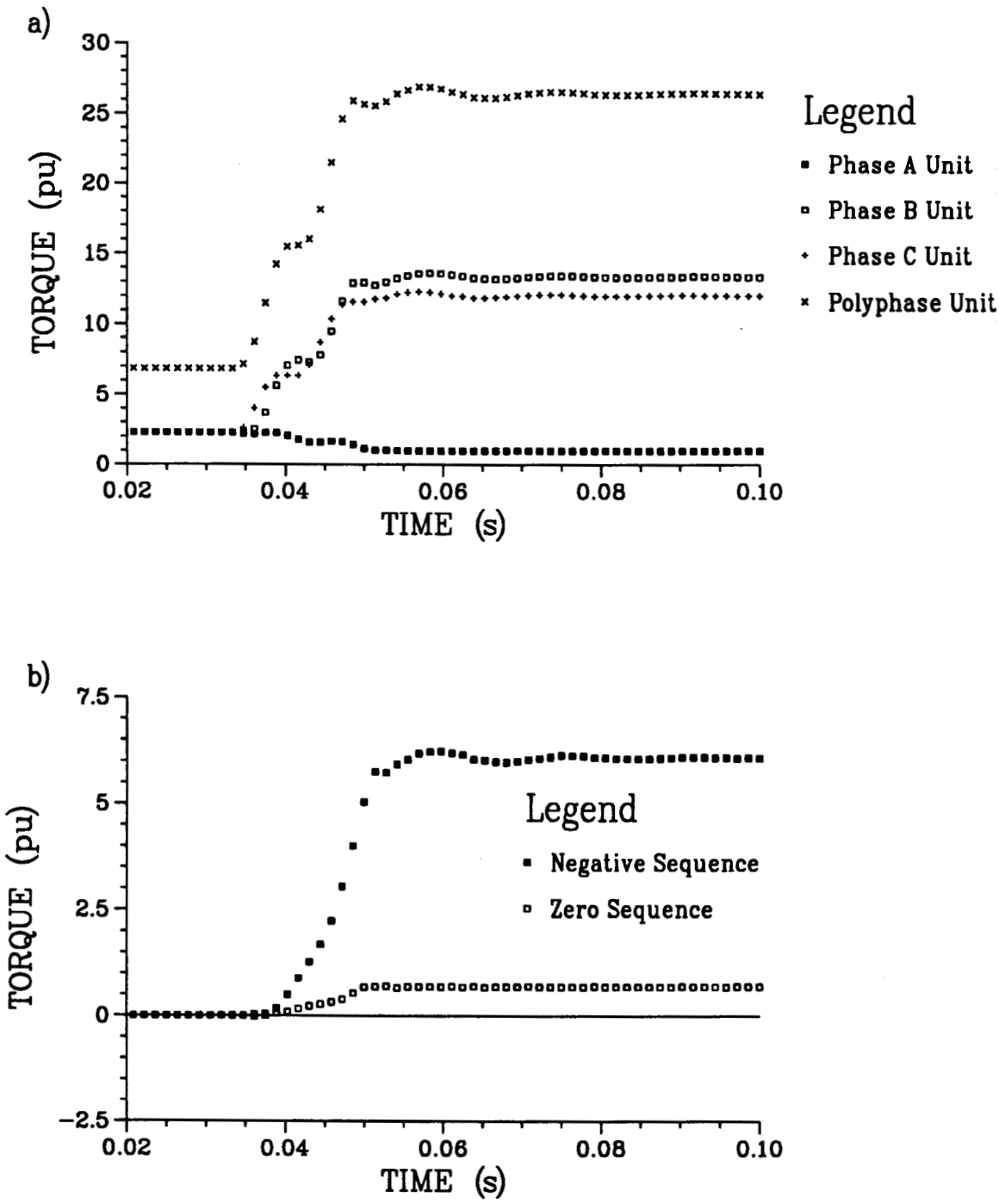

Figure 5.21: Torques developed by the relay for line P2C at bus PR for a two-phase-to-ground fault with a) a MTA of 30° for the directional phase units and b) MTA's of –60° and 90° for the directional ground unit when polarized with zero and negative sequence quantities respectively.

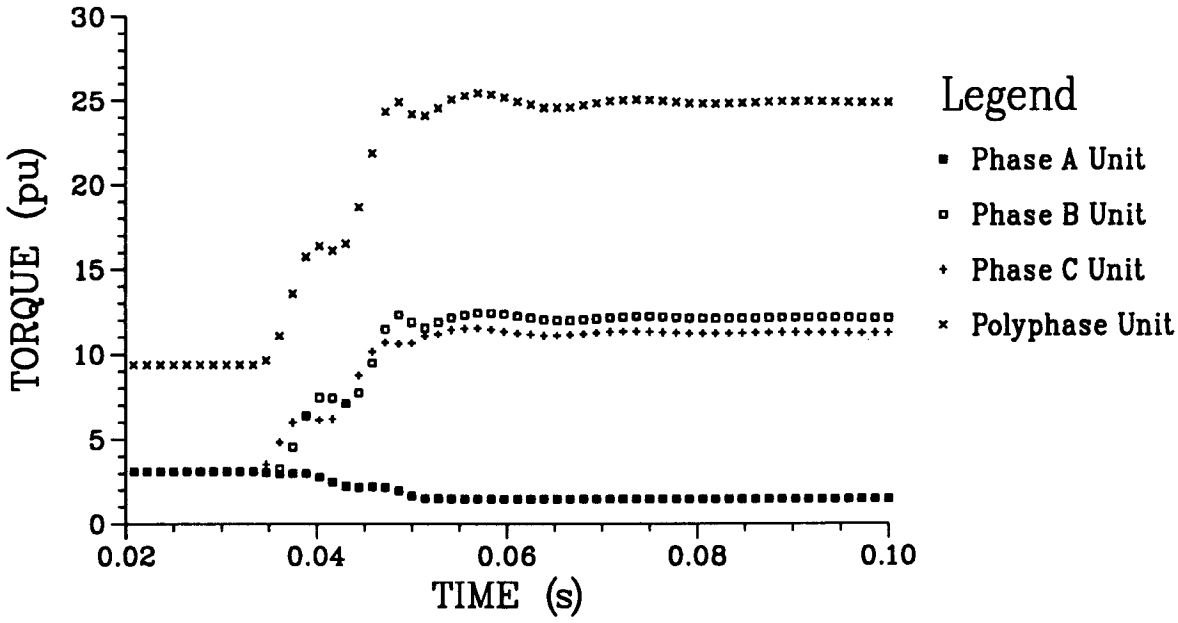

Figure 5.22: Torques developed by the relay for line P2C at bus PR for a two-phase-to-ground fault with a MTA of 45° for the directional phase units.

5.4. System Studies Using SPC Data

Further system studies with the relay were carried out using actual fault data collected by SPC on its transmission network which corresponds to the six-bus test system already described. The data was sampled at 360 Hz until an abnormal condition occurred and then the sampling rate was increased to 1200 Hz, the data has already been pre-filtered.

A new LES filter with a data window size of 21 samples, centered in the middle, was developed for this data. Table 5.7 lists the new filter coefficients. From the filter coefficients it can be shown that the noise introduced by the cosine and the sine filters is $0.2906\ \sigma_n^2$ and $0.09356\ \sigma_n^2$ respectively; therefore, both filters suppress noise effectively with the noise suppression of the sine filter best.

Table 5.7: The filter coefficients for a 21 point LES filter centered in the middle.

Coefficient Number	Cosine Coefficients	Sine Coefficients
x[-10]	0.3018314	-0.0645161
x[-9]	0.0096380	-0.0747387
x[-8]	-0.0984317	-0.0841275
x[-7]	-0.0758444	-0.0651095
x[-6]	-0.0755211	-0.0276759
x[-5]	-0.1105985	0.0032258
x[-4]	-0.1057042	0.0276759
x[-3]	-0.0687191	0.0571349
x[-2]	-0.0539980	0.0841275
x[-1]	-0.0436030	0.0956166
x[0]	0.0000000	0.0967742
x[1]	0.0436030	0.0956166
x[2]	0.0539980	0.0841275
x[3]	0.0687191	0.0571349
x[4]	0.1057042	0.0276759
x[5]	0.1105985	0.0032258
x[6]	0.0755211	-0.0276759
x[7]	0.0758444	-0.0651095
x[8]	0.0984317	-0.0841275
x[9]	-0.0096380	-0.0747387
x[10]	-0.3018314	-0.0645161

5.4.1. Single-Phase-To-Ground Fault

Figures 5.23(a) and (b) show the voltage and current waveforms recorded at bus CON for a single-phase-to-ground fault at an undetermined location on line P2C. Figure 5.24(a) shows the torques developed by the directional phase units with a MTA of 30°. The torques are shown after the detection of the fault at 0.1278 seconds and this represents time zero on this and subsequent torque profiles. After an initial transient region the unfaulted phase units generate negative torque indicating power flow towards bus CON from bus PR while the faulted phase unit generates positive torque indicating power flow towards bus PR. The generation of positive torque represents power flow in the tripping direction and will allow the overcurrent phase unit to increment its trip counter and generate a trip signal. The diagrams also show the torques after a single pole trip has been initiated. This is evident from the faulted phase unit torque dropping to zero.

Figure 5.24(b) shows the torques developed by the ground unit using the different directional voltage-current pairs for ground relaying. Both the zero and negative sequence torque start at zero, climb to a steady state value and then proceed to zero after the circuit breaker has been tripped. The figure indicates that either quantity could effectively torque control the overcurrent ground unit.

5.4.2. Two-Phase Fault

Figures 5.25(a) and (b) show the voltage and current waveforms recorded at bus CON when a cat shorted two phases of an autotransformer behind the relays for line P2C. Figure 5.26(a) shows the torques developed by the directional phase units, with a MTA of 30°. They are shown after the detection of the fault at 0.1278 seconds. After an initial transient region all phase unit torques remain negative indicating power flow towards bus CON from bus PR. The generation of negative torque represents power flow in the non-tripping direction and the relay will not allow the overcurrent units to increment their trip counters and generate a trip signal.

Figure 5.26(b) shows the torques developed by the ground unit using the different

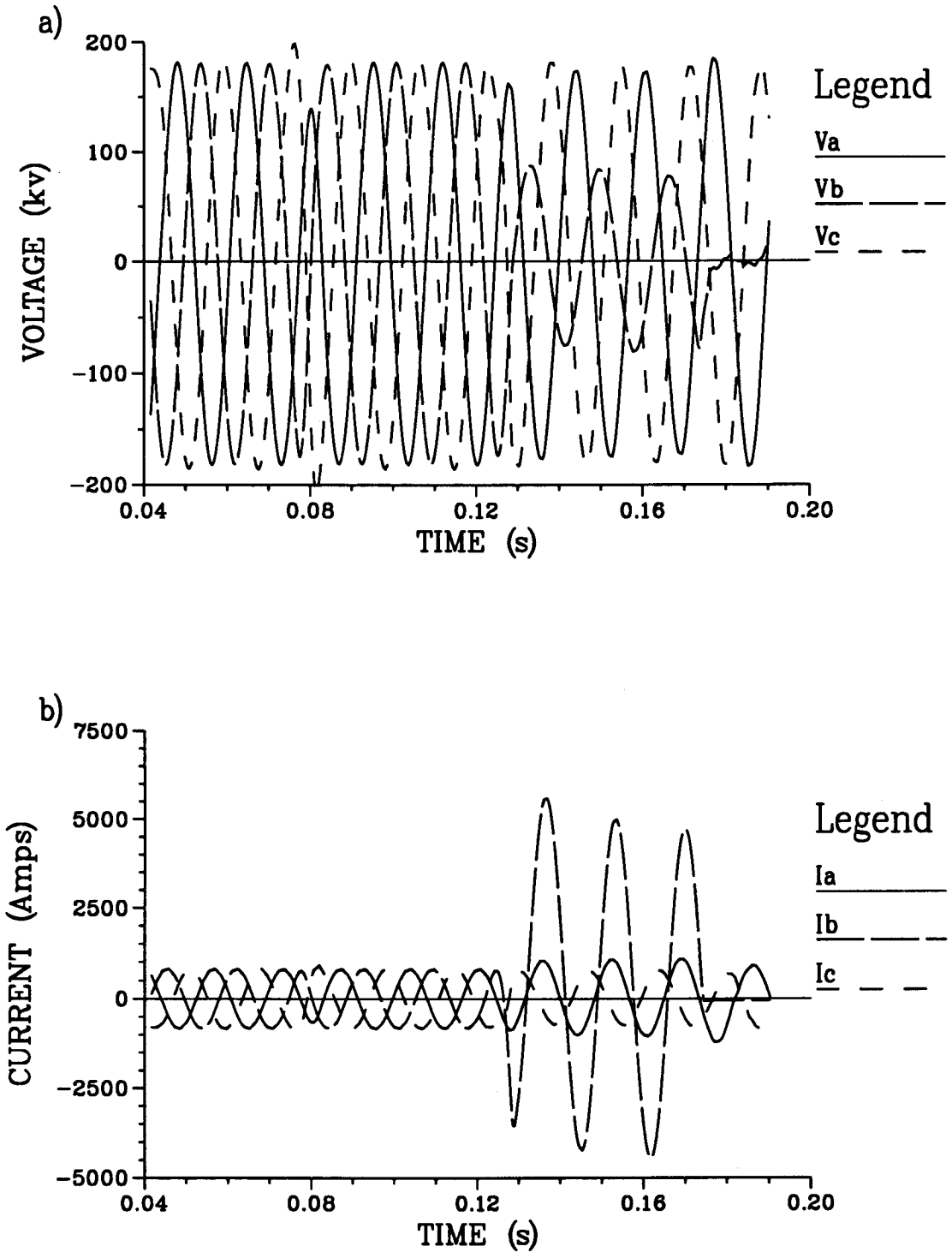

Figure 5.23: The a) voltage and b) current waveforms recorded at bus CON for a single-phase-to-ground fault on line P2C at an undetermined location.

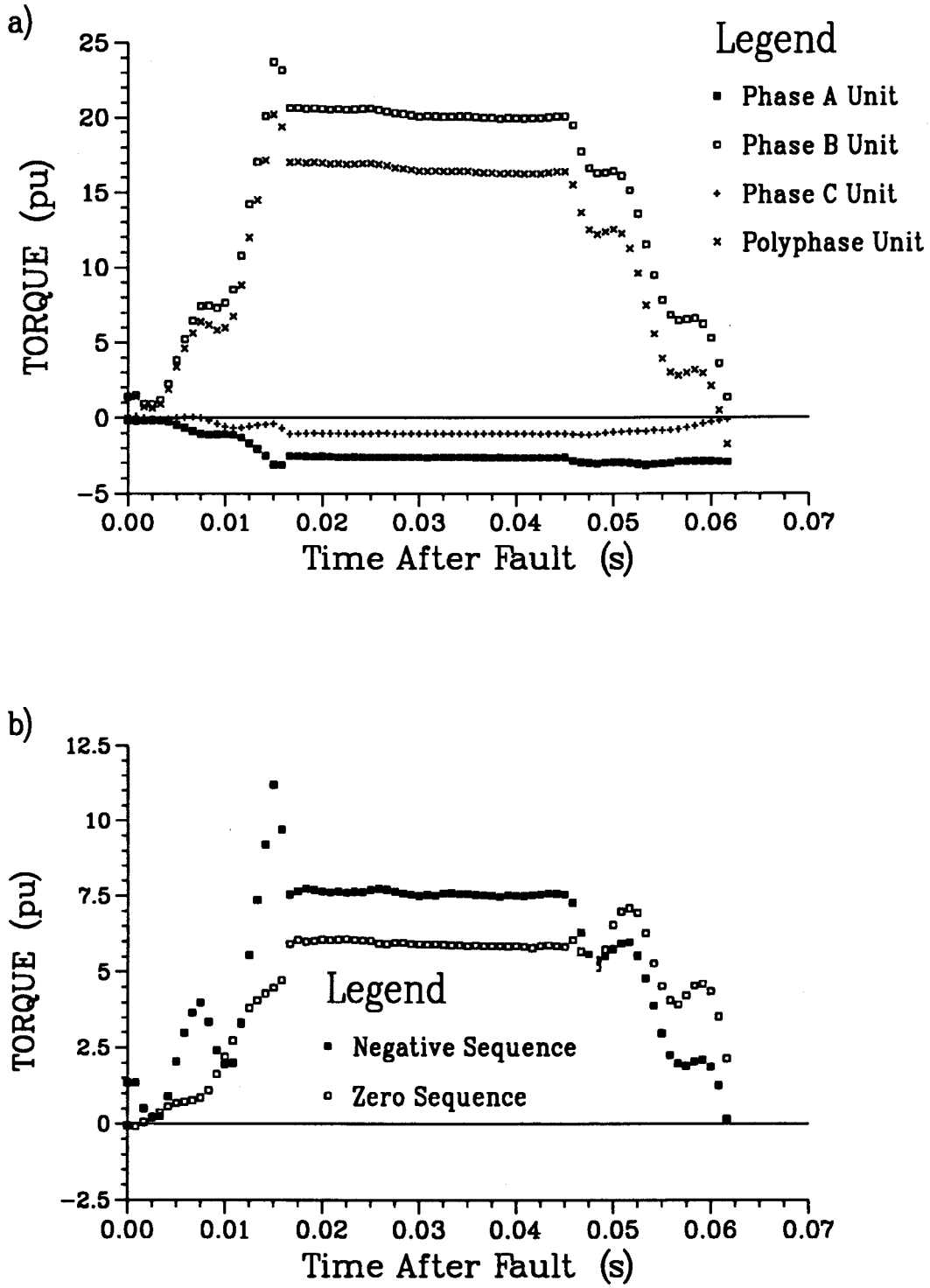

Figure 5.24: Torques developed by the relay for line P2C at bus CON for a single-phase-to-ground fault at an undetermined location with a) a MTA of 30° for the directional phase units and b) MTA's of –60° and 90° for the directional ground unit when polarized with zero and negative sequence quantities respectively.

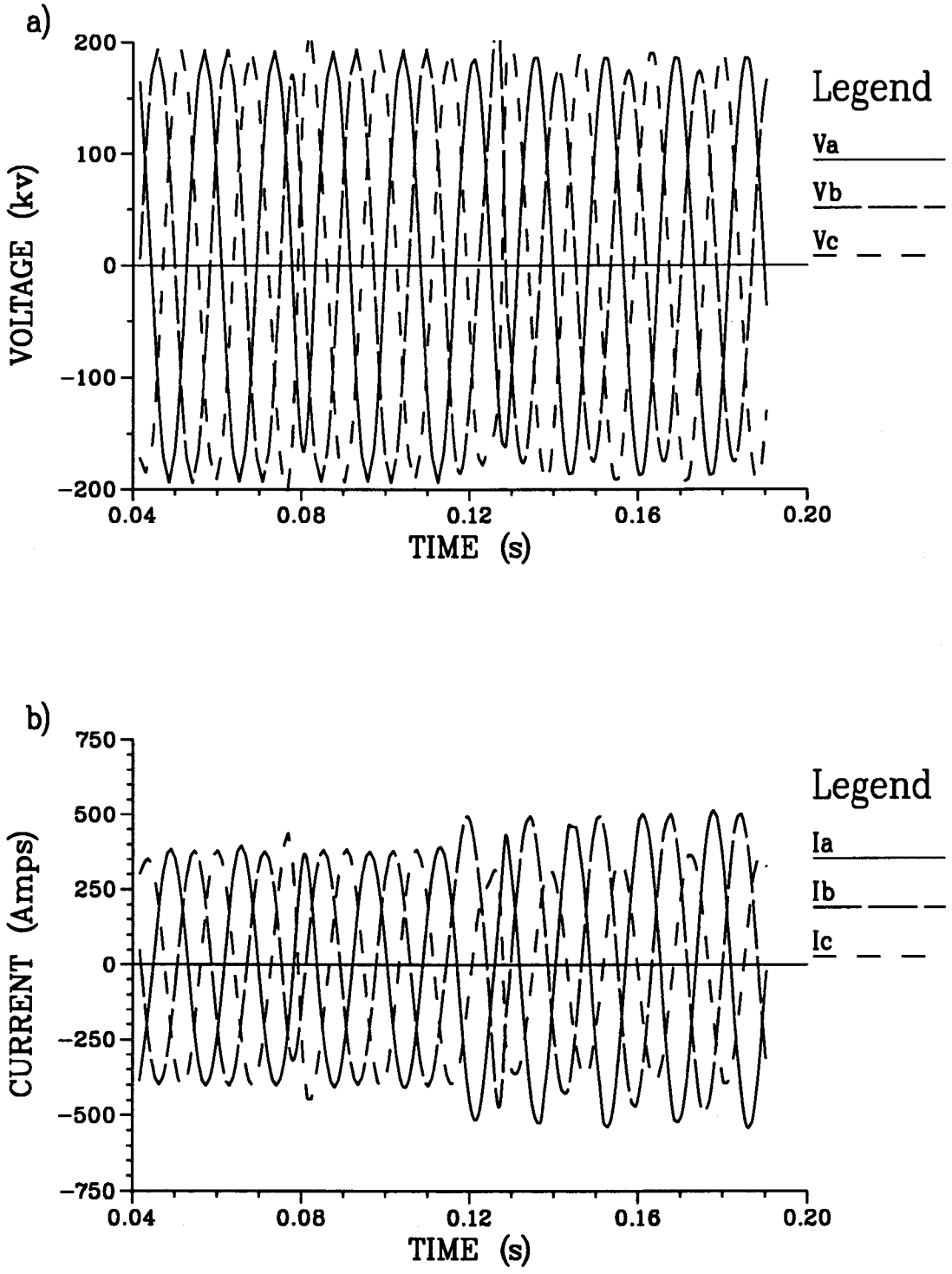

Figure 5.25: The a) voltage and b) current waveforms at bus CON when a cat shorted two phases of an autotransformer behind the P2C relays.

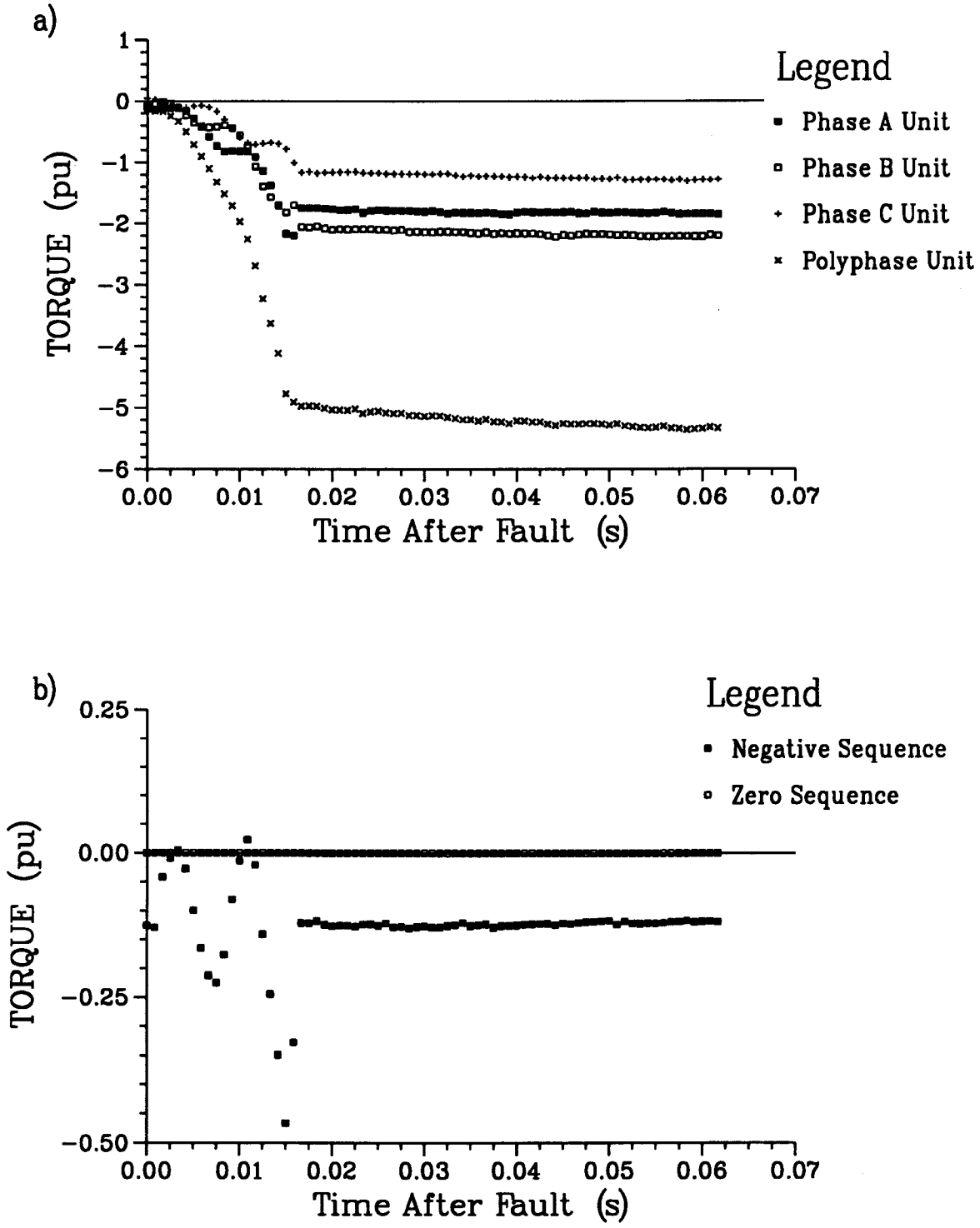

Figure 5.26: Torques developed by the relay for line P2C at bus CON for a two-phase fault behind the P2C relays with a) a MTA of 30° for the directional phase units and b) MTA's of –60° and 90° for the directional ground unit when polarized with zero and negative sequence quantities respectively.

directional voltage-current pairs for ground relaying. The zero sequence torque remains at zero while the negative sequence torque, after a transient region, descends to a negative steady state value. With zero sequence polarization no fault is indicated but negative sequence polarization indicates a fault behind the relay, but both quantities would not allow the ground overcurrent unit to increment its trip counter. However, from the figure it is evident that zero sequence polarization is more reliable as it has no transient and indicates no ground fault at all.

5.5. Summary

In summary, this chapter has presented the tests and system studies that were carried out to demonstrate the capabilities of the designed relay. The directional element was shown to provide accurate results as to the generation of torque from pre- and post-fault waveforms. It was proven that the overcurrent element can accurately emulate the three IEC current-time characteristics. System studies done, using either EMTP or SPC data, demonstrate the capable performance of the relay to different kinds of shunt faults. As well, memory polarization was shown to be effective during close-in three-phase faults. From the results presented in this chapter it is apparent that the microprocessor-based directional overcurrent relay can determine the direction of power flow for a variety of fault conditions. This is accomplished by using an algorithm based on Equation 2.1, directional flags (set by the directional units) thus providing effective torque control over the operation of the overcurrent units and weighting functions to provide the current-time characteristics.

6. SUMMARY AND CONCLUSIONS

The basic concepts behind the protection of power systems from faults and abnormal conditions have been presented in the first chapter. As well, the underlying reasons for the development of microprocessor-based relays have also been discussed. The main objective of this research was to design and develop a versatile microprocessor-based directional overcurrent relay capable of functioning in distribution networks, transmission networks or for other power flow applications.

The various applications of and general theory behind directional relaying for power system protection, with emphasis on directional overcurrent relaying for line protection and other power flow applications, such as generator and transformer protection, have been reviewed in Chapter 2. Relaying algorithms and their fundamental mathematical concepts have been briefly presented in Chapter 3. Nonrecursive algorithms presented are trigonometric, correlation and least squares; the recursive algorithms presented are the Kalman filter and recursive DFT. The digital relaying algorithm chosen to estimate the parameters of interest was the least squares technique.

The design of the microprocessor-based relay is described in Chapter 4; it details how the directional and overcurrent elements are modelled. Previously proposed techniques for modelling overcurrent relay characteristics have also been presented. The design of the LES filter, that estimates the real and imaginary components of the of the sampled voltages and currents, is also discussed. The relay is implemented on an Ariel DSP-C25 board using TMS320C25 C and assembly language, with a Lattice C interface program for communication between the host PC and its DSP-C25 board. Most functions are performed using fixed point arithmetic, but some use floating point. Chapter 5 lists the results from testing the directional and overcurrent elements and the system studies done with EMTP and SPC data.

Further research into the feasibility of using negative sequence polarization for phase fault monitoring could be investigated. This would be advantageous because negative sequence torque is normally zero and it would reduce some of the transit time between pre and post-fault torque levels. As well, system studies using modal quantities to polarize directional relays could be done as modal equations are easier to implement than symmetrical component equations.

Enhancements to the relay could be the addition of voltage-restrained phase units allowing the relay to operate correctly when the fault current in the tripping direction can be at or slightly below the maximum load current. This augmentation would also minimize undesired tripping during severe power swings. Different current-time characteristics, such as definite time and long time earth fault characteristics could be added to improve the versatility of the relay.

In conclusion, the design and implementation of a versatile microprocessor-based directional overcurrent relay has been described in this thesis. The theory for determining the direction of power flow and how to torque control the operation of an overcurrent element has also been presented. The proposed design has been implemented on an Ariel DSP-C25 board and off-line testing confirms the validity and versatility of this design.

REFERENCES

1. Mason, C. Russel, *The Art and Science of Protective Relaying,* John Wiley and Sons, Inc., New York;Chapman and Hall, Ltd.,London, 1956.

2. Warrington, A.R. van C., *Protective Relays: Their Theory and Practice,* Chapman and Hall, Ltd., London, Vol. 1, 1968.

3. Blackburn, J. Lewis, *Protective Relaying Principles and Applications,* Marcel Dekker, Inc., New York, New York, 1987.

4. Rockefeller, G.D., "Fault Protection with a Digital Computer", *IEEE Transactions on Power Apparatus and Systems*, Vol. PAS-88, April 1969, pp. 438-462.

5. Gilcrest, G.B., Rockefeller, G.D. and Udren, E.A., "High Speed Distance Relaying Using A Digital Computer; Part I - System Description", *IEEE Transactions on Power Apparatus and Systems*, Vol. PAS-91, No. 3, May/June 1972, pp. 1235-1243.

6. Sachdev, M.S. (Coordinator), *Computer Relaying,* IEEE Tutorial Course Text, Publication No. 79 EH0148-7-PWR, New York, 1979.

7. Sachdev, M.S. (Coordinator), *Microprocessor Relays and Protection Systems,* IEEE Tutorial Course Text, Publication No. 88 EH0269-1-PWR, Piscataway, New Jersey, 1988.

8. Phadke, Arun G. and Thorp, James S., *Computer Relaying For Power Systems,* Research Studies Press Ltd., Taunton, Somerset, England and John Wiley & Sons Inc., New York, 1988.

9. Wood, H.C., Sidhu, T.S., Sachdev, M.S. and Nagpal, M., "A General Purpose Hardware For Microprocessor Based Relays", *Conference Proceedings of the International Conference on Power System Protection '89, Singapore*, September 13-14 1989, pp. 43-59.

10. Singh, J., Sachdev, M.S., Fleming, R.J. and Krause, A.E., "Digital IDMT Directional Overcurrent Relay", *Developments in Power System Protection, IEE Conference Publication No. 185*, April 1980, pp. 84-87.

11. Murty, Y.V.V.S. and Smolinski, W.J., "Design and Implementation of a Versatile Digital Directional Overcurrent Relay", *Electric Power Systems Research*, January 1990, pp. 47-55.

12. GEC Alsthom, *Protective Relays Application Guide,* GEC Alsthom Measurements Limited; Stafford, England, 1987.

13. Graybeal, Troy D., "Factors Which Influence the Behavior of Directional Relays", *Transactions A.I.E.E.*, Vol. 61, 1942, pp. 942-952.

14. Sonnemann, W.K., "A Study of Directional Element Connections for Phase Relays", *Transactions A.I.E.E.*, Vol. 69, 1950, pp. 1438-1451.

15. Baldwin, C.J. and Goffard, B.N., "An Analysis of Polyphase Directional Relay Torques", *Transactions A.I.E.E.*, Vol. 72, 1953, pp. 752-759.

16. Westinghouse Electric Corporation, *Instructions, Type CO Overcurrent Relay,* I.L. 41-101 ed., 1976.

17. Blackburn, J.L. and Elmore, W.A., "Negative-Sequence Directional Ground Relaying", *IEEE Transactions on Power Apparatus and Systems*, Vol. 64, February 1963, pp. 913-921.

18. Mann, B.J. and Morrison, I.F. , "Digital Calculation of Impedance for Transmission Line Protection", *IEEE Transactions on Power Apparatus and Systems*, Vol. PAS-90, January/February 1971, pp. 270-276.

19. Rockefeller, G.D. and Udren, E.A., "High Speed Distance Relaying Using A Digital Computer; Part II - Test Results", *IEEE Transactions on Power Apparatus and Systems*, Vol. PAS-91, No. 3, May/June 1972, pp. 1244-1258.

20. Makino, J. and Miki, Y., "Study of Operating Principles and Digital Filters for Protective Relays with Digital Computer", *IEEE Publication No. 75 CH0990-2 PWR, Paper No. C75 197 9, IEEE PES Winter Power Meeting, New York,* January 1975, pp. 1-8.

21. Ramamoorty, M., "A Note on Impedance Measurement Using Digital Computer", *IEE-IRE Proceeding (India)*, Vol. 9, No. 6, November/December 1974.

22. Phadke, A.G., Hlibka, T. and Ibrahim, M., "A Digital Computer System for EHV Substation: Analysis and Field Tests", *IEEE Transactions on Power Apparatus and Systems*, Vol. PAS-95, No. 1, January/February 1976, pp. 291-301.

23. Hope, G.S. and Umamaheswaran, V.S., "Sampling for Computer Protection of Transmission Lines", *IEEE Transactions on Power Apparatus and Systems*, Vol. PAS-93, No. 5, September/October 1974, pp. 1522-1533.

24. Schweitzer, E.O., "The Design and Test of a Digital Relay for Transformer Protection", *IEEE Transactions on Power Apparatus and Systems*, May/June 1979, pp. 795-805.

25. Luckett, R.G., Monday, P.J. and Murray, B.E., "Substation Based Computer Control and Protection", *IEE Conference Publication No. 125, Developments in Power System Protection*, March 1975, pp. 252-260.

26. Brooks, A.E., "Distance Relaying Using Least Error Squares Estimates of Voltage, Current and Impedance", *Proceedings of the 10th Power Industry Computer Application Conference Publication No. 77 CH1131-2-PWR*, May 1977, pp. 394-402.

27. Sachdev, M.S. and Baribeau, M.A., "A New Algorithm for Digital Impedance Relays", *IEEE Transactions on Power Apparatus and Systems*, Vol. PAS-98, November/December 1979, pp. 2232-40.

28. Phadke, A.G., Thorp, J.S. and Adamiak, M.G., "A New Measurement Technique for Tracking Voltage Phasors, Local System Frequency, and Rate of Change of Frequency", *IEEE Transactions on Power Apparatus and Systems*, Vol. PAS-102, No. 5, May 1983, pp. 1025-1038.

29. Girgis, A.A. and Brown, R.G., "Application of Kalman Filtering in Computer Relaying", *IEEE Transactions on Power Apparatus and System*, Vol. PAS-91, July 1981, pp. 3387-3397.

30. Dasgupta, K.S., Malik, O.P. and Hope, G.S., "Kalman Filtering Approach to Impedance Protection", *Transactions of the CEA, Paper No. 83-SP-171*, Vol. 221983, pp. 1-14.

31. Sachdev, M.S., Wood, H.C. and Johnson, N.G., "Kalman Filtering Applied To Power System Measurements for Relaying", *IEEE Transactions on Power Apparatus and System*, Vol. PAS-104, December 1985, pp. 3365-3373.

32. Kreyszig, Erwin, *Advanced Engineering Mathematics,* John Wiley and Sons, Inc., New York , 1983.

33. Computer Representation of Overcurrent Relay Characteristics Working Group of the Power System Relaying Committee, IEEE, "Computer Representation of Overcurrent Relay Characteristics", *IEEE Transactions on Power Delivery*, Vol. 4, No. 3, July 1989, pp. 1659-1667.

34. Hieber, J.E., "Empirical Equations of Overcurrent Relay Curves for Computer Applications", *IEEE CP 31-CP-65-90*, 1965, pp. 1-11.

35. IEC Standard, Publication No. 255-4, *Single Input Energizing Quantity Measuring Relays With Dependent Specified Time,* International Electrotechnical Commission, Geneva, Switzerland, 1976.

36. Albrecht, R.E., Nisja, M.J., Peero, W.E., Rockefeller, G.D., and Wagner, C.L., "Digital Computer Protective Device Coordionation Program - General Program Description", *IEEE Transactions on Power Apparatus and System*, Vol. PAS-83, No. 4, April 1964, pp. 402-411.

37. Radke, G.E., "A Method for Calculating Time-Overcurrent Relay Settings by Digital Computer", *IEEE Transactions on Power Apparatus and System-Special Supplement*, Vol. PAS-82, 1963, pp. 189-205.

38. Singh, J., Sachdev, M.S. and Fleming, R.J., "Mathematical Models Representing Time-Current Characteristics of Overcurrent Relays for Computer Applications", *IEE PES Winter Meeting, New York, NY, Paper No. A78 131-5*, Jan./Feb. 1979, pp. 1-8.

39. Damborg, M.J., Ramaswami, R., Venkata, S.S. and Postforoosh, J.M, "Computer Aided Transmission Protection System Design", *IEEE Transactions on Power Apparatus and System*, Vol. PAS-103, No. 1, January 1984, pp. 51-59.

40. Sidhu, T.S., Sachdev, M.S. and Wood, H.C., "Design Of A Microprocessor-Based Overcurrent Relay", *The IEEE Western Canada Conference On Computer, Power And Communication Systems In A Rural Enviroment Proceedings, Regina Canada*, 1991, pp. 41-46.

41. Nagpal, Mukesh, *Design And Implementation Of A Microprocessor-Based System For Protecting Three-Phase Transformers,* PhD dissertation, University Of Saskatchewan, 1991.

42. Sidhu, T.S., "Computer-Aided Design and Performance Evaluation of Digital Relays", Master's thesis, University Of Saskatchewan, 1985.

43. Sidhu, T.S., *A Microprocessor-Based System For Protection of Power Transformers,* PhD dissertation, University Of Saskatchewan, 1989.

44. Sachdev, M.S. and Wood, H.C., "Introduction and General Methodology of Digital Protection", *Transactions Canadian Electrical Association, Engineering and Operating Division, Power System Planning and Operation Section*, March 1986.

45. Kernighan, Brian W. and Ritchie, Dennis M., *The C Programming Langauge,* Prentice-Hall Inc., Englewood Cliffs, New Jersey, 1978.

46. Gottfried, Byron S., *Programming With C, Schaum's Outline Series,* McGraw-Hill Publishing Company, New York, 1990.

47. Technical Publications, Texas Instruments Incorporated, *TMS320C25 C Compiler, Reference Guide,* SPRU024A ed., 1989.

48. Technical Publications, Texas Instruments Incorporated, *TMS320C1x/TMS320C2x Assembly Langauge Tools, User's Guide,* SPRU018A ed., 1989.

49. Technical Publications, Texas Instruments Incorporated, *Second-Generation TMS320, User's Guide,* SPRU014A ed., 1989.

50. Ariel Corporation, *Operating Manual For The DSP-C25 TMS320C25 DSP Board,* Highland Park, New Jersey, 1989.

51. Ariel Corporation, *DSP 16 Operating Manual,* Highland Park, New Jersey, 1986.

52. Hamming, R.W., *Digital Filters,* Prentice Hall Inc., Englewood Cliffs, New Jersey, 1977.

53. Taylor, Fred J., *Digital Filter Design Handbook,* Marcel Dekker, Inc., New York, 1983.

54. Antoniou, Andreas, *Digital Filters: Analysis and Design,* McGraw-Hill Book Company, New York, 1979.

55. White, Donald R.J., *A Handbook on Electrical Filters Synthesis, Design and Applications,* Don White Consultants, Inc., Gainesville, Virginia, 1980.

56. Schweitzer, E.O. and Aliaga, A., "Digital Programmable Time-Parameter Relay Offers Versatility and Accuracy", *IEEE Transactions on Power Apparatus and Systems*, Vol. PAS-99, Jan./Feb. 1980, pp. 152-157.

57. Bonneville Power Administration, *ElectroMagnetic Transients Program (EMTP) Rule Book,* Portland, Oregon, 1983.

A. ANTI-ALIASING FILTER DESIGN

Low pass filters are used in digital relaying to band limit the input voltage signals and to remove any high frequency components present. According to the Nyquist criterion the cut-off frequency f_c of the low pass filter should be less than one half of the sampling frequency so that the effects of aliasing are minimized [52, 53, 54]. Since a sampling frequency of 720 Hz is used in this design f_c must be equal to or less than 360 Hz. To fulfill this requirement a second order low pass Butterworth filter with f_c=270 Hz was designed. A Butterworth filter was chosen because of its maximally flat pass-band response and it is readily available and easily implemented in a variety of formats, e.g., switched capacitors. The cut-off frequency of 270 Hz was chosen to limit the amount of the sixth harmonic delivered to the 13 point LES sine filter as much as possible while still maintaining a small group delay.

The transfer function of a second order Butterworth filter is given by the following equation:

$$H(s) = \frac{1}{\frac{s}{\omega_c^2}+\frac{s}{\omega_c}1.4142+1}, \qquad (A.1)$$

where:

s is complex frequency and

ω_c is equal to $2\pi f_c$.

Which can be rewritten as:

$$H(s) = \frac{\omega_c^2}{s^2+s\,1.4142\,\omega_c+\omega_c^2}. \qquad (A.2)$$

The group delay (τ_d) of the filter can be determined from Equation A.3.

$$\tau_d = -\frac{d\phi(\omega)}{d\omega}. \qquad (A.3)$$

where:

$\phi(\omega)$ is the argument of the transfer function.

Applying Equation A.3 the group delay of a n^{th} order low pass Butterworth filter can be shown to be [55]:

$$\tau_d = \frac{\frac{1}{B}\sum_{k=1}^{n} \frac{\left(\frac{\omega}{B}\right)^{2k-2}}{\sin((2k-1)\pi/2n)}}{1+\left(\frac{\omega}{B}\right)^{2n}}, \qquad (A.4)$$

where:

ω is the frequency of interest,

B is the bandwidth of the filter and

n is the order of the filter.

Using Equation A.4 the group delay of the designed 2^{nd} order Butterworth filter at 60 Hz is 0.8727 ms and at 270 Hz is 0.8336 ms. The group delay response is shown in Figure A.1.

In this project the analog low pass Butterworth filter was simulated by a digital filter implemented in Fortran on a Sun Sparc workstation. Analog filters can be transformed into digital filters by using the bilinear transformation and frequency prewarping. Frequency prewarping is performed as follows:

$$H(s) = \frac{\Omega_c^2}{s^2+s\,1.4142\,\Omega_c+\Omega_c^2}, \qquad (A.5)$$

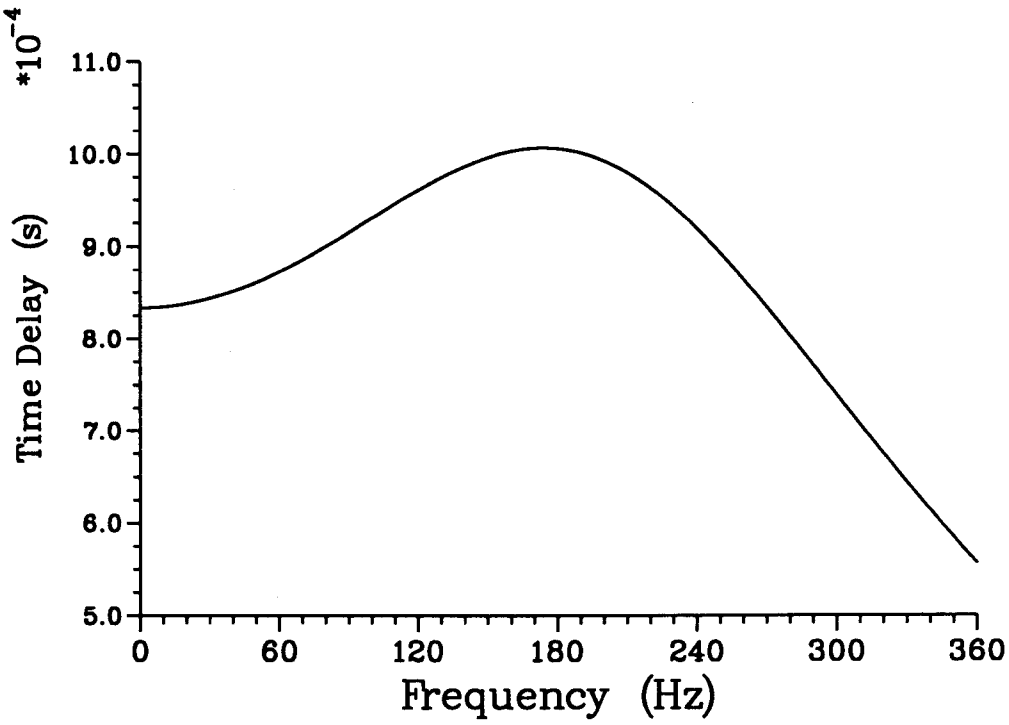

Figure A.1: The group delay response of the 2nd order low pass butterworth filter.

$$\Omega_c = 2\pi F', \tag{A.6}$$

$$F' = \frac{F_s}{\pi}\tan\frac{\pi F}{F_s}, \tag{A.7}$$

where:

Ω_c is the digital cut-off frequency and

F' is the pre-warped analog cut-off frequency.

The bilinear transformation is given in Equation A.8.

$$s = \frac{2}{\Delta T}\,\frac{1-z^{-1}}{1+z^{-1}}. \tag{A.8}$$

Using the preceding equations Equation A.5 can be transformed into:

$$H(z) = \frac{0.00542649\,(1+2z^{-1}+z^{-2})}{3.797071z^{-2}-7.989147z^{-1}+4.213782}. \qquad (A.9)$$

The frequency response can now be determined by substituting $z=e^{-j\omega\Delta T}$ into Equation A.9. Figure A.2 shows the frequency response of the filter and it is apparent that high frequency components are attenuated.

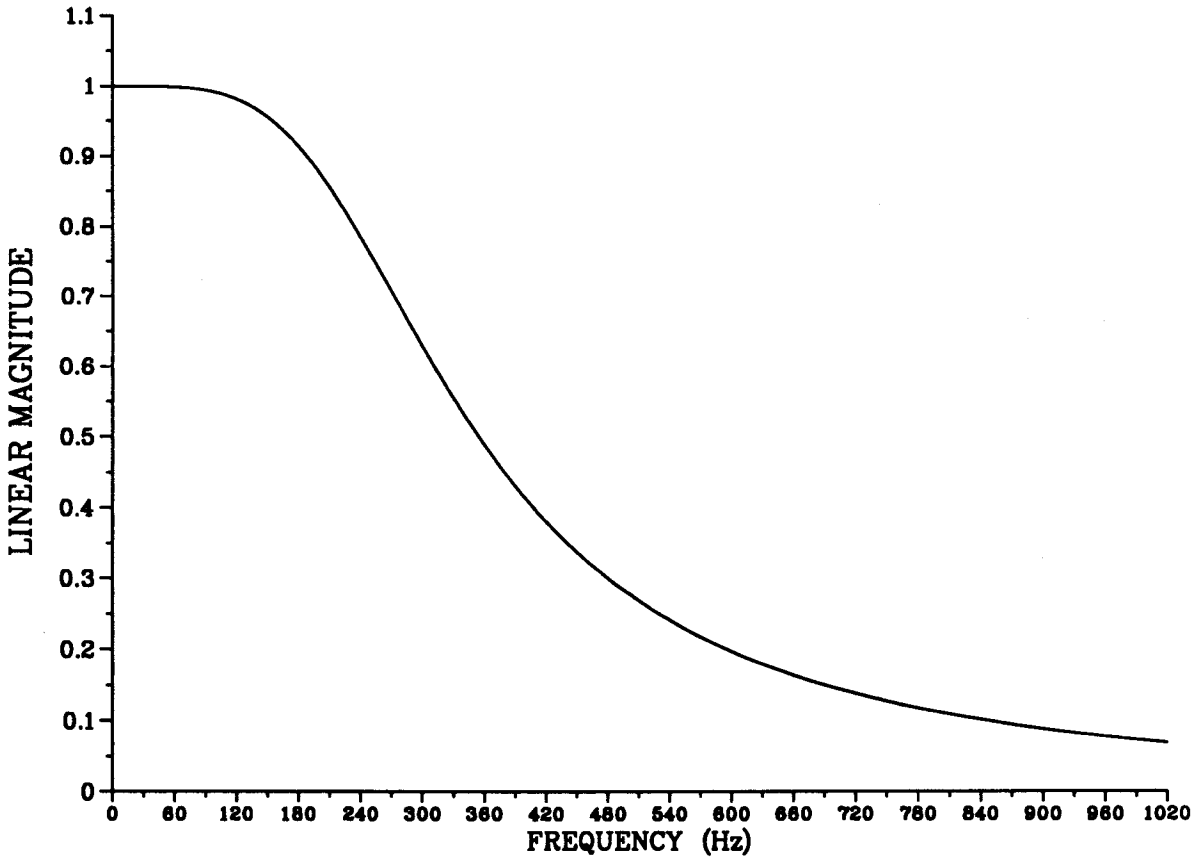

Figure A.2: The frequency response of the 2nd order low pass butterworth filter.

Equation A.9 can then be written in terms of the time delay of n sampling intervals.

$$Y(z) = X(z)H(z). \tag{A.10}$$

$$y(n) = x(n)h(n). \tag{A.11}$$

$$\begin{aligned} y(n) = {} & 0.00128780(x(n)+2x(n-1)+x(n-2)) \\ & +1.895956\,y(n-1)-0.901108\,y(n-2). \end{aligned} \tag{A.12}$$

Equation A.12 is then implemented as a digital filter.

B. AMPLITUDE ESTIMATOR

The rms amplitude of a phasor is needed in many relaying applications and can be determined from its real and imaginary components, requiring two squaring operations and one square root operation to be carried out. Performing these operations on a microprocessor requires extensive amounts of computational time, the square root operation being the most time consuming. To avoid this heavy computational burden a piecewise linear approximation approach [56] [42] can be used to determine the square root of a phasor. This approach requires only additions and multiplications by constants and error in the approximation can be made arbitrarily small by increasing the size of the model.

Consider R and I to be the real and imaginary components of a phasor having a magnitude M. These components represent a point in the complex plane and M is the distance from the origin to that point. M is unaffected by the sign and order of the components, points (R, I) and (I, R) are equidistant from the origin. Let,

$$L = max(|R|, |I|), \tag{B.1}$$

$$S = min(|R|, |I|). \tag{B.2}$$

The point (L, S) is now in the first octant at a distance M from the origin. As a first approximation let,

$$\overline{M} = xL + yS, \tag{B.3}$$

where:

$\overline{M}$ is the estimated peak value and

x and y are the coefficients that minimize the error $\overline{M} - M$.

Equation B.3 is the case when only one region of approximation is considered. Additional accuracy is obtained by subdividing the first octant into multiple regions and using a different set of coefficients for each region. But, as the number of regions increase the processing time will increase as well. In general, for n regions there will be a set of n coefficients, $(x_1, y_1) \ldots (x_n, y_n)$, and each set is valid for a particular range of $\frac{S}{L}$ ratios. The values for each set of coefficients, for a particular region, can be calculated using the least squares fit of the data to a linear form of Equation B.3. If k is the number of data points used to fit the data from the n^{th} region then,

$$\underset{k\times 1}{[M]} = \underset{1\times 1}{[x_n]}\,\underset{k\times 1}{[L]} + \underset{1\times 1}{[y_n]}\,\underset{k\times 1}{[S]}, \tag{B.4}$$

$$\underset{k\times 1}{[M]} = \underset{k\times 2}{[L \;\; S]}\,\underset{2\times 1}{\begin{bmatrix} x_n \\ y_n \end{bmatrix}}. \tag{B.5}$$

Using Equation B.6 the values of the coefficients, (x_n, y_n), for the n^{th} region can be determined.

$$\begin{bmatrix} x_n \\ y_n \end{bmatrix} = [L \;\; S]^{+}\,[M], \tag{B.6}$$

where:

$[L \;\; S]^{+}$ is the psuedo-inverse of $[L \;\; S]$.

The use of these coefficients in Equation B.3 provides the estimated peak values; when the coefficients are premultiplied by $\sqrt{2}$ rms values are produced.

C. ANALOG TO DIGITAL CONVERTER MODELLING

An analog to digital (A/D) converter converts an analog electrical quantity to its corresponding digital representation. An A/D converter simulation uses the following parameters;

- the word size of the A/D converter,
- the range of the input signal that the converter can handle and
- the quantization type.

Equation C.1 is the mathematical expression for an A/D converter of $b + 1$ bits.

$$FSR = V_{ref(+)} - V_{ref(-)}, \qquad (C.1)$$

where:

FSR	is the fullscale range of the A/D converter,
$V_{ref(+)}$	is the positive voltage saturation level of the A/D converter and
$V_{ref(-)}$	is the negative voltage saturation level of the A/D converter.

If the input is x volts, then the output of the converter is an integer number determined from Equation C.2. This equation represents an A/D converter with $b + 1$ bits with two's complement representation for negative numbers.

$$NUMB_{10} = Truncation\ or\ Rounding\ of\ \frac{x + \frac{FSR}{2}}{FSR} 2^{b+1} - 2^{b}, \qquad (C.2)$$

where:

$NUMB$	is an integer value with base 10,

D. SPC SIX BUS TEST SYSTEM

For the simulation of transmission line faults a six bus representation of a portion of the Saskatchewan Power Corporation (SPC) transmission system was used. Refer to Figure 5.1.

The system consists of six load buses, three of which are directly connected to generating units, and six transmission lines. The generating units are located at Poplar River (PR), Boundary Dam (BD), and the Queen Elizabeth (QE) generating stations. The substations are at Condie (CON), Regina (RG) and Wolverine (WOL).

The electrical parameters of the six bus test system are listed in the following tables. A base voltage of 230 kv and a base apparent power of 100 MVA were used to calculate the per unit values.

Table D.1: The transmission line data for the six bus SPC test system.

Line Name	Length (km)	Positive Sequence (pu)			Zero Sequence (pu)		
		R_1	X_1	B_1	R_0	X_0	B_0
B2R	182.8	0.0210	0.1214	0.4506	0.0940	0.3877	0.2404
B3R	182.8	0.0210	0.1214	0.4506	0.0940	0.3877	0.2404
C1W	158.5	0.0172	0.1428	0.2909	0.0950	0.3614	0.2016
P2C	174.4	0.0151	0.1134	0.4377	0.0966	0.3568	0.2612
R4C	21.4	0.0023	0.0181	0.0362	0.0118	0.0469	0.0235
Q1W	104.6	0.0913	0.2651	0.0685	0.2308	0.7811	0.0450

Table D.2: The generator data for the six bus SPC test system.

Generator Number	Generator Bus	Positive Sequence (pu)		Zero Sequence (pu)	
		R_1	X_1	R_0	X_0
1	BD	0.000606	0.037343	0.000543	0.016062
2	PR	0.000897	0.054236	0.000807	0.023177
3	QE	0.002160	0.096514	0.001291	0.045230

Table D.3: The pre-fault load flow data for the six bus SPC test system.

Bus	Load		Generation		Voltage	
	P (pu)	Q (pu)	P (pu)	Q (pu)	Magn. (pu)	Phase (°)
BD	0.798	0.177	2.784	0.129	1.0496	0.00
PR	0.250	0.100	2.910	0.184	1.0497	11.81
QE	2.709	0.680	2.200	0.775	1.0110	-20.40
CON	0.608	0.055	0.0	0.0	1.0165	-4.33
WOL	0.419	0.075	0.0	0.0	1.0246	-12.07
RG	2.925	0.735	0.0	0.0	1.0099	-6.27

Table D.4: The load data for the six bus SPC test system.

Bus	P (pu)	Q (pu)	Equivalent Impedance (pu)
BD	0.798	0.1770	1.3158 + j0.2919
PR	0.250	0.1000	3.7996 + j1.5198
QE	2.709	0.6800	0.3549 + j0.0891
CON	0.608	0.0545	1.6859 + j0.1511
WOL	0.419	0.0750	2.4277 + j0.4346
RG	2.925	0.7350	0.3280 + j0.0824

E. THE ELECTRO-MAGNETIC TRANSIENTS PROGRAM

This appendix briefly describes the simulation of transmission line faults using the Electro-Magnetic Transients Program (EMTP) [57]. EMTP uses trapezoidal integration to solve linear algebraic equations that represent algebraic, differential and integral equations that describe the resistive, inductive and capacitive elements of a power system. To simulate a transmission line shunt fault EMTP closes time dependent switches at an imaginary node located at the fault location. An imaginary node is used because these dependent switches can not be directly connected into the transmission line network. The output generated by EMTP consists of instantaneous voltages and currents corresponding to a multiple of the inter-sampling time. In this project the inter-sampling time was set at 4.3403 x10^{-9} s, this corresponds to a sampling frequency, f_s, of 23040 Hz. This high rate of sampling simulates a continuous time signal that can contain frequency components up to $\frac{1}{2}f_s$. The voltage measurement at a node was obtained by inserting a large resistance between the node and ground and measuring the voltage drop across the resistor or by measuring the drop across an already existing circuit branch at the node to ground. The current measurements were obtained by inserting a small resistance in series with an element and measuring the current flow through the resistor.

E.1. Modelling of System Components

EMTP can model generators, transformers, transmission lines and loads for fault studies in several different ways. The models used in the SPC six bus test system were as follows.

1. The generating units were modelled as constant voltage sources and were assumed to be operating in a steady state condition before the inception of the fault. Each generator was represented by the voltage magnitude and phase angle computed from a load flow program. The generator

impedances were combined with the transformer impedances into an equivalent impedance, which consisted of resistive and inductive elements connected in series, and then mutually coupled.

2. The transmission lines were modelled using distributed parameters of resistance, inductive reactance and capacitive reactance. The transmission lines were also assumed to be continuously transposed.
3. The loads at each bus were assumed to be balanced and have a constant impedance.

F. FURTHER RESULTS

Table F.1: The performance of the extremely inverse current-time characteristic at TMS=0.5.

Current Multiple	Relay Time (s)	IEC Time (s)	Percent Difference	Cycle Difference
1.5	32.008333	32.000000	0.026042	0.500000
2.0	13.336111	13.333333	0.020833	0.166667
2.5	7.620833	7.619048	0.023438	0.107143
3.0	5.001389	5.000000	0.027778	0.083333
3.5	3.556944	3.555556	0.039063	0.083333
4.0	2.668056	2.666667	0.052083	0.083333
4.5	2.051389	2.077922	-1.276910	-1.591991
5.0	1.668056	1.666667	0.083333	0.083333
5.5	1.356944	1.367521	-0.773437	-0.634615
6.0	1.143056	1.142857	0.017361	0.011905
6.5	0.965278	0.969697	-0.455729	-0.265152
7.0	0.834722	0.833333	0.166667	0.083333
7.5	0.720833	0.723982	-0.434896	-0.188914
8.0	0.636111	0.634921	0.187500	0.071429
8.5	0.559722	0.561404	-0.299479	-0.100877
9.0	0.501389	0.500000	0.277778	0.083333
9.5	0.447222	0.448179	-0.213542	-0.057423
10.0	0.404167	0.404040	0.031250	0.007576
12.5	0.258333	0.257649	0.265625	0.041063
15.0	0.179167	0.178571	0.333333	0.035714
17.5	0.131944	0.131040	0.690104	0.054259
20.0	0.101389	0.100251	1.135417	0.068296

Table F.2: The performance of the extremely inverse current-time characteristic at TMS=1.6.

Current Multiple	Relay Time (s)	IEC Time (s)	Percent Difference	Cycle Difference
1.5	102.425000	102.400000	0.024414	1.500000
2.0	42.715278	42.666667	0.113932	2.916667
2.5	24.390278	24.380952	0.038249	0.559524
3.0	16.001389	16.000000	0.008681	0.083333
3.5	11.380556	11.377778	0.024414	0.166667
4.0	8.534722	8.533333	0.016276	0.083333
4.5	6.565278	6.649351	-1.264377	-5.044372
5.0	5.334722	5.333333	0.026042	0.083333
5.5	4.340278	4.376068	-0.817871	-2.147436
6.0	3.658333	3.657143	0.032552	0.071429
6.5	3.084722	3.103030	-0.590007	-1.098485
7.0	2.668056	2.666667	0.052083	0.083333
7.5	2.306944	2.316742	-0.422906	-0.587858
8.0	2.031944	2.031746	0.009766	0.011905
8.5	1.791667	1.796491	-0.268555	-0.289474
9.0	1.601389	1.600000	0.086806	0.083333
9.5	1.430556	1.434174	-0.252279	-0.217087
10.0	1.293056	1.292929	0.009766	0.007576
12.5	0.823611	0.824477	-0.104980	-0.051932
15.0	0.572222	0.571429	0.138889	0.047619
17.5	0.419444	0.419328	0.027669	0.006962
20.0	0.320833	0.320802	0.009766	0.001880

Table F.3: The performance of the very inverse current-time characteristic at TMS=0.5.

Current Multiple	Relay Time (s)	IEC Time (s)	Percent Difference	Cycle Difference
1.5	13.501389	13.500000	0.010288	0.083333
2.0	6.751389	6.750000	0.020576	0.083333
2.5	4.501389	4.500000	0.030864	0.083333
3.0	3.376389	3.375000	0.041152	0.083333
3.5	2.701389	2.700000	0.051440	0.083333
4.0	2.251389	2.250000	0.061728	0.083333
4.5	1.929167	1.928571	0.030864	0.035714
5.0	1.688889	1.687500	0.082305	0.083333
5.5	1.501389	1.500000	0.092593	0.083333
6.0	1.351389	1.350000	0.102881	0.083333
6.5	1.227778	1.227273	0.041152	0.030303
7.0	1.126389	1.125000	0.123457	0.083333
7.5	1.038889	1.038462	0.041152	0.025641
8.0	0.965278	0.964286	0.102881	0.059524
8.5	0.901389	0.900000	0.154321	0.083333
9.0	0.844444	0.843750	0.082305	0.041667
9.5	0.794444	0.794118	0.041152	0.019608
10.0	0.751389	0.750000	0.185185	0.083333
12.5	0.587500	0.586957	0.092593	0.032609
15.0	0.483333	0.482143	0.246914	0.071429
17.5	0.409722	0.409091	0.154321	0.037879
20.0	0.355556	0.355263	0.082305	0.017544

Table F.4: The performance of the very inverse current-time characteristic at TMS=1.6.

Current Multiple	Relay Time (s)	IEC Time (s)	Percent Difference	Cycle Difference
1.5	43.220833	43.200000	0.048225	1.250000
2.0	21.601389	21.600000	0.006430	0.083333
2.5	14.402778	14.400000	0.019290	0.166667
3.0	10.801389	10.800000	0.012860	0.083333
3.5	8.641667	8.640000	0.019290	0.100000
4.0	7.201389	7.200000	0.019290	0.083333
4.5	6.172222	6.171429	0.012860	0.047619
5.0	5.401389	5.400000	0.025720	0.083333
5.5	4.801389	4.800000	0.028935	0.083333
6.0	4.320833	4.320000	0.019290	0.050000
6.5	3.927778	3.927273	0.012860	0.030303
7.0	3.601389	3.600000	0.038580	0.083333
7.5	3.323611	3.323077	0.016075	0.032051
8.0	3.086111	3.085714	0.012860	0.023810
8.5	2.880556	2.880000	0.019290	0.033333
9.0	2.701389	2.700000	0.051440	0.083333
9.5	2.541667	2.541176	0.019290	0.029412
10.0	2.401389	2.400000	0.057870	0.083333
12.5	1.879167	1.878261	0.048225	0.054348
15.0	1.543056	1.542857	0.012860	0.011905
17.5	1.309722	1.309091	0.048225	0.037879
20.0	1.137500	1.136842	0.057870	0.039474

Table F.5: The performance of the standard inverse current-time characteristic at TMS=0.5.

Current Multiple	Relay Time (s)	IEC Time (s)	Percent Difference	Cycle Difference
1.5	8.598611	8.597109	0.017467	0.090101
2.0	5.015278	5.014514	0.015241	0.045856
2.5	3.786111	3.784855	0.033182	0.075352
3.0	3.151389	3.150965	0.013438	0.025406
3.5	2.759722	2.758971	0.027237	0.045088
4.0	2.490278	2.489878	0.016054	0.023983
4.5	2.302778	2.292183	0.462197	0.635664
5.0	2.140278	2.139860	0.019522	0.025065
5.5	2.023611	2.018288	0.263737	0.319378
6.0	1.919444	1.918596	0.044210	0.050893
6.5	1.838889	1.835074	0.207883	0.228888
7.0	1.765278	1.763871	0.079743	0.084394
7.5	1.705556	1.702291	0.191752	0.195851
8.0	1.648611	1.648387	0.013607	0.013458
8.5	1.602778	1.600713	0.128984	0.123879
9.0	1.558333	1.558175	0.010163	0.009501
9.5	1.522222	1.519926	0.151100	0.137796
10.0	1.486111	1.485299	0.054656	0.048708
12.5	1.352778	1.351033	0.129115	0.104664
15.0	1.258333	1.257759	0.045685	0.034476
17.5	1.188889	1.188169	0.060579	0.043187
20.0	1.134722	1.133678	0.092093	0.062642

Table F.6: The performance of the standard inverse current-time characteristic at TMS=1.6.

Current Multiple	Relay Time (s)	IEC Time (s)	Percent Difference	Cycle Difference
1.5	27.523611	27.510750	0.046749	0.771658
2.0	16.052778	16.046443	0.039476	0.380073
2.5	12.112500	12.111537	0.007953	0.057794
3.0	10.086111	10.083089	0.029967	0.181298
3.5	8.830556	8.828706	0.020945	0.110948
4.0	7.969444	7.967610	0.023027	0.110080
4.5	7.368056	7.334987	0.450836	1.984124
5.0	6.848611	6.847552	0.015465	0.063540
5.5	6.476389	6.458522	0.276640	1.072010
6.0	6.140278	6.139508	0.012539	0.046191
6.5	5.883333	5.872237	0.188961	0.665775
7.0	5.645833	5.644388	0.025609	0.086727
7.5	5.455556	5.447332	0.150958	0.493390
8.0	5.275000	5.274838	0.003075	0.009733
8.5	5.127778	5.122282	0.107292	0.329747
9.0	4.987500	4.986160	0.026876	0.080404
9.5	4.868056	4.863762	0.088277	0.257615
10.0	4.754167	4.752958	0.025434	0.072532
12.5	4.326389	4.323307	0.071289	0.184924
15.0	4.026389	4.024828	0.038783	0.093657
17.5	3.804167	3.802141	0.053273	0.121531
20.0	3.629167	3.627770	0.038494	0.083789

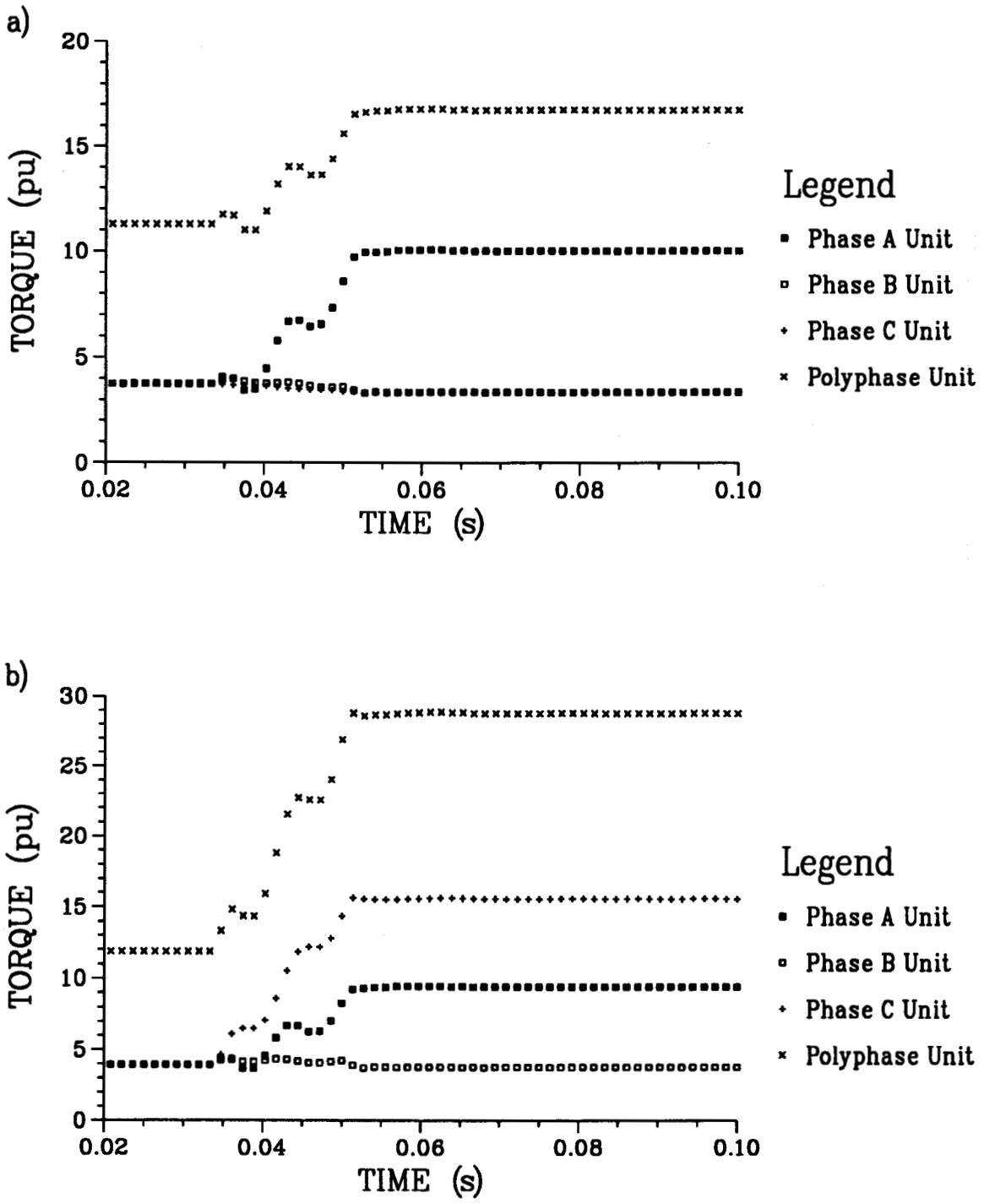

Figure F.1: Torques developed by the relay for line P2C at bus PR for a single-phase-to-ground fault with a MTA of 0° for the directional phase units: a) the 30° connection and b) the 60° delta connection. Data was generated using EMTP.

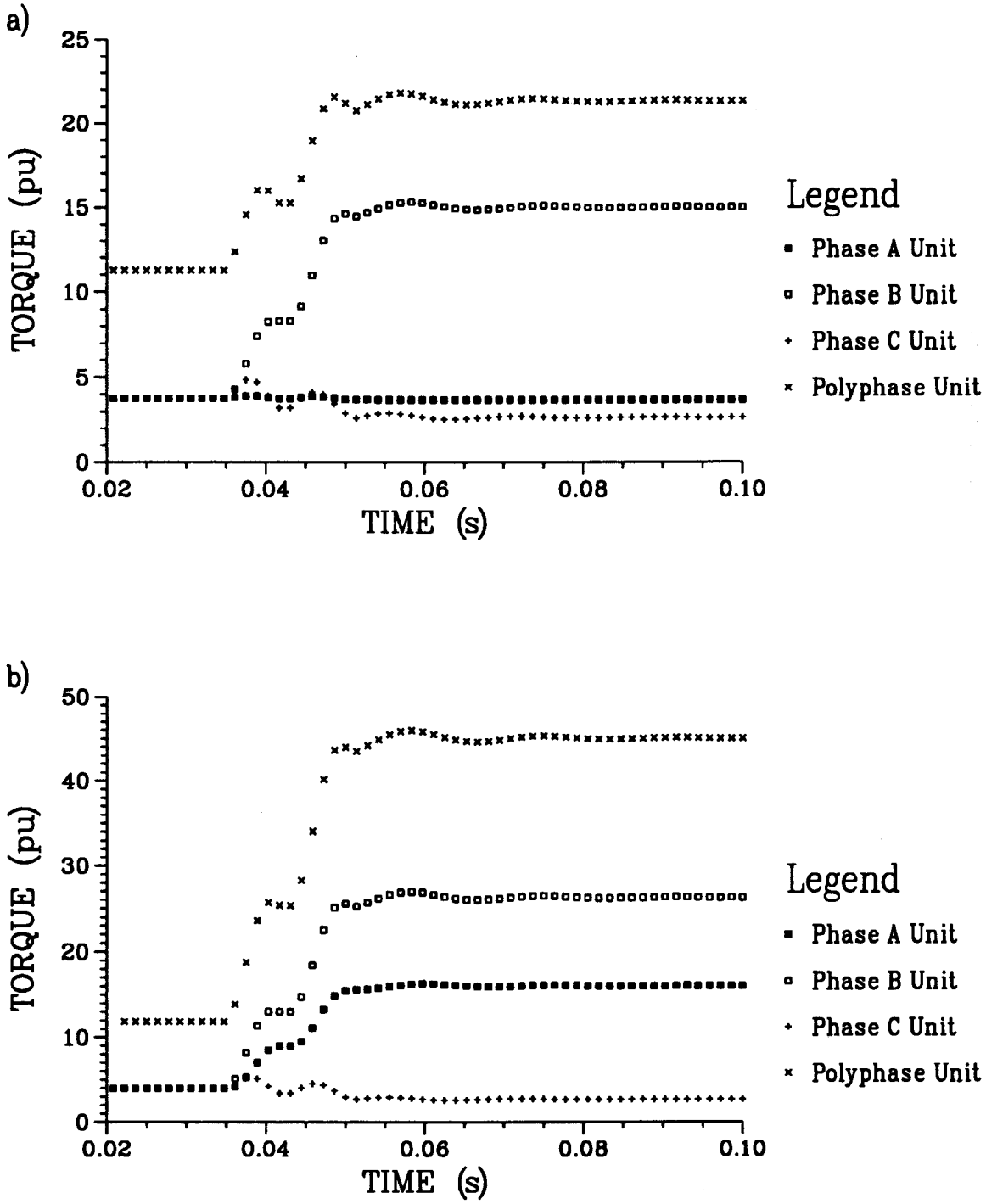

Figure F.2: Torques developed by the relay for line P2C at bus PR for a two-phase fault with a MTA of 0° for the directional phase units: a) the 30° connection and b) the 60° delta connection. Data was generated using EMTP.

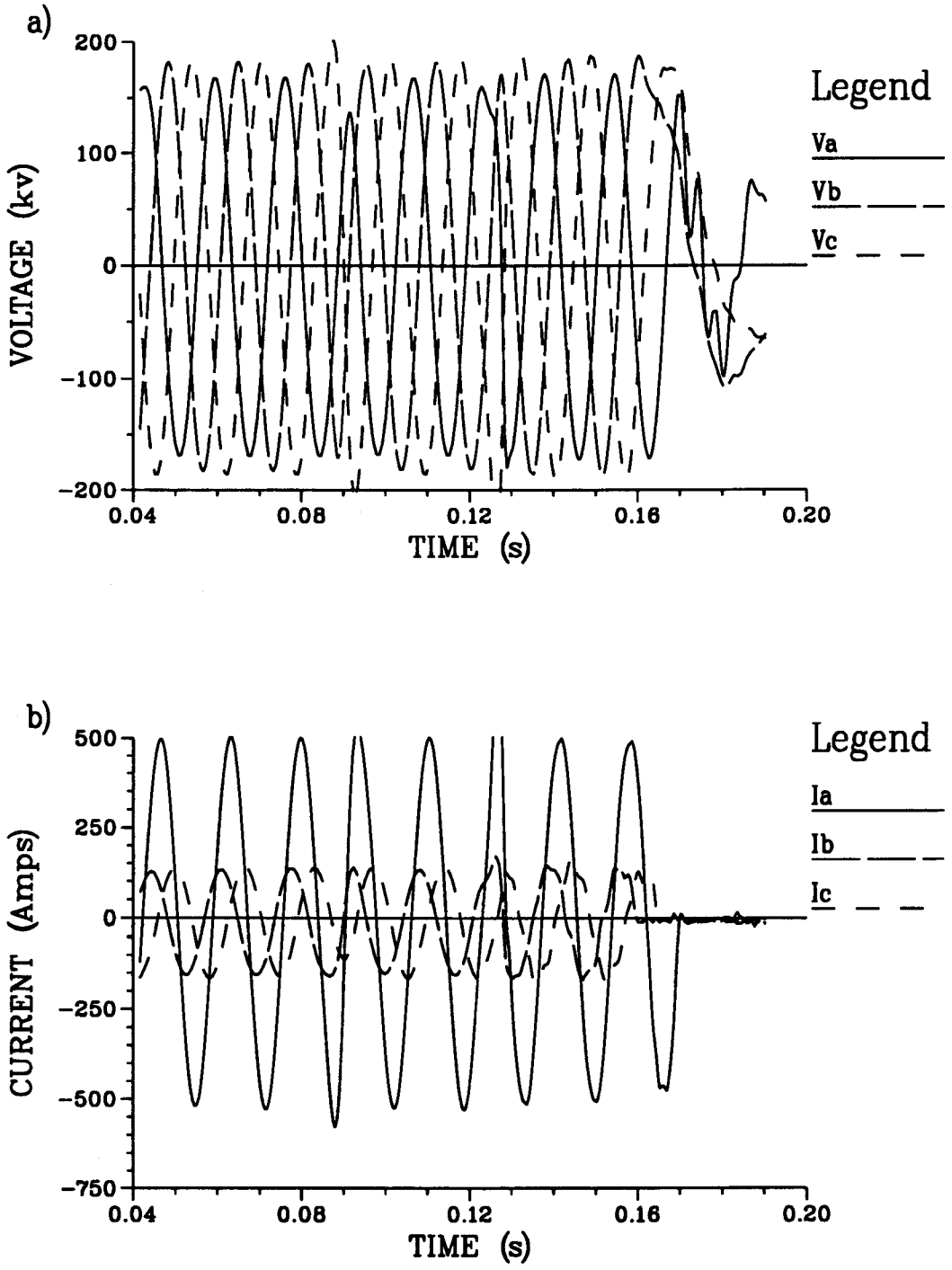

Figure F.3: The a) voltage and b) current waveforms recorded at bus CON by SPC when one pole of the disconnect switch at bus PR, on line P2C, malfunctioned.

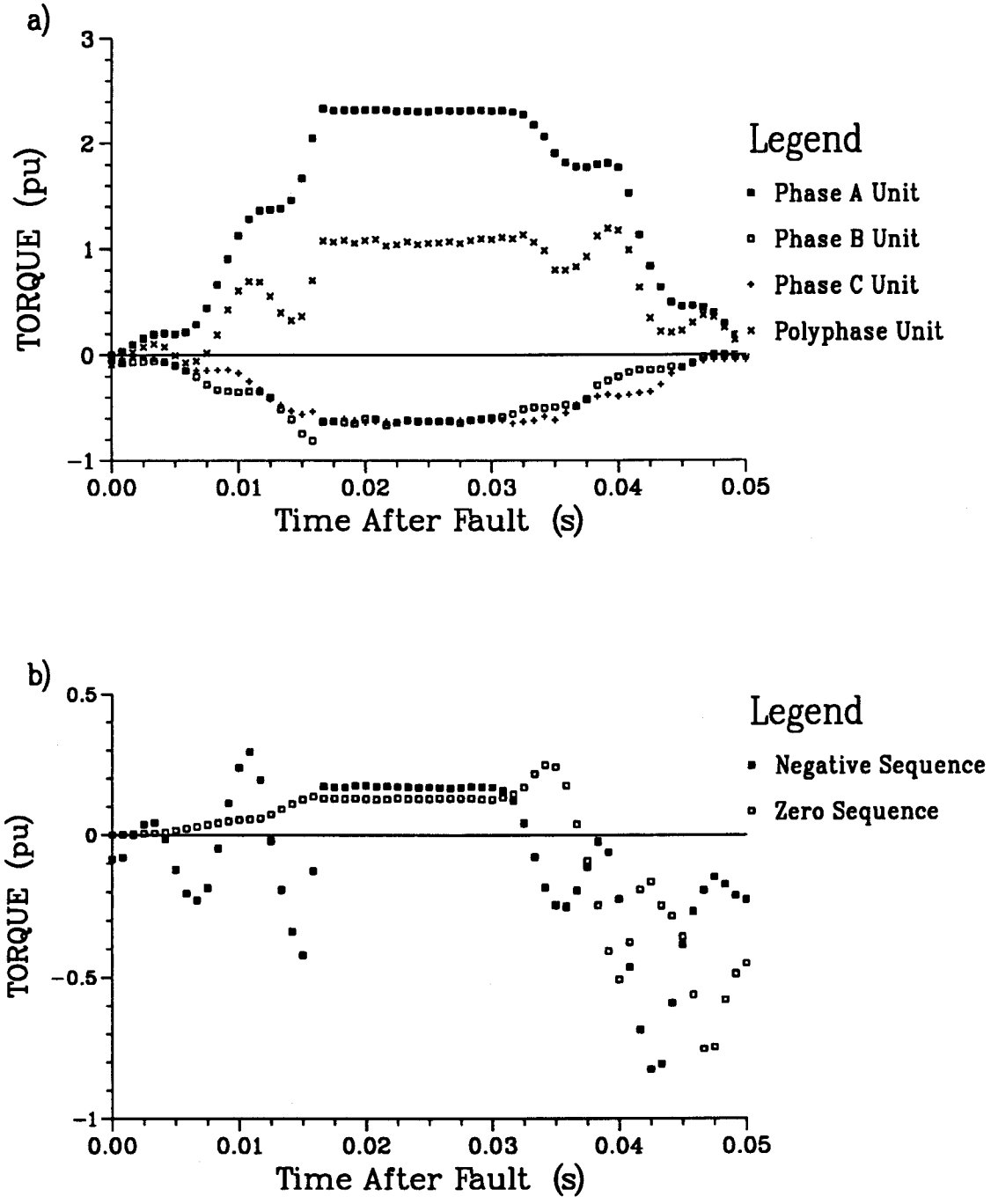

Figure F.4: Torques developed by the relay for line P2C at bus CON for the waveforms shown in Figure F.3. Using a) a MTA of 30° for the directional phase units and b) MTA's of −60° and 90° for the directional ground unit when polarized with zero and negative sequence quantities respectively.

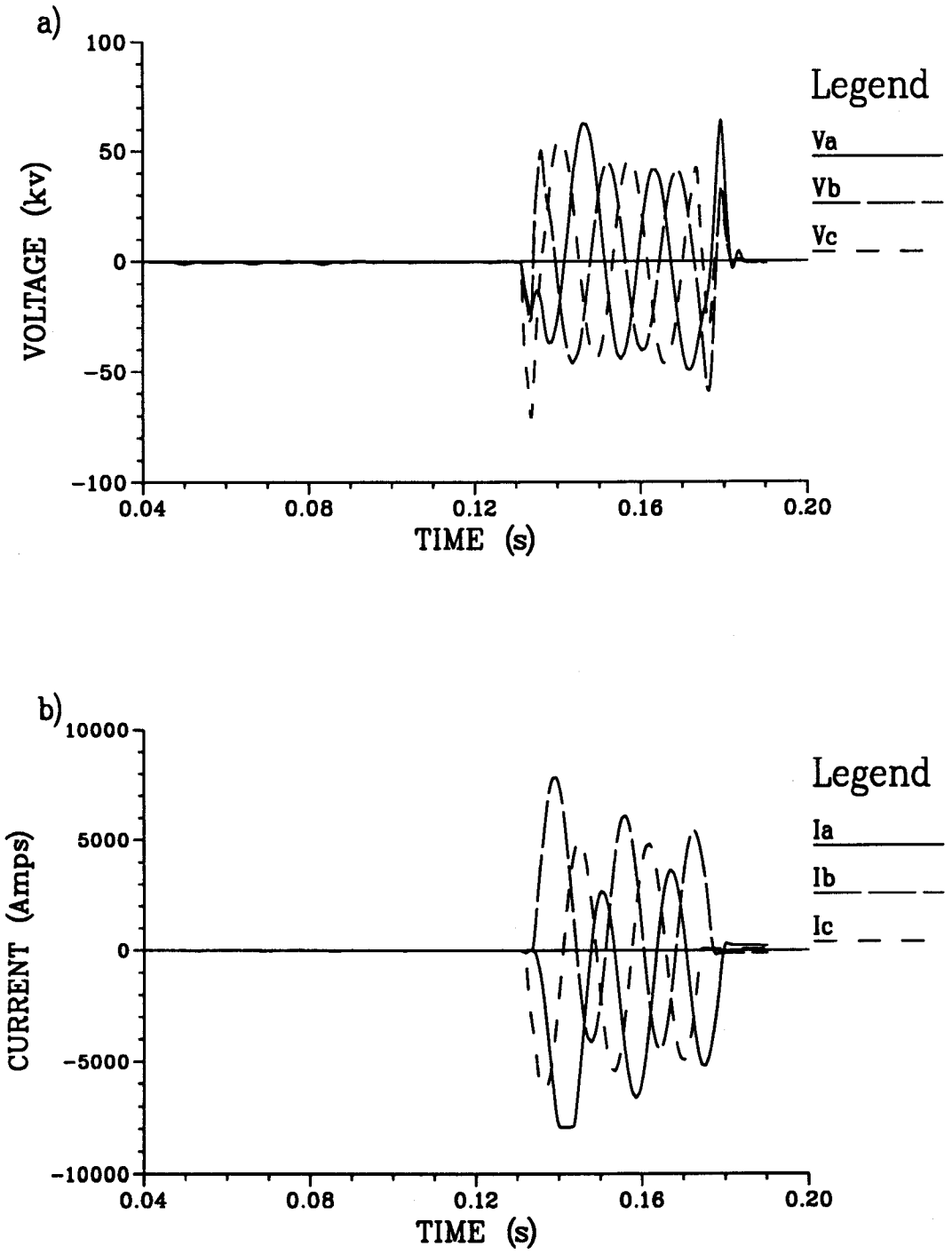

Figure F.5: The a) voltage and b) current waveforms recorded at bus CON by SPC for a first unsuccessful attempt to reclose P2C onto a solid three-phase-to-ground fault approximately 25.5 km from bus CON.

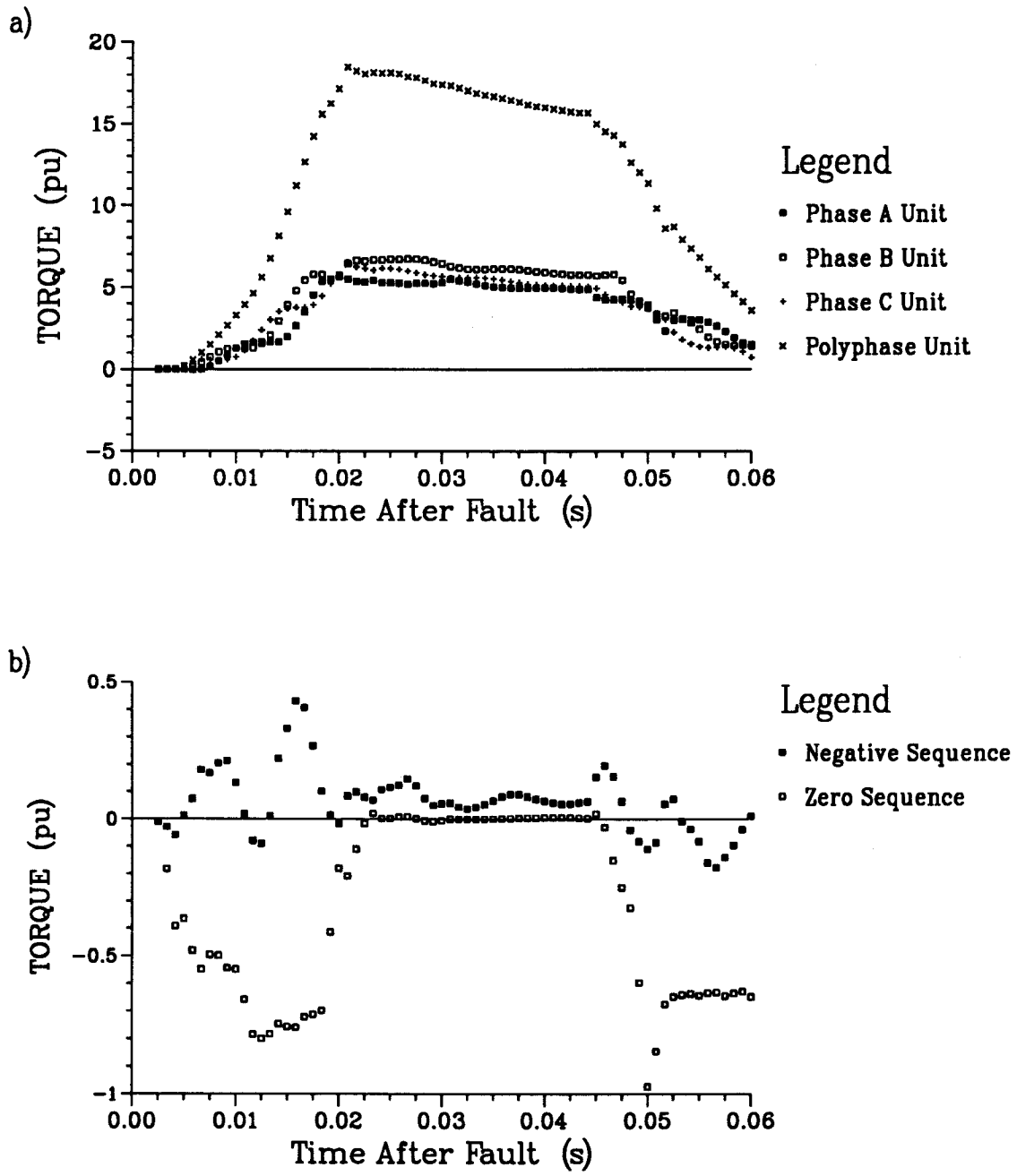

Figure F.6: Torques developed by the relay for line P2C at bus CON for the waveforms shown in Figure F.5. Using a) a MTA of 30° for the directional phase units and b) MTA's of –60° and 90° for the directional ground unit when polarized with zero and negative sequence quantities respectively.

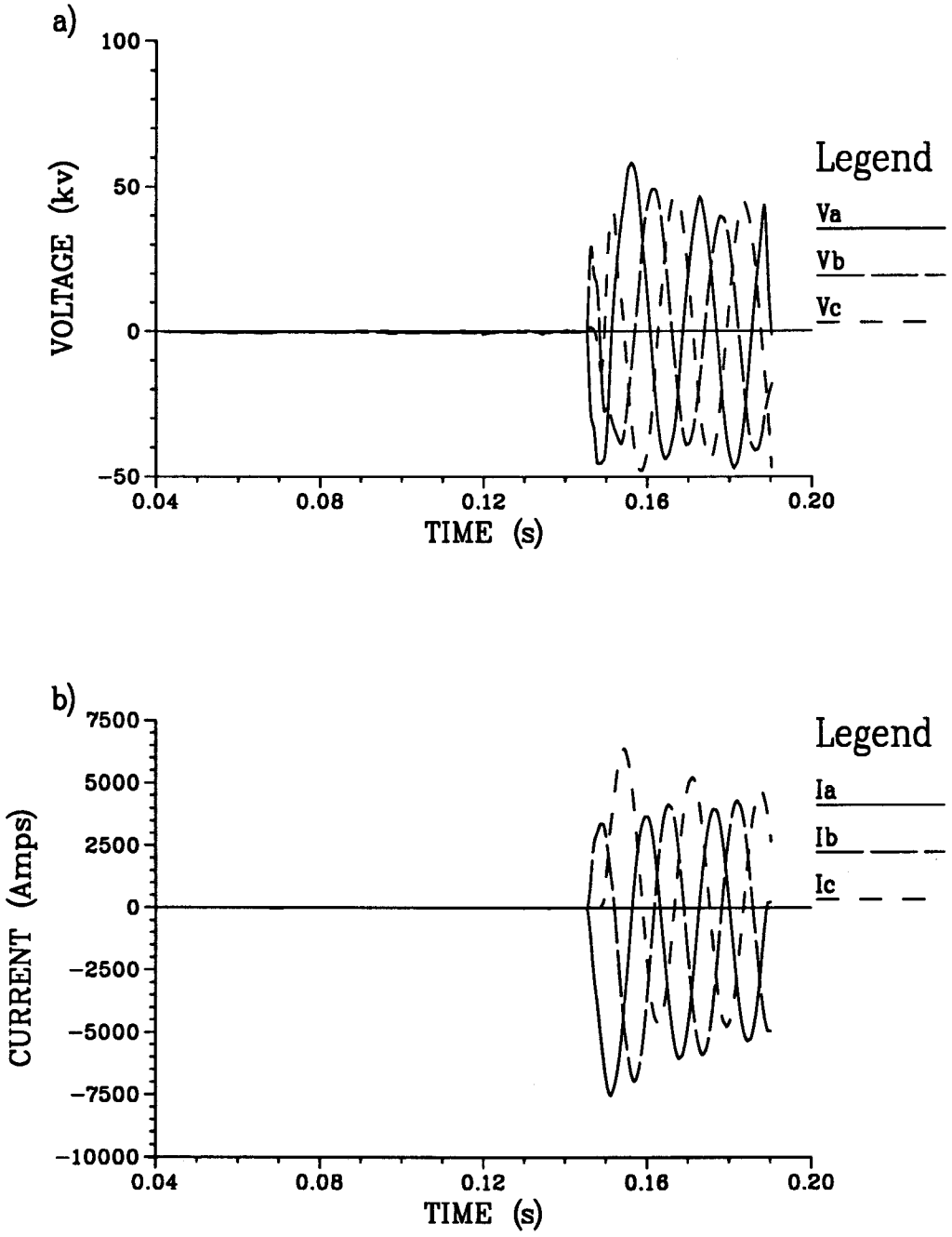

Figure F.7: The a) voltage and b) current waveforms recorded at bus CON by SPC for a second unsuccessful attempt to reclose P2C onto a solid three-phase-to-ground fault approximately 25.5 km from bus CON.

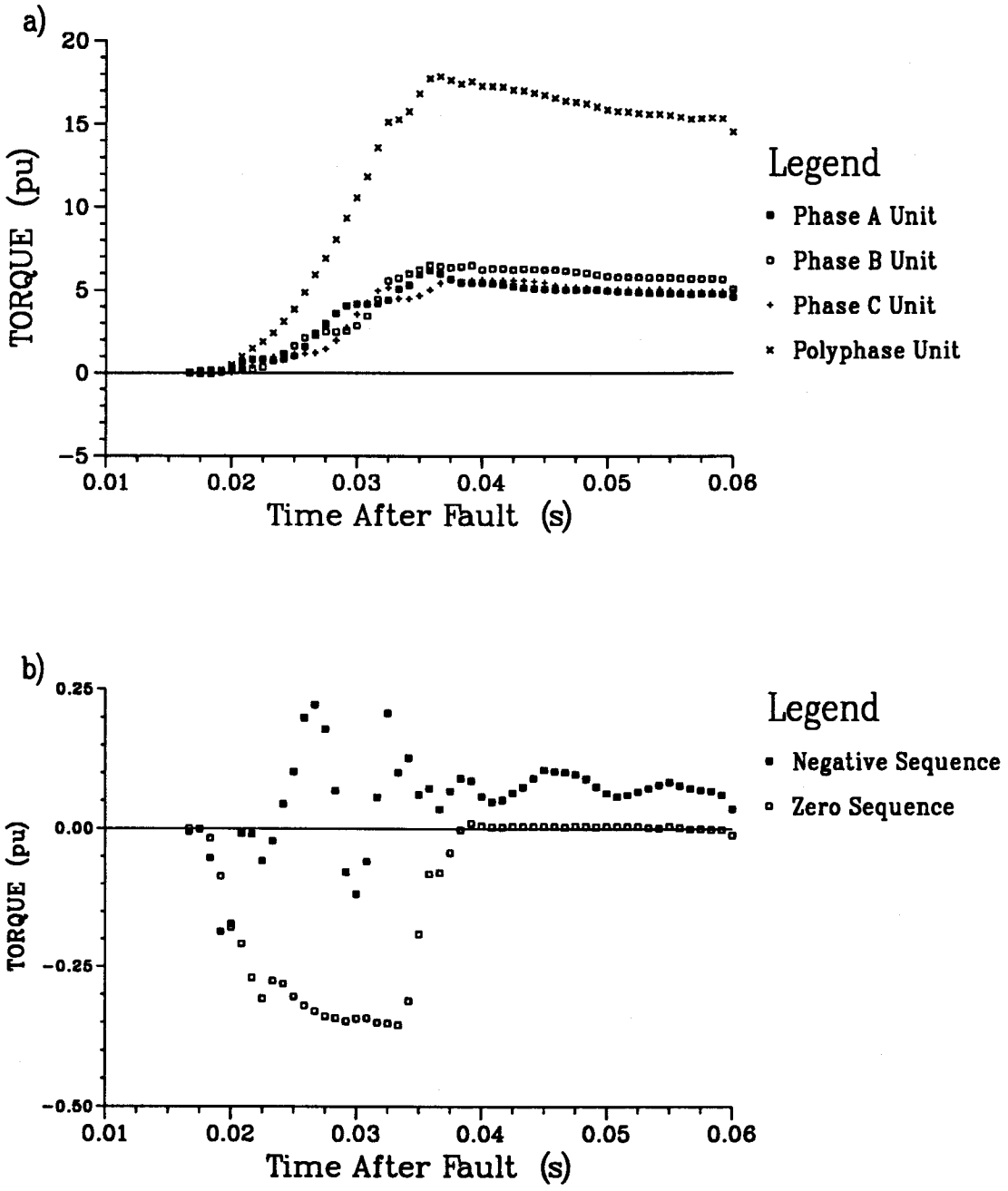

Figure F.8: Torques developed by the relay for line P2C at bus CON for the waveforms shown in Figure F.7. Using a) a MTA of 30° for the directional phase units and b) MTA's of −60° and 90° for the directional ground unit when polarized with zero and negative sequence quantities respectively.

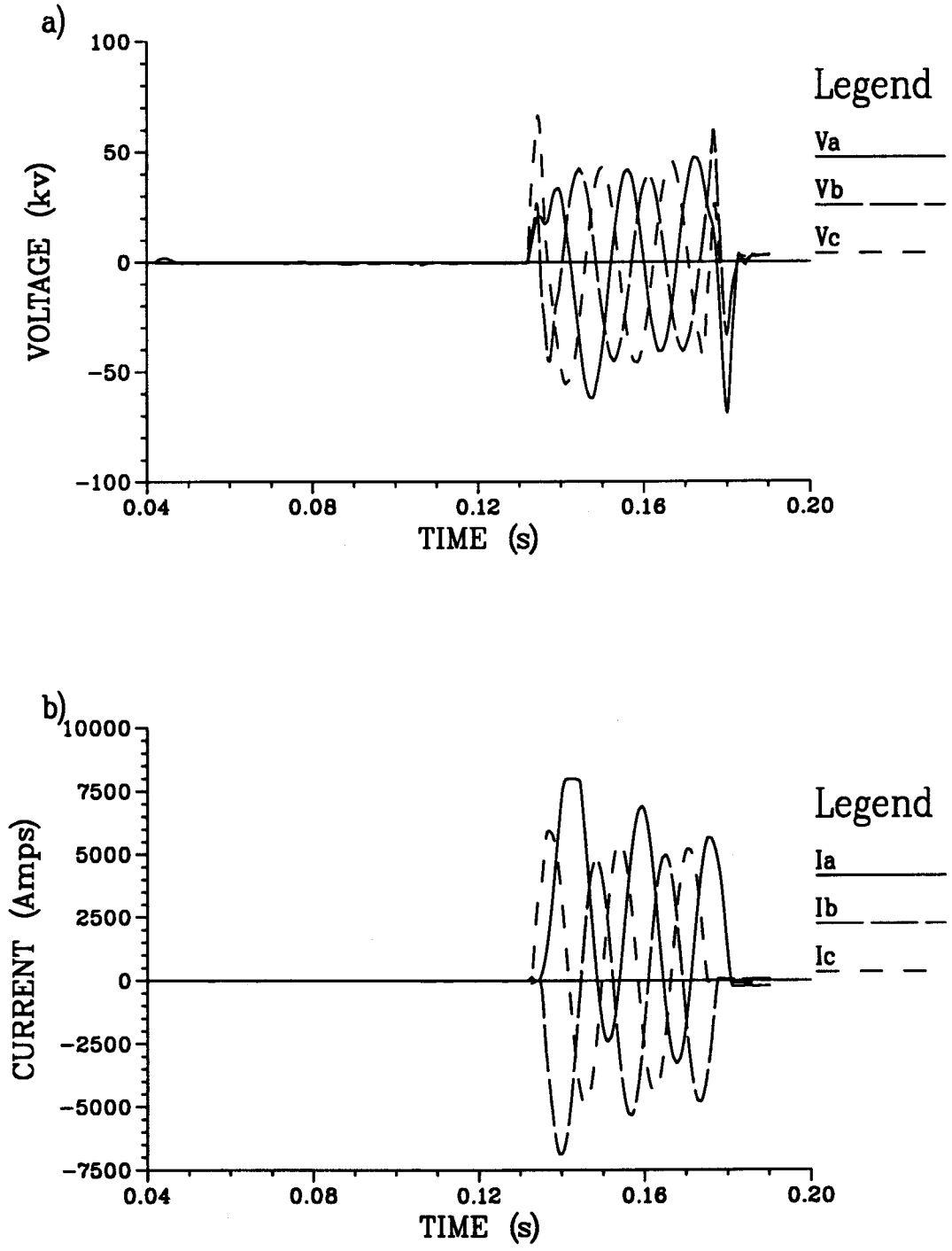

Figure F.9: The a) voltage and b) current waveforms recorded at bus CON by SPC for a third unsuccessful attempt to reclose P2C onto a solid three-phase-to-ground fault approximately 25.5 km from bus CON.

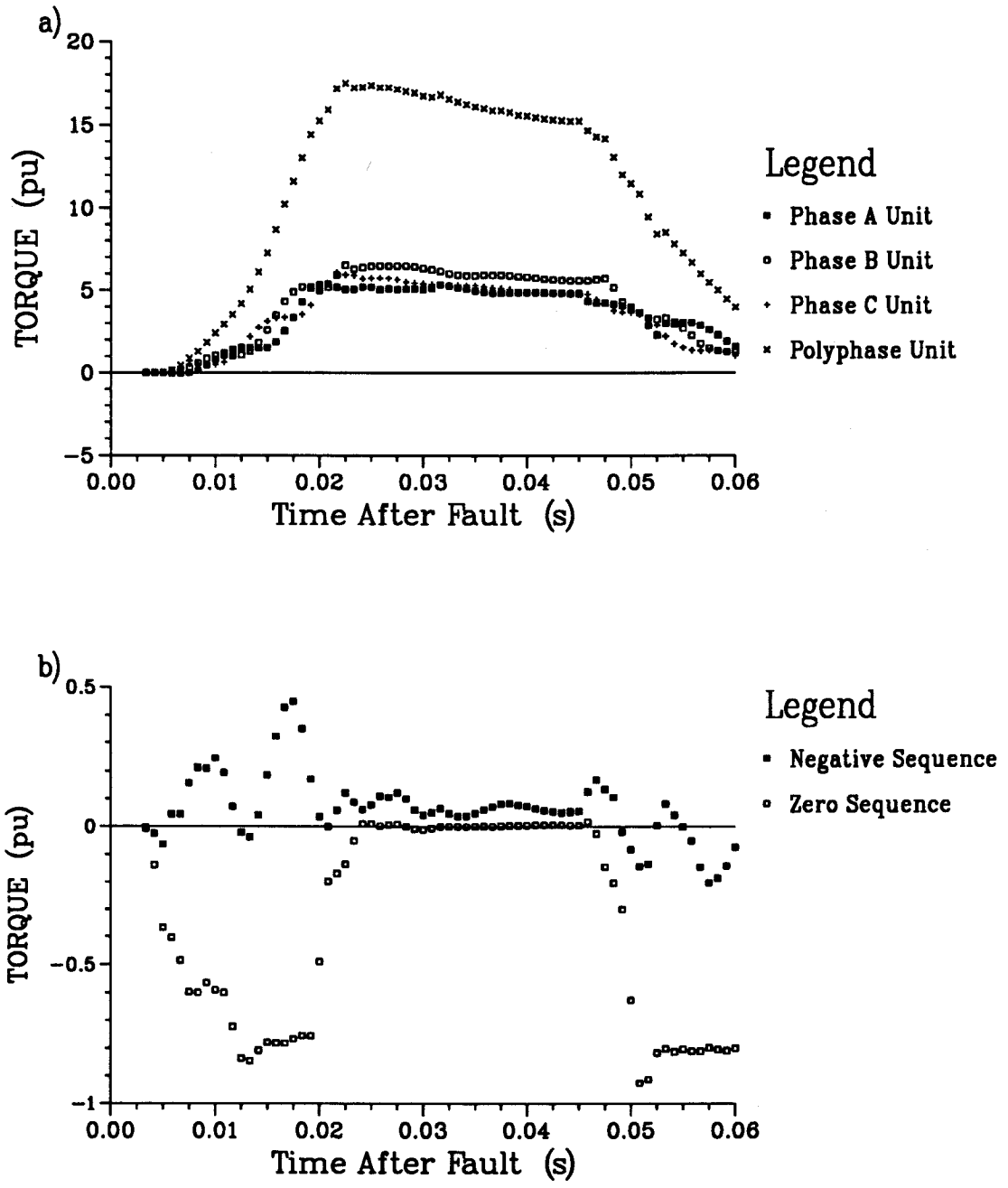

Figure F.10: Torques developed by the relay for line P2C at bus CON for the waveforms shown in Figure F.9. Using a) a MTA of 30° for the directional phase units and b) MTA's of –60° and 90° for the directional ground unit when polarized with zero and negative sequence quantities respectively.